

**Toward understanding the polyglutamine disorder
Spinocerebellar Ataxia type 3 using mouse models of
disease**

by

Biswarathan Ramani

**A dissertation submitted in partial fulfillment
of the requirements for the degree of
Doctor of Philosophy
(Neuroscience)
in the University of Michigan
2015**

Doctoral Committee:

**Professor Henry L. Paulson, Chair
Professor Roger L. Albin
Professor Andrew P. Lieberman
Professor Miriam H. Meisler
Professor Jack M. Parent**

© Biswarathan Ramani

2015

Acknowledgements

I would firstly like to thank my dissertation mentor Dr. Henry Paulson, who has been an outstanding source of inspiration, support, knowledge, and wisdom. I thank my dissertation committee members Dr. Roger Albin, Dr. Andrew Lieberman, Dr. Miriam Meisler, and Dr. Jack Parent for their enthusiasm and support of my work with valuable advice during and outside committee meetings. I thank the members of the Paulson laboratory for helping me over the years and for keeping the lab environment productive and professional. I thank both current and former lab members that have directly contributed to this dissertation work: Rogerio Huang (my student), Dr. Ginny Harris, Dr. Maria do Carmo Costa, Bo Wang, Svetlana Fischer, and Dr. Takahiro Seki. I also thank Dr. Graham Atkin and Lijie Gong for teaching me techniques. I thank Dr. Peter Todd, Dr. Vikram Shakkottai, and Dr. Aaron Goldstrohm for helpful conversations over various aspects of the thesis. I thank the many staff of the Medical Scientist Training Program and the Neuroscience Graduate Program for their support over the many years. I thank our collaborators in the Computational Medicine & Bioinformatics department, including Dr. Richard McEachin, Dr. Yuanfang Guan, and Dr. Bharat Panwar, for help with analysis of our RNA-sequencing data. Other collaborators, contributors, and sources of funding are acknowledged throughout the dissertation.

Table of Contents

Acknowledgements.....	ii
List of Figures.....	v
List of Tables	vii
Abstract.....	viii
Chapter 1: Introduction.....	1
1.1 Toward understanding the polyglutamine diseases	1
1.1.1 The polyglutamine disease genes and proteins.....	1
1.1.2 Disease protein misfolding and aggregation: central to pathogenesis?	4
1.1.3 Transcriptional dysregulation and gene expression profiling in polyQ disease	9
1.2 Knock-in mouse models of polyglutamine disease	11
1.2.1 Mouse models of polyQ disease and general features of knock-in mice.....	12
1.2.2 Lessons from knock-in mouse models of polyQ disease.....	14
1.3 Toward understanding Spinocerebellar Ataxia type 3.....	16
1.3.1 Clinical and pathological features of SCA3.....	17
1.3.2 The <i>ATXN3</i> gene, splice isoforms, and aggregation	18
1.3.3 <i>ATXN3</i> as a deubiquitinating enzyme.....	19
1.3.4 <i>ATXN3</i> function and dysfunction in the nucleus	20
1.4 Summary and aims of the dissertation	21
Chapter 2: Materials and Methods.....	28
2.1 Generation of the SCA3 knock-in mice.....	28
2.2 Animals and ethical use	30
2.3 Genotyping and CAG repeat sizing.....	30
2.4 Tissue lysate preparation, SDS-PAGE, SDS-Agarose, and western blot analysis	31
2.5 Immunohistochemistry, immunofluorescence, and scoring <i>ATXN3</i> accumulation....	32
2.6 Motor behavior testing and fear conditioning.....	33
2.7 RNA extraction, RNA sequencing, RT-PCR, quantitative PCR, and 3' RACE	33
2.8 Primers	35
2.9 Plasmids and cell culture experiments.....	36
2.10 Statistical analysis.....	37

Chapter 3: A knock-in mouse model of Spinocerebellar Ataxia type 3 exhibits prominent aggregate pathology and aberrant splicing of the disease gene transcript	39
3.1 Abstract	39
3.2 Introduction	40
3.3 Results	42
3.3.1 Generation of the SCA3 knock-in mouse and mutant ATXN3 expression	42
3.3.2 Neuropathological and behavioral characterization of the SCA3 knock-in mouse	43
3.3.3 Alternative processing of the mutant ataxin-3 transcript	46
3.4 Discussion	50
3.5 Acknowledgements	53
Chapter 4: Isoform-driven aggregation of the polyglutamine disease protein ATXN3 elicits early transcriptional changes in the brain	64
4.1 Abstract	64
4.2 Introduction	65
4.3 Results	67
4.3.1 Distinct SCA3 knock-in lines express different mutant <i>Atxn3</i> transcripts	67
4.3.2 ATXN3 accumulation in neuronal nuclei and aggregation differs in the two SCA3 knock-in lines	69
4.3.3 Transcriptional alterations are associated with ATXN3 nuclear accumulation and aggregation in SCA3 mouse models	71
4.3.4 Cre-recombinase expression in Q82 mice alters <i>Atxn3</i> splicing and attendant aggregation	74
4.4 Discussion	75
4.5 Acknowledgements	81
Chapter 5: Conclusions and future directions	93
5.1 Diverse uses of SCA3 knock-in mice and extended characterization	93
5.2 ATXN3 isoforms and protein context in polyQ disease	97
5.3 Disease protein aggregation in polyQ disease	99
5.4 Understanding transcriptional changes in polyQ disease	101
5.5 Oligodendrocytes and glial contributions to polyQ disease	104
5.6 Concluding remarks	106
References	108

List of Figures

Figure 1.1 Pathogenic factors from CAG expansion to disease	24
Figure 1.2 Basic model of polyQ disease protein aggregation	24
Figure 1.3 SCA3 mutant gene, transcript, and protein	27
Figure 2.1 Retained sequences in the mutant <i>Atxn3</i> locus of SCA3 knock-in mice.....	38
Figure 3.1 Generation of a SCA3 knock-in mouse expressing mutant ATXN3 (Q82).....	55
Figure 3.2 Mutant ATXN3 accumulation in the SCA3 knock-in mouse brain	56
Figure 3.3 ATXN3 and p62 co-immunostaining in a heterozygous Q82/Q6 mouse.....	57
Figure 3.4 Cresyl-violet staining of Q82/Q6 brain	57
Figure 3.5 Extranuclear inclusions in the hippocampus of SCA3 knock-in mice	58
Figure 3.6 Examples of scoring ATXN3 accumulation in an immunohistochemically- stained SCA3 knock-in mouse brain.....	59
Figure 3.7 ATXN3 solubility and aggregation in different brain regions of Q82/Q6 mice.....	60
Figure 3.8 Alternative splicing of the mutant <i>Atxn3</i> transcript is enhanced in SCA3 knock-in mice.....	61
Figure 3.9 The mutant <i>Atxn3</i> transcript in SCA3 knock-in mice does not exhibit obvious abnormalities outside the exon 10-intron 10 junction.....	62
Figure 3.10 Expression of 10 exon <i>Atxn3</i> / <i>ATXN3</i> transcript in SCA3 mouse models and SCA3 human fibroblasts	63
Figure 4.1 SCA3 knock-in mouse lines express different <i>Atxn3</i> transcript.....	82
Figure 4.2 Human and murine ATXN3-10e isoforms are predicted to have greater hydrophobicity	83

Figure 4.3 ATXN3 accumulation and aggregation is increased in SCA3 knock-in mice expressing <i>Atxn3</i> -10e	84
Figure 4.4 ATXN3 accumulation and aggregation remains low in homozygous variant SCA3 knock-in mice.....	85
Figure 4.5 Increased aggregation-propensity of ATXN3 associates with robust distinct transcriptional changes in the pons	86
Figure 4.6 Transcripts associated with ATXN3 aggregation are enriched in biological processes linked to oligodendrocytes.....	87
Figure 4.7 Transcriptional alterations in Q82/Q82 mice are minimally associated with ATXN3 loss of function.....	88
Figure 4.8 Validation of altered transcripts in Q82 versus Q82V SCA3 knock-in mice ..	89
Figure 4.9 Expression of Cre-recombinase in the brain of Q82/Q6 mice reduces <i>Atxn3</i> -10e expression, ATXN3 aggregation, and transcriptional changes	90
Figure 4.10 Overexpressing mouse mutant ATXN3 isoforms in cell culture did not show differences in puncta/inclusion formation	91
Figure 4.11 Identifying the origin and heritability of different mutant <i>Atxn3</i> phenotypes in SCA3 knock-in mice.....	92

List of Tables

Table 1.1 The diversity of polyglutamine (polyQ) disease genes, proteins, and function	23
Table 1.2 Knock-in mouse models of HD	25
Table 1.3 Knock-in mouse models of polyQ disease excluding HD	26
Table 3.1 Regional differences in ATXN3 accumulation in SCA3 knock-in mouse brain	59

Abstract

The polyglutamine (polyQ) diseases, including Spinocerebellar Ataxia type 3 (SCA3), are inherited neurodegenerative diseases caused by glutamine-encoding CAG expansions in disease genes. All polyQ diseases exhibit accumulation and aggregation of the disease protein in affected brain regions, yet central questions remain regarding the pathogenesis of these untreatable disorders, including which factors can influence disease protein aggregation, the extent to which aggregation drives disease, and the processes by which aggregation might contribute to toxicity.

My thesis addresses these questions in a novel knock-in mouse model of SCA3. Chapter 1 reviews central features of polyQ disease, the use of knock-in mouse models to study polyQ disease, and aspects of SCA3. Chapter 2 provides the materials and methods used for the dissertation. Chapter 3 describes the generation and characterization of a SCA3 knock-in mouse model. SCA3 knock-in mice show striking mutant ATXN3 accumulation and aggregation in brain. This accompanies aberrant splicing of the mutant *Atxn3* transcript, emulating an important feature of the human *ATXN3* transcript. Chapter 4 further explores how alternative *Atxn3* splicing influences aggregation in a “variant” SCA3 knock-in mouse that exhibits minimal aggregate pathology. Using various mouse models I explore the relationship between mutant ATXN3 aggregation and transcriptional alterations in the pons, a susceptible brain region. Chapter 5 concludes the dissertation with thoughts regarding moving forward with this work.

This thesis establishes the utility of SCA3 knock-in mice for studying early molecular pathogenic events and provides evidence supporting a critical role for alternative splicing in influencing disease protein aggregation. The results further suggest a molecular link between the process of ATXN3 aggregation and transcriptional dysregulation in the brain. Together, these findings support a pathogenic role for disease protein aggregation in SCA3 and perhaps other polyQ diseases.

Chapter 1

Introduction

Spinocerebellar ataxia type 3 (SCA3), also known as Machado-Joseph disease (MJD), is a hereditary neurodegenerative disorder caused by a glutamine-encoding CAG repeat expansion in the *ATXN3* gene. This dissertation utilizes, among a diverse set of resources, novel knock-in mouse models of disease to study the intriguing relationship between alternative splicing of the disease transcript, disease protein aggregation, and transcriptional alterations in the brain. SCA3 also belongs to a larger group of polyglutamine (polyQ) diseases caused by CAG expansions in different genes. Despite considerable advances in the last two decades in understanding the molecular pathogenesis of these diseases, central questions remain unresolved. In this introductory Chapter, I review the central features of polyQ disease, the role of knock-in mouse models in polyQ disease research, and the clinical and molecular features of SCA3. This overview seeks to put into context the dissertation work on SCA3 disease pathogenesis described in subsequent chapters.

1.1 Toward understanding the polyglutamine diseases

1.1.1 The polyglutamine disease genes and proteins

Abnormally expanded CAG nucleotide repeat expansions in coding regions of distinct genes are responsible for a group of neurodegenerative disorders known as the

polyglutamine (polyQ) diseases. The CAG expansion in the X-linked androgen receptor gene *AR* was first identified in 1991 as the cause of spinal and bulbar muscular atrophy (SBMA) (1). SBMA has since been joined by eight other polyQ diseases caused by CAG expansions in different genes. These diseases include Huntington disease (HD), the Spinocerebellar Ataxias (SCA) types 1, 2, 3, 6, 7, 17, and dentatorubralpallidoluysian atrophy (DRPLA). With the exception of SBMA, which is an X-linked disease, the polyQ diseases are autosomal dominantly inherited.

Despite sharing CAG repeat expansions, the polyQ disease genes and their encoded proteins are diverse. Table 1.1 lists the polyQ diseases and highlights some of these features. One point of diversity is the number of different exons/introns in polyQ disease genes, with the CAG repeat located in different exons. Consequently, the location of the polyQ tract in the different disease proteins differs greatly. For example, the polyQ tract resides close to the N-terminus of HTT in HD and close to the C-terminus in *ATXN3* in SCA3, while some polyQ tracts are found towards the center of their respective disease protein. Table 1.1 also shows the relative size of the polyQ proteins by primary amino acid length, with HTT being the largest (>300 kD) and *ATXN3* and TBP (disease protein in SCA17) the smallest (<50 kD), with other polyQ disease proteins being intermediate in length. The size range of polyQ expansions and threshold for disease-causing repeat length also varies. For example, while expansions greater than approximately 60 CAG repeats in *ATXN3* cause SCA3, repeat lengths as small as 20 in *CACNA1A* cause SCA6; the other diseases show threshold lengths in the mid to upper 30s. Finally, the functions of the polyQ disease proteins are diverse and distinct. While several polyQ proteins are associated with transcriptional function, they are rarely linked

to the same cellular pathways. The fact that distinct clinical disorders are caused by similar CAG expansions in different genes likely reflects one or more of these several points of diversity.

Nonetheless, the shared CAG expansion still leads to important common features among the different polyQ diseases. The polyQ diseases are generally late-onset disorders associated with selective dysfunction and degeneration of the nervous system, even though the polyQ disease proteins are expressed throughout the body. The affected regions of the CNS differ among the polyQ diseases, yet some brain regions like the cerebellum and brainstem are particularly vulnerable, as indicated by seven of the nine known polyQ disorders showing prominent brainstem and cerebellar degeneration (2, 3). All polyQ diseases are characterized by the misfolding, accumulation, and aggregation of the disease protein in the nervous system, which I will further discuss below. These shared features between polyQ diseases suggest common disease mechanisms. Thus, the study of a specific polyQ disorder could shed light on others. Conversely, studying individual polyQ diseases may help solve the puzzle of selective regional vulnerability among the polyQ diseases.

Protein misfolding and aggregation is not a unique feature of polyQ diseases. A number of other neurodegenerative diseases, including Alzheimer disease (AD), Parkinson Disease (PD), and amyotrophic lateral sclerosis (ALS) are characterized by the accumulation of different aggregated disease proteins in the nervous system (4). In most affected individuals, these diseases occur sporadically with no known genetic mutation or family history, though all of them can be caused by specific mutations in the respective disease proteins. While hundreds of thousands of individuals with polyQ disease may

benefit from an effective therapy, the polyQ diseases are rare compared to AD and PD. Nonetheless, the polyQ diseases serve as a simpler paradigm to study the relationship between protein misfolding, aggregation, and neurodegeneration. A better understanding of these relationships could provide insight on the neurodegenerative processes of more common diseases.

1.1.2 Disease protein misfolding and aggregation: central to pathogenesis?

Despite their monogenic inheritance pattern, polyQ diseases have a complex etiology involving widespread cellular effects, and disease pathogenesis can be influenced by various factors along the pathogenic cascade. Figure 1.1 depicts a simplified model of the path from expanded CAG repeat to neurodegeneration that includes disruption of several important cellular processes. This figure also highlights some of the pathogenic properties that may be exerted directly by mutant RNAs and proteins and lists several factors that can modify disease pathogenesis. At the DNA level, the length of the repeat and its stability within tissues are important factors that influence disease onset and severity. The transcribed RNA itself can potentially exert toxicity by sequestering RNA binding proteins, or the mutant disease transcript can be misspliced to produce more toxic isoforms. MicroRNAs can influence the stability or translation of the disease transcript. The misfolded and aggregated polyQ protein can misbehave in different ways to exert toxicity: it can engage in altered interactions with its normal binding partners, initiate new toxic interactions with other proteins, sequester important cellular factors, and alter/impair the native function of the disease protein. The toxic properties of a polyQ disease protein can be further influenced by other factors including the differing solubility of alternate disease protein isoforms, post-translational

modifications (e.g. proteolytic processing), and protein clearance pathways (e.g. chaperones and autophagy). The impaired clearance of the aggregated polyQ protein leads to its accumulation in the nervous system and in different cellular compartments, especially in the nucleus of neurons. Eventually, these proteotoxic processes lead to several possible downstream consequences, including disrupted transcriptional processes, organelle (e.g. mitochondria) dysfunction, ion channel/electrophysiological dysfunction, DNA damage with apoptotic pathway activation, altered protein quality control systems, among others. Ultimately, these processes lead to neuronal and non-neuronal dysfunction, disrupted neuro-circuitry, and neurodegeneration. While this chapter will not cover all the different aspects of polyQ disease introduced here, it will touch on certain important features that are relevant to the work presented later in the dissertation.

A key early event and potential central mediator of disease processes is disease protein aggregation. Pioneering studies examining polyQ disease brains immunostained for the mutant protein revealed large intraneuronal inclusions in various brain regions (5, 6). These inclusions co-immunostain for ubiquitin, molecular chaperones, and proteasome subunits, suggesting that cellular degradation machinery is engaged in the clearance of the disease protein (7, 8). The presence of inclusions of the disease protein in the nervous system is now recognized as a pathologic hallmark of polyQ diseases. Importantly, longer CAG repeat lengths in the disease gene are associated with earlier disease-onset, in some cases accelerated disease progression, and increased disease protein aggregation in the brain (9–11). In conjunction with the dominantly-inherited nature of all but one polyQ disease, these early findings led to the hypothesis that polyQ

expansions cause disease through toxic gain-of-function mechanisms exerted by disease protein misfolding and aggregation.

A large body of evidence establishes a strong association between polyQ disease aggregation and toxicity in numerous models of disease. Overexpression of the polyQ protein or polyQ-containing fragments recapitulate aggregate formation and toxicity in various systems, including cell culture, yeast, worms, fruit flies, and mice. Studies in these models established that altering protein quality control factors implicated in the proper folding or clearance of misfolded proteins, namely molecular chaperones and associated proteins, could affect aggregation and toxicity (12–21). This prior work includes previous studies in our lab showing that the loss of CHIP, a ubiquitin ligase that interacts with molecular chaperones, accelerates aggregation and lethality in a transgenic mouse model of SCA3 (16). Conversely, overexpression of specific chaperones or CHIP can reduce aggregation and disease-associated phenotypes (12, 18, 22).

Just as the length of the polyQ tract can alter disease protein solubility and toxicity, so too can the sequence of the disease protein outside the polyQ tract. For example, early studies established that fragments of polyQ disease proteins are highly aggregate-prone and toxic in cell culture and mouse models, suggesting a “toxic fragment hypothesis” (23–26). Caspase and calpain proteases are primary suspects in driving polyQ disease protein cleavage, including in SCA3 and HD (27–31). Recent studies have shown in mouse models of SCA3 that increasing or decreasing the levels of calpastatin, an endogenous inhibitor of calpain, respectively attenuates or accelerates ATXN3 aggregation and disease-associated phenotypes (32, 33). These findings underscore the importance of the protein sequence that harbors the polyQ tract (i.e. protein context) in

polyQ disease and provide additional correlative evidence between polyQ protein aggregation and disease pathogenesis.

Several studies, however, called into question the role of aggregation in disease pathogenesis and suggested instead benign or even protective roles for aggregates. This debate is reviewed by Todd and Lim (34). Initial observations of polyQ disease brain pathology showed that the presence of inclusions in disease brain did not correlate (directly or inversely) with the regions most affected in disease (35–37). A landmark study by Arrasate and colleagues used automated microscopy to longitudinally examine neurons overexpressing a polyQ-containing fragment of mutant HTT and found that neurons that formed large HTT inclusions survived longer than those that did not (38). Further mismatch between aggregation-pathology and behavior phenotypes in mouse models raised questions on the role of aggregation in disease. A mouse model of HD expressing a mutant HTT fragment exhibited widespread neuronal inclusions but no behavioral phenotype (39) and, conversely, a transgenic mouse model of SCA3 exhibits a motor phenotype in the absence of detectable aggregate pathology (40). While chaperones could rescue toxicity in different disease models as mentioned above, a study by Chafekar et al showed that activated Hsp70 solubilizes aggregated polyQ proteins and increased toxicity (41). Together, studies have raised understandable concerns that polyQ aggregation may not necessarily represent a pathogenic disease process.

The potential disconnect between polyQ disease protein aggregation and toxicity may stem from the different toxic properties associated with different polyQ aggregate species. It is now generally accepted that microscopically visible polyQ protein inclusions are unlikely to be directly neurotoxic, but increasing evidence suggests the

polyQ protein may still exert toxicity through misfolded monomeric or oligomeric species (11, 42, 43) (Figure 1.2). Nagai et al demonstrated that purified misfolded monomers of polyQ expanded protein in a β -sheet conformation can induce toxicity in cell culture (44). Automated longitudinal microscopy also revealed that the binding of an antibody that recognizes specific misfolded conformers of the polyQ monomer correlated with neuronal death (45, 46). Legleiter et al. have proposed that misfolded monomers and oligomers adopt multiple conformations and can access or initiate several gain-of-function interactions which may be toxic (11). In contrast, polyQ proteins sequestered into aggregates would not be able to exert these toxic properties.

While the toxicity of different conformers has been demonstrated *in vitro*, directly isolating and demonstrating the relative toxicity of different polyQ species *in vivo* remains challenging. To support the potentially differing roles of aggregate species *in vivo*, overexpressing p62 improved motor symptoms in a mouse model of SBMA with a concomitant increase in the number and size of AR inclusions in the spinal cord (47). These mice also showed decreased monomeric and oligomeric AR detected biochemically (47).

In summary, the extent to which aggregation propensity of the polyQ disease protein directly drives pathogenesis *in vivo* remains debated. While overexpressing chaperones, protease inhibitors, or other factors can reduce aggregation and toxicity, these broad-acting factors may exert beneficial effects indirectly. Work presented in this dissertation avoids this potential pitfall by demonstrating that expressing different mutant ATXN3 isoforms with the same polyQ tract length, but differing solubility, leads to

marked differences in aggregate formation *in vivo* and subsequent molecular events, particularly transcriptional changes.

1.1.3 Transcriptional dysregulation and gene expression profiling in polyQ disease

The mechanisms that drive polyQ toxicity remain the subject of investigation, but key observations support a critical role for nuclear localization of the disease protein.

Firstly, a central feature of all polyQ diseases is the nuclear concentration and aggregation of the disease protein in neurons. Secondly, SBMA preferentially affects males due to androgen dependent effects of the polyQ-expanded AR protein that requires nuclear residence, and this is supported by mouse models of SBMA. Only male mice carrying mutant AR develop motor behavior symptoms, which diminish with castration (48) or by removing nuclear localization signals from AR (49). Other studies have added nuclear localization/export signals to the mutant polyQ proteins in mouse models, including for HD(50), SCA1(51), and SCA3 (52), which preferentially show disease phenotypes when there is nuclear localization of the disease protein. These observations and the fact that transcriptional roles have been suggested for all polyQ proteins have led to the major hypothesis that transcriptional dysregulation contributes to disease pathogenesis (53)

PolyQ expansions can alter transcriptional activities of the disease protein through different means, as recently reviewed by Mohan et al (54). The polyQ expansion in HTT alters its interactions with or sequesters important transcription factors, including CREB-binding protein (55, 56), Sp1 (57), or REST/NRSF (58). PolyQ expansions can alter transcription factor activities of the disease protein, as seen with AR in SBMA (59). AR's ability to bind DNA is also required for mutant AR-induced toxicity in flies (60). The

polyQ expansion in ATXN1 alters its interaction with different transcriptional factors, including the transcriptional repressor Capicua, and this leads to both loss- and gain-of-function changes in target genes (61, 62). Direct alterations in transcription-associated functions of expanded polyQ have also been observed in SCA7 (63) and SCA17 (64, 65).

A useful way to assess transcriptional dysregulation is through gene profiling of affected human disease tissue and equivalent brain regions in mouse models of disease. Transcriptional profiling has been a powerful tool in identifying early molecular correlates to disease including dysregulated transcriptional pathways (66). Extensive transcriptional profiling in HD, as reviewed by Seredenina and Luthi-Carter (67), has revealed numerous perturbed biological pathways associated with mutant HTT expression: neurotransmitter signaling, calcium signaling and homeostasis, mitochondrial function, and others. Transcriptional profiling of SCA17 recently identified that the loss of an important age-related transcription factor, MANF, could accelerate disease (68). Transcriptional profiling in SCA1 and SCA7 revealed robust downregulation of *Igfbp5* to indicate possible converging pathways in SCAs (69). Profiling of DRPLA mouse models has shown CAG repeat length- and age-dependent transcriptional alterations in pathways associated with calcium-dependent signaling and neuropeptide signaling (70). Profiling of muscle tissue in mouse models of SBMA has indicated alterations in mitochondrial and metabolic pathways (71, 72).

In short, gene expression profiling has implicated possible transcriptional pathways in the pathophysiology of multiple polyQ diseases. Characterizing these disrupted transcriptional networks in polyQ disease could help move the field toward therapies by either identifying critical factors (e.g. transcription factors) that elicit

observed transcriptional changes or by identifying pharmacologically accessible downstream targets (e.g. ion channels) that exacerbate neuronal dysfunction. At a minimum, gene expression profiles provide a sensitive and early readout of disease-associated processes *in vivo* (73). Kuhn et al showed that expression profiles of seven different HD mouse models showed good concordance with profiles of human HD caudate (74), supporting the view that expression profiling of mouse models can provide insight into human disease pathogenesis. However, agreement between human disease tissue and animal model expression profiling cannot be assumed for all disease models, and confidence in the data set of any profiling experiment improves with validation of one or more predicted changes in human disease tissue.

To date, polyQ disease gene expression profiles largely have utilized microarray technology. The advent of next-generation sequencing technology, such as RNA-sequencing, has greatly increased the sensitivity of detecting altered transcripts, and performing RNA sequencing today is equally if not more cost-effective than performing microarrays. Moreover, continually improving bioinformatic analytical tools allow scientists to better characterize transcriptional networks and the processes that might drive their disruption. Work in this dissertation utilizes RNA-sequencing to comprehensively identify transcripts associated with mutant ATXN3 aggregation.

1.2 Knock-in mouse models of polyglutamine disease

The ability to address important questions about polyQ disease pathogenesis hinges on the availability of appropriate model systems. The range of model systems in polyQ disease research is vast, spanning from the *in vitro* characterization of purified disease protein (75) to the insertion of disease genes into non-human primates (76). Each

disease model has advantages and disadvantages and can provide complementary information on different aspects of disease. Work in this dissertation extensively uses knock-in mouse models of disease, which are particularly suited to study early molecular pathogenic events *in vivo* under pathophysiological expression conditions. This section reviews the major aspects of knock-in mouse models and their utility in studying polyQ disease pathogenesis.

1.2.1 Mouse models of polyQ disease and general features of knock-in mice

The study of polyQ disease *in vivo* extensively utilizes mice, which are valuable for several reasons: 1) they breed quickly, allowing faster assessment of disease features, 2) they are relatively easy to genetically manipulate compared to other vertebrate models, and 3) as mammals they exhibit good morphological and functional similarity to the human brain and its cellular components, including neurons, glia, other cell types, and functional circuitry. Modeling these diseases has been aided by the fact that transgenic overexpression of mutant polyQ proteins from human mutant cDNAs often elicits robust neuropathological and behavioral changes in mice, consistent with the dominant inheritance of disease in humans. Even the transgenic insertion of a full-length human disease gene through a bacterial or yeast artificial chromosome (BAC or YAC) can lead to robust expression of the disease protein. Of course, mice cannot recapitulate every feature of disease in humans, who have more complicated nervous systems and harbor CAG mutations for decades before exhibiting symptoms. An unsolved challenge in the polyQ field has been defining the best type of mouse model and the most critical features of mouse models that will best predict the success of therapeutic interventions in humans.

Nonetheless, mouse models of polyQ disease have been useful in exploring the properties and effects mutant polyQ proteins expressed in a mammalian nervous system.

Among the possible types of mouse models are knock-in mouse models of polyQ disease. Knock-in models take advantage of the presence of closely related orthologues to human disease genes in mice. Knock-in mouse models of polyQ disease, in which the endogenous CAG repeat within the gene of interest is expanded, represent a genetically precise *in vivo* approximation of human polyQ disease. In contrast to overexpression mouse models, knock-in mice express the mutant transcript and protein at physiological concentrations, which are regulated by endogenous murine regulatory factors and elements. Some polyQ knock-in mice exhibit key features of human disease, including neuropathological and behavioral abnormalities. By being genetically precise and within the animal genomic and protein contexts, knock-in mice allow scientists to identify the consequences, for a given mutant protein, of loss-of-function, disrupted native interactions, and novel interactions, and to identify cis- and trans-acting gene regulatory elements that control the mutant gene's expression.

Importantly, the physiological nature of knock-mice makes them well suited to investigate early molecular changes associated with expression of a disease gene in the brain. To date, several disease-modifying polyQ disease therapeutic trials have been performed in symptomatic subjects and so far have failed (77–79). Earlier presymptomatic interventions may be necessary for improved outcomes. Therefore, defining early molecular changes in disease using knock-in mouse models may be the key to identifying early presymptomatic biomarkers of disease processes en route to finding effective therapies.

Knock-in mouse models, however, present several caveats and challenges. The most evident drawback is that most knock-in mice do not exhibit robust behavioral abnormalities even at relatively advanced age. The exception is in knock-in mouse models expressing hyper-expanded repeats (that is, well beyond known human disease repeat lengths or so long as to cause an atypical infantile onset disease in humans). Hyperexpanded repeats may not be the most appropriate models of the common, adult-onset form of disease. In addition, subtle differences between mouse and human genes and proteins can pose a challenge for designing and testing therapeutic targets that are specific to the human disease gene or protein. The mouse and human proteins also may behave differently when an expanded polyQ tract is inserted. These considerations underscore the importance, when using mouse models to identify disease-related changes, of striving to validate critical findings in human disease tissue. One could argue knock-in mice provide the best prediction of early molecular changes, since they most closely mimic the genetic cause of the disease in humans. However, such a comparative analysis has not been systematically performed across the different polyQ disease mouse models and the respective diseases they model.

1.2.2 Lessons from knock-in mouse models of polyQ disease

The greatest number of available knock-in mice is for HD (Table 1.2) and, with the exception of DRPLA, all other polyQ diseases now have at least one knock-in mouse model available (Table 1.3). Table 1.3 includes two recently reported knock-in mouse models of SCA3, one of which was generated in our lab and is utilized throughout this dissertation. All published polyQ disease knock-in mice were generated through homologous recombination techniques to replace the endogenous murine CAG repeat

with a segment containing a long CAG repeat. Some knock-in mice were generated using a human exon with the expanded CAG tract to replace the mouse exon, resulting in a chimeric human/mouse exon. Other groups have simply expanded the endogenous CAG repeat in the mouse exon. All knock-in mouse models express the mutant polyQ protein and exhibit some degree of intraneuronal accumulation of the mutant protein, thus recapitulating a key early disease feature. Only a few knock-in mouse models with especially long CAG expansions exhibit behavioral phenotypes, and most do not show clear neurodegenerative changes.

The study of knock-in mouse models of polyQ disease has been instrumental to understanding different aspects of disease pathogenesis including behavior of the mutant gene, transcript and protein, and their effects on downstream processes. To highlight a few key findings: Several polyQ disease knock-in mouse models exhibit intergenerational and somatic instability of the CAG repeat (80–82), and reducing repeat instability in HD knock-in mice correlates with reduced aggregation in the brain (83, 84); knock-in mice of HD and SCA6 have helped characterize alternative splicing of their respective disease transcripts (85, 86); SCA1 knock-in mice have paved the understanding of how polyQ-driven alterations of native interactors, for example via a specific phosphorylation site, can affect disease pathogenesis (87, 88); Chua and colleagues recently altered SUMOylation sites in SBMA knock-in mice to demonstrate that functional recovery of expanded AR protein was associated with improved muscle function (72); a conditional knock-in mouse model of SCA17 helped identify critical age-associated factors and their contribution to disease (68); Finally, knock-in mice have been useful for pre-clinical testing of several novel therapies (89–92).

In general, knock-in mouse models have proved to be a valuable tool, but the concurrent use of other disease models is important to identify converging affected pathways or to confirm hypotheses. These additional models include transgenic mice that overexpress the human disease protein. Transgenic mice expressing the full-length disease gene containing all introns and exons can be especially useful for investigating disease gene splicing *in vivo*. The work in this dissertation uses multiple SCA3 mouse models and human tissues samples to strive for findings that have a high probability of occurrence in human disease. Ultimately, there is no perfect model of disease until we clearly identify predictive markers or interventions that translate directly from model to disease. Until then, a combinatorial and interdisciplinary approach with models for disease is most likely to bring us closer to therapies.

1.3 Toward understanding spinocerebellar ataxia type 3

The studies described here on SCA3 are motivated by several factors. Although SCA3 is among the most prevalent of the polyQ diseases, no SCA3 knock-in mouse model was published at the time my dissertation work began. The size of the SCA3 disease gene, transcript, and protein are all fairly small, which allows straightforward visualization and manipulation of these elements *in vivo*. The function of the ATXN3 protein is also well characterized, which facilitates investigation of both loss-of-function and gain-of-function contributions to disease. Together, these factors helped ensure my capacity to make important contributions toward understanding SCA3 pathogenesis. An improved understanding of SCA3 could benefit the substantial number of individuals affected by SCA3, as well as other polyQ diseases. The remainder of this introduction highlights some of the major clinical and pathogenic features of SCA3 and how this

dissertation aims to address critical questions on polyQ disease pathogenesis using SCA3 knock-in mice.

1.3.1 Clinical and pathological features of SCA3

Several reports in the 1970s described an ataxic disorder in different families of Portuguese ancestry, particularly those of Azorean descent (93–96). The mysterious disease at the time went by different names such as nigro-spino-dentatal degeneration, striatonigral degeneration, or Azorean disease. The study of two different families with this ataxic disorder who were respective descendants of William Machado and Antone Joseph led to the name Machado-Joseph disease (97). Geneticists in Europe in the 1990s had also designated what seemed to be a distinct hereditary ataxia as SCA3. The identification of the causative mutation in 1994 unified Machado-Joseph disease and SCA3 as one disorder that is now believed to be the most common dominantly inherited ataxia in the world (98, 99).

Along with ataxia, SCA3 is clinically characterized by a constellation of signs and symptoms that can vary greatly among affected persons. These symptoms include speech difficulty, rigidity, spasticity, proptosis, ophthalmoplegia, eye movement and vision difficulties (100). Some affected individuals exhibit prominent Parkinsonism. SCA3 can be phenotypically classified into four subtypes, which are not clinically very helpful but demonstrate the heterogeneous presentation of disease (101). Increasing studies also recognize cognitive symptoms associated with SCA3 (102–104).

Post-mortem analysis in SCA3 brain has shown prominent degeneration of the deep cerebellar nuclei, as well as various associated nuclei of the brainstem and spinal cord (2, 105). The pons is especially affected as signified by some of SCA3's alternative

names: *olivopontocerebellar* degeneration and *spinopontine* atrophy. As such, work in this dissertation frequently examines molecular alterations in the pons. As described above, these brain regions exhibit large intraneuronal ATXN3 inclusions. Furthermore, large axonal ATXN3 inclusions can also be found along different fiber tracts, particularly in the brainstem (106). Degeneration is not prominent in the SCA3 cortex and hippocampus, but aggregate pathology in these regions has not yet been systematically assessed.

1.3.2 The *ATXN3* gene, splice isoforms, and aggregation

The genetic structure of the ~48 kb *ATXN3* gene and the location of the CAG repeat in the 10th exon are shown in figure 1.3. Also shown are the spliced full-length *ATXN3* transcript, containing all 11 coding exons, and a schematic of the encoded protein. When the disease gene was initially cloned by Kawaguchi and colleagues, the cDNA and gene were reported to contain only 10 exons (98). Three years later another group identified the 11th coding exon (107). Bettencourt et al reported up to 50 different *ATXN3* splice isoforms in patient blood samples though how many of these are expressed in specific tissues is unknown (108). The splice isoform encoded by full-length transcript with 11 exons (*ATXN3*-11e) appears to be most abundantly expressed (109), but the relative abundance of different *ATXN3* isoforms has not yet been clearly established. A fair portion of published work on SCA3 studies the first identified 10 exon (*ATXN3*-10e) isoform, including studies using SCA3 mouse models that overexpress this minor isoform (110).

Different *ATXN3* isoforms exhibit differences in solubility and their expression may influence disease pathogenesis. The *ATXN3*-10e transcript does not splice to exon 11

and instead retains intron 10, which encodes a more hydrophobic stretch at the C-terminus. Our lab previously determined that the ATXN3-10e isoform is more aggregation-prone in cell culture (109). However, the extent to which the expression of different ATXN3 isoforms can drive differences in aggregation and pathogenesis *in vivo* has not been explored. A significant part of this dissertation aims to show that the expression of a mouse ATXN3-10e isoform markedly accelerates ATXN3 aggregation *in vivo*.

1.3.3 ATXN3 as a deubiquitinating enzyme

The full-length ATXN3 protein is a small deubiquitinase (~42 kD, ~355 amino acids) with an evolutionarily conserved, globular catalytic domain at the N-terminus (so called Josephin domain), and an unstructured, flexible C-terminus (Figure 1.3). The Josephin domain contains two ubiquitin binding sites and a catalytic cysteine at the 14th residue (not depicted). The unstructured C-terminus stretch of the full-length isoform contains three ubiquitin interacting motifs (UIMs) as depicted in figure 1.3.

ATXN3 localizes diffusely throughout the cell, found in both the cytoplasm and nucleus, where it functions in protein surveillance pathways. Using its multiple UIMs and enzyme activity, ATXN3 binds and trims polyubiquitinated chains conjugated to proteins, particularly Ub chains containing four or more ubiquitin (111, 112). As a result of ATXN3's broad substrate activity, ATXN3 knockout mouse brains exhibit elevated total levels of polyubiquitinated proteins (113, 114). Of note, the third UIM is encoded by exon 11 and is therefore missing in the ATXN3-10e isoform. this does not, however, lead to obvious differences in the ubiquitin binding or deubiquitinating activity of ATXN3 (109).

The deubiquitinating role of ATXN3 has raised the intriguing possibility that its enzymatic activity may influence its own aggregation and disease pathogenesis. In support of this concept, a fly model of SCA3 showed that overexpressing wild-type ATXN3 protects against eye degeneration, and that this protection required ATXN3's deubiquitinating activity (115). However, a protective effect of ATXN3 was not confirmed in mammalian models overexpressing wild-type ATXN3 (116, 117). Work in our lab by Dr. Li Zeng also found that knocking out endogenous ATXN3 did not alter disease progression in a knock-in mouse model of HD (118). ATXN3 does not seem to be an essential protein since ATXN3 knockout mice are healthy (113), suggesting that the toxicity of mutant ATXN3 predominantly arises from gain-of-function mechanisms. This does not, however, exclude the possibility that ATXN3's function and polyQ-dependent dysfunction may influence disease pathogenesis and selective regional vulnerability.

1.3.4 ATXN3 function and dysfunction in the nucleus

ATXN3 plays an active role in the nucleus and mutant ATXN3 dysfunction in the nucleus may contribute to disease pathogenesis. ATXN3 can freely shuttle between the cytoplasm and nucleus (119) and concentrates in the nucleus with heat or oxidative stress (120). ATXN3 has been reported to act as a transcriptional co-repressor (121), and ATXN3 can work in concert with HDAC3 and NCor to repress transcription (122). Mutant ATXN3 is not as effective at this repression (122), which may lead to dysregulation of various target genes. ATXN3 also interacts with the transcription factor FOXO4 to upregulate superoxide dismutase 2 (SOD2), a protein that helps break down oxygen radicals (123). Mutant ATXN3 expression reduces SOD2 transcription, possibly increasing cellular vulnerability to oxidative stress (123). While ATXN3 has clear effects

on the transcription, the extent to which ATXN3 acts as a traditional transcription cofactor rather than as a deubiquitinase that regulates other transcription factors is unclear.

Emerging evidence on the role of ATXN3 in DNA damage repair supports a role for impaired DNA repair in SCA3 pathogenesis (124). ATXN3 is well-known to interact with DNA repair-associated proteins, including RAD23A (125–127). Recently, mutant ATXN3 was shown to interact with and inhibit mammalian polynucleotide kinase 3'-phosphatase (PNKP), an enzyme involved in DNA repair, leading to increased DNA damage and activated apoptotic pathways, which may drive cell death in disease (128, 129). The authors further showed that induction of apoptotic pathways by mutant ATXN3 is mediated by the protein ataxia telangiectasia mutated (ATM) (129), an important DNA damage checkpoint component of the cell cycle that is mutated in a childhood onset form of ataxia. ATM mediates toxicity in models of HD, and its reduction can reduce mutant HTT-induced toxicity (130). As other studies converge on DNA damage in polyQ diseases (131–133), disrupted nuclear processes continue to be a dominant theme in polyQ disease pathogenesis.

1.4 Summary and aims of the dissertation

SCA3, caused by a CAG repeat expansion in the *ATXN3* gene, is likely the most common of the polyQ diseases with many unresolved questions regarding disease pathogenesis. Like other polyQ diseases, SCA3 appears to be predominantly mediated by toxic gain-of-function mechanisms, and emerging evidence implicates important roles of ATXN3 dysfunction in disease pathogenesis, particularly in the nucleus. However, the extent to which mutant polyQ protein aggregation contributes to disease pathogenesis is

still debated. To address this further, I sought to identify factors that modify mutant ATXN3 aggregation in a physiologically-relevant disease model.

Current understanding of SCA3 pathogenesis benefits from various disease models that include worms, fruit flies, cell cultures, mice, and rats. With the exception of patient fibroblasts and iPSC-derived neurons, prior models of SCA3 have overexpressed mutant disease protein and few had explored molecular pathogenesis of SCA3 under physiological expression conditions. This prompted me to approach the disease in a new way by using a knock-in mouse model. The generation of a knock-in model was started by Dr. Ginny Harris in the Paulson lab during her dissertation and completed by me.

By approaching SCA3 using a novel and previously uncharacterized knock-in mouse model of disease, this dissertation addresses three main aims. The first aim is to demonstrate features of the SCA3 knock-in mouse model and its suitability for modeling disease, particularly with respect to disease protein aggregation and splicing of the disease transcript. Characterization of these mice led to the serendipitous identification of two separate lines of SCA3 knock-in mice that differentially express mutant *Atn3* splice isoforms, leading me to the second aim: determine the extent to which alternative splicing of *Atn3* contributes to ATXN3 aggregation. The third and final aim takes advantage of differences in aggregation in nearly identical SCA3 knock-in mice to address the extent to which mutant ATXN3 aggregation contributes to pathogenesis, assessed through transcriptional profiling of these knock-in and other SCA3 mouse models.



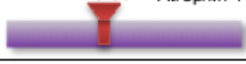






PolyQ Disease	Exon w/ CAG-repeat	Total exons	Disease protein with pathogenic polyQ repeat range	General function
Huntington's Disease (HD)	1	67	36-121 Huntingin (HTT) 	Scaffolding protein, diverse functions in development, nervous system health
Spinal-Bulbar Muscular Atrophy (SBMA)	1	8	38-62 Androgen receptor (AR) 	Androgen-activated steroid receptor
Dentatorubral-pallidoluysian atrophy (DRPLA)	5	10	49-88 Atrophin-1 (ATN1) 	Transcriptional cofactor
Spinocerebellar Ataxia Type 1 (SCA1)	8	9	39-83 Ataxin-1 (ATXN1) 	Transcriptional co-repressor
SCA2	1	25	32-200 Ataxin-2 (ATXN2) 	Endoplasmic reticulum function and RNA processing
SCA3	10	11	60-87 Ataxin-3 (ATXN3) 	Deubiquitinating enzyme
SCA6	47	47 or 48	α 1A subunit of the voltage-gated calcium channel (CACNA1A) 21-33 	Voltage-gated calcium channel subunit
SCA7	3	13	37-306 Ataxin-7 (ATXN7) 	Transcriptional co-activator
SCA17	3	8	45-63 TATA-binding protein (TBP) 	Core transcriptional factor

Table 1.1: The diversity of polyglutamine (polyQ) disease genes, proteins, and function. Provided are the list of diseases, the exon in which the CAG repeat is expanded in disease, and the total number of exons in the gene. The diagrams show the relative size of the disease protein with the relative location of the polyQ expansion and includes the range of polyQ expansions known to cause disease. A general description of the protein's known function is also given.

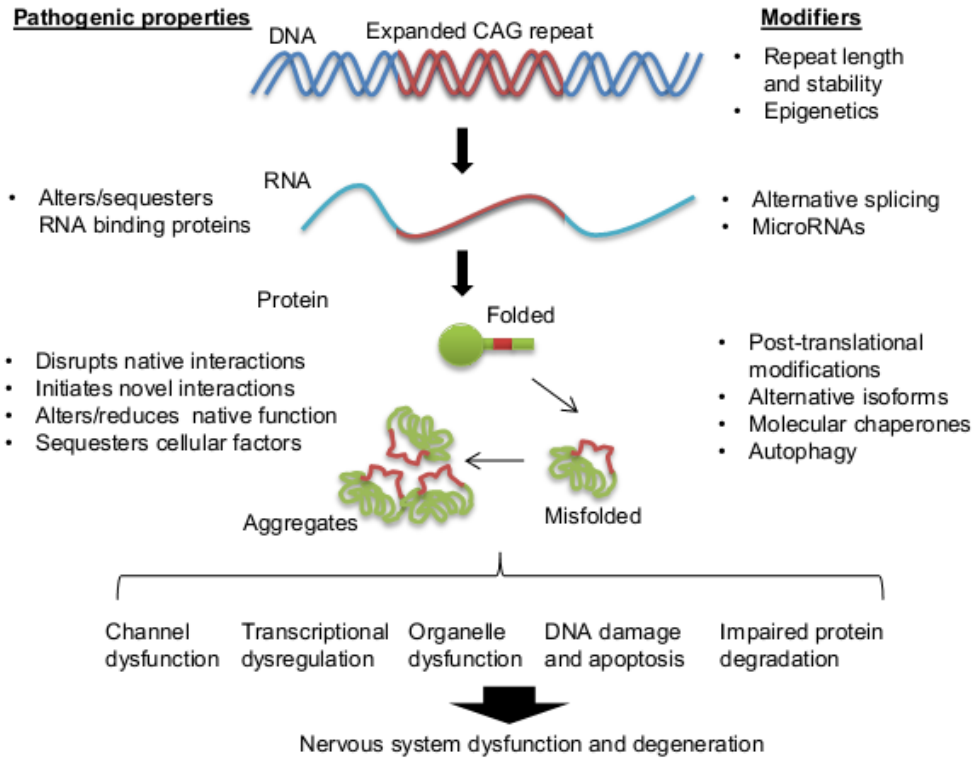


Figure 1.1: Pathogenic factors from CAG expansion to disease. This simplified diagram shows the CAG repeat expansion leading to mutant RNA expression, mutant protein expression, and aggregation. Left, a list of properties directly exhibited by disease transcript and disease protein (and its aggregation) that may drive toxicity. Right, a list of factors at the level of the disease gene, transcript, and protein that can further influence pathogenesis. The misfolding and aggregation of disease protein may critically drive several downstream events listed below that lead to neurodegeneration.

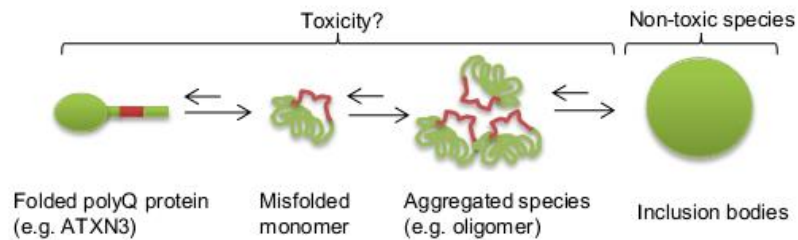


Figure 1.2: Basic model of polyQ disease protein aggregation. This diagram shows that the polyQ expanded protein has a tendency to misfold and aggregate, ultimately leading to the formation of microscopically visible puncta and inclusions in cells that are not directly toxic. Although a proteotoxic species in polyQ disease has not been clearly defined, increasing evidences suggests that monomeric and oligomeric states of disease protein may drive toxicity. Other intermediate species not depicted include amorphous aggregates, protofibrils, and fibrils.

HD knock-in mouse	Neuropathological findings	Behavioral changes	Refs
Q50 (<i>HD/Hdh</i> exon 1)	No known abnormalities	No known abnormalities	(134)
Q71 (<i>HD/Hdh</i> exon 1)	No known abnormalities	No known abnormalities	(135)
Q72-80	Increased nuclear localization neuronal intranuclear inclusions (NIIs), neuropil aggregates, axonal degeneration at >2 years	Aggression (~3 months), motor deficits at 4 months	(136)
Q77 (<i>HD</i> exon 1)	Nuclear localization, NIIs, and neuropil aggregates	Increased aggression >1 year	(81, 137)
Q80	Rare nuclear inclusions (up to 22 months)	Mild gait deficit at 10 months	(138)
Q94 (<i>HD/Hdh</i> exon 1)	Increased nuclear localization and NIIs	Altered activity and motor deficits at ~2 years	(135, 139)
Q92 (<i>HD/Hdh</i> exon 1)	Nuclear localization and NIIs in neurons	Mild motor and memory deficits in homozygous mice >14 months	(82, 140, 141)
Q111 (<i>HD/Hdh</i> exon 1)	Nuclear localization and NIIs, gliosis, neuropil aggregates at 2 years	Anxious/depressive-like behavior at 4 months, memory deficits at 8 months, mild motor deficits at ~2 years,	(82, 140)
Q140-175 (<i>HD/Hdh</i> exon 1)	Nuclear localization and NIIs, neuropil aggregates. Reduced DARPP-32 in striatum, brain atrophy and neuronal loss	Altered activity and motor deficits at ~1 year	(142, 143)
Q140 (N-term Flag tag)	Nuclear localization and NIIs (6 months)	Not reported	(144)
Q150-250	Q150-200: Nuclear localization and NIIs, neuropil aggregates, axonal degeneration, reduced neurotransmitter receptor binding, autophagic changes, gliosis in striatum Q250+: Reduced DARPP-32 in striatum, myelination defects	Q150: Hindlimb dragging, claspings, and activity 4 months, motor deficits 100 weeks, weight loss in homozygotes ~1.5 years Q200: Weight loss ~5 months, reduced grip strength ~1.5 years, motor deficits ~1 year Q250: Motor deficits ~6 months	(138, 145–148)

Table 1.2: Knock-in mouse models of HD

Disease	Knock-in mouse	Neuropathological findings	Behavioral changes	Refs
SBMA	Q113 (AR/Ar ex 1)	Neuronal intranuclear inclusions (NIIs) in spinal cord and skeletal muscle; neuromuscular pathology	Decreased fertility, androgen-dependent early death, progressive motor deficits	(48)
SCA1	Q78	Not reported	Mild motor incoordination in homozygous mice	(80)
	Q154	Early nuclear accumulation and NIIs; synaptic deficits, Purkinje neuron atrophy and loss	Weight loss, robust motor behavior and learning deficits	(149)
SCA2	Q42	NIIs in Purkinje neurons	Motor deficits in homozygous mice (>18 months)	(150)
SCA3	Q82	Robust nuclear accumulation and NIIs; dystrophic neurites in hippocampus	No detectable motor phenotype in heterozygous mice (1 year)	(151)
	Q91 (ATXN3 ex 11)	Nuclear accumulation, NIIs	Mild motor behavior deficit in aged (>1 year) mice	(152)
SCA6	Q84	Mutant Cav2.1 aggregates in Purkinje neurons	Progressive motor deficits	(85)
SCA7	Q266+	Neuronal accumulation and NIIs	Weight loss, visual and motor deficits, early death, robust motor behavior deficit	(153)
SCA17	Q105	Nuclear accumulation and NIIs, Purkinje neuron atrophy and loss	Weight loss, moderate motor behavior deficits, Purkinje neuron loss	(154)
DRPLA	N/A	N/A	N/A	

Table 1.3: Knock-in mouse models of polyQ disease excluding HD

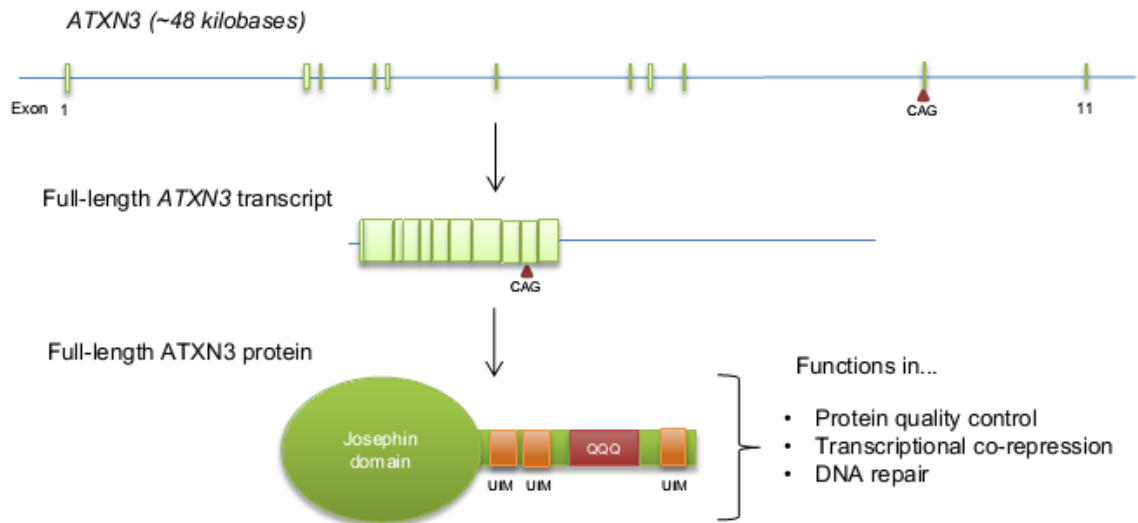


Figure 1.3: SCA3 mutant gene, transcript, and protein. The *ATXN3* gene is ~48 kb with 11 coding exons with large introns (shown to scale), with the CAG repeat in the 10th exon. The *ATXN3* protein is ~42 kD consisting of a globular Joseph domain and an unstructured C-terminal stretch containing the polyQ stretch (red) and three ubiquitin interacting motifs (UIM, orange). *ATXN3* primarily functions as a deubiquitinating enzyme, but plays diverse roles in cellular pathways. The sizes of the *ATXN3* gene, transcript, and protein are not drawn in scale relative to each other.

Chapter 2

Materials and methods

This chapter provides information on the materials and methods used in both Chapters 3 and 4. The majority of the protocols given here are used in the work of both Chapters with few minor differences. Most of the information in this chapter has been published in Ramani et al (151).

2.1 Generation of SCA3 knock-in mice

The protocol described in this section was performed by Dr. Ginny Harris as part of her dissertation. A more comprehensive protocol is provided in her thesis (155). For the reader's convenience, I have provided the protocol from our published report of the SCA3 knock-in mouse (151). The generation of these mice was aided by collaboration with Dr. Thomas Saunders and the Transgenic Animal Model Core (<http://www.med.umich.edu/tamc/>).

Genomic murine *Atn3* DNA from a C57BL/6-tyr(c-2J) albino embryonic stem (ES) cell line (Millipore, Cat SCR011) was used to amplify a 4 kb upstream flanking arm derived from intron 9-10 and a 2.6 kb downstream flanking arm that spans exon 10. NotI and SalI restriction sites were engineered to flank the upstream flanking arm and a novel KpnI restriction site was engineered onto the 5' end of the downstream flanking arm. The 5' flanking arm was then subcloned into pBY49a upstream of a FRT-PGK-Neo-FRT positive selection cassette. The 3' flanking arm was subcloned into pBluescript SK(-) and

the CAG repeat was expanded using a modified QuickChange approach (156). Briefly, a human expanded CAG template (At3-Q129-GFP and At3-Q166-GFP) was amplified with partially complementary primers to generate an expanded (CAG)_n “megaprimer” flanked by murine genomic sequence. This double-stranded megaprimer was used to insert an expanded (CAG)_n repeat into the *Atn3* gene using the QuickChange Mutagenesis method (Stratagene). One clone generated was chosen for additional repeat expansion through splicing by overlap extension (157). We inserted the 3' flanking arm from one clone of the megaprimer expansion series, which contained a Q3KQ82-encoding expansion, into the targeting vector between the FRT-PGK-Neo-FRT positive selection cassette and the PGK-TK negative selection cassette, using KpnI and EcoRI restriction sites.

The complete targeting vector was purified with NdeI and electroporated into Bruce4.G9 ES cells (158). G418 and ganciclovir selection were used to enrich for ES cell colonies with the positive selection cassette and loss of the negative selection cassette. Each colony was screened for homologous recombination and CAG repeat expansion by PCR- and Southern blot-based strategies. ES cell clones containing the expansion and confirmed to be sufficiently euploid were microinjected into homozygous albino B6(Cg)-Tyr^{c-2J}/J blastocysts. Microinjected blastocysts were introduced then into the uterine horns of pseudopregnant female mice. Chimeras were crossed to albino B6(Cg)-Tyr^{c-2J}/J mice, and all black pups were assayed for germline transmission of the knock-in allele by PCR.

For *in vivo* excision of the FRT-site flanked positive selection cassette, F1 heterozygous knock-in animals were crossed with homozygous FLP recombinase

transgenic mice driving FLPe expression under the human β -actin promoter (Jackson Laboratories, strain B6.Cg-g(ACTFLPe)9205Dym/J). F2 mice positive for the Q82 knock-in expansion were crossed with C57BL/6 mice (Jackson Laboratories) to remove the FLPe transgene and outbred for at least four generations. Homozygous Q82/Q82 mice were generated and sequenced across the FRT site to ensure removal of the neomycin cassette and identify the remaining sequences in intron 9 (Figure 2.1)

2.2 Animals and ethical use

YAC-84Q and YAC-15Q mice (159) and ATXN3 knockout mice (120) are described previously. Mice used here are available from Jackson Laboratories including YAC-84Q mice (B6;CBA-Tg(ATXN3*)84.2Cce/IbezJ), Q82/Q6 mice (B6(Cg)-Atxn3tm1Hlp/J), and Nestin-Cre mice (B6.Cg-Tg(Nes-cre)1Kln/J). The Nestin-Cre mice were kindly provided by Corinne Weisheit of Dr. William Dauer's lab (University of Michigan). All mice are maintained by veterinarians and animal care staff from the University of Michigan Unit for Laboratory Animal Medicine (ULAM). All manipulations and handling were performed in accordance with guidelines of the University of Michigan Committee on Use and Care of Animals.

2.3 Genotyping and CAG repeat sizing

DNA was extracted from clipped mouse tails using a DNeasy Tissue kit (Qiagen) and used for genotyping by PCR. Primers flanked the endogenous CAG repeat of exon 10 of *Atxn3* (see section 2.8 for primers). The PCR conditions are as follows: 95 deg C/2 min, 30 cycles of 95 deg/30s, 51degC/30s, 72degC/1m, 1 cycle 72degC/10min. Products were run on a 1.5% agarose gel and visualized with ethidium bromide. Purified tail DNA was submitted for CAG repeat sizing to Laragen, Inc. (Culver City, CA, USA).

2.4 Tissue lysate preparation, SDS-PAGE, SDS-agarose, and western blot analyses

Tissue lysates were prepared as previously described (16) with minor modifications. Briefly, frozen tissue was homogenized in 10 vol RIPA + protease inhibitor (PI) cocktail containing RIPA buffer (50 mM Tris-HCl pH 7.4, 150 mM sodium chloride, 0.1% SDS, 0.5% sodium deoxycholate, 1% NP-40) and protease inhibitors (Complete Mini tablets, Roche). Homogenates were centrifuged at 1500g for 15 min at 4 deg C, and supernatants (soluble fraction) was transferred to a new tube and assayed for protein concentration using bicinchoninic acid (Pierce). The soluble fractions were diluted to a final concentration of 4 µg/µl in RIPA + PI + loading buffer (from 6X concentration of 0.35 M Tris-HCl, 10.3% SDS, 36% glycerol, 0.6 M dithiothreitol, and 12% bromophenol blue), and boiled for 5 min. Samples were separated by 10%, 3% SDS-PAGE, or 2% SDS-Agarose (with 0.1% SDS), transferred onto polyvinylidene fluoride membrane (PVDF), and blotted as previously described (16). The 3% gel was transferred onto PVDF using the BioRad TransBlot SD semi-dry apparatus on 10V for 30 min.

For an alternative method for detecting high molecular weight ATXN3 aggregates (Chapter 4 only), a mouse brain hemisphere was homogenized in 1 ml RIPA + PI, sonicated briefly, and centrifuged at 12,000g for 20 min. The supernatant was saved and assayed for protein concentration. 1 mg of protein was then incubated overnight in 1 µl of 1H9 antibody + 20 µl protein A beads (Life Technologies). The protein A beads were then pelleted, washed, eluted by boiling 5 min in 2x loading buffer, resolved on a 3-12% Tris-acetate gel, transferred to PVDF, and blotted with anti-MJD.

For work in Chapter 4, human disease brainstem tissues from three Alzheimer's disease and three SCA3 cases were kindly provided by the University of Michigan Health System Brain Bank. Roughly 0.5 cm³ of brain stem tissue was used for western blot analysis using the protocol described above.

Antibodies: 1H9 1:2000 (MAB5360, Millipore), anti-MJD 1:10,000 (160), β -tubulin 1:5000 (Cell signaling), ACY3 1:2000 (Proteintech).

2.5 Immunohistochemistry, immunofluorescence, and scoring ATXN3 accumulation

Mice were transcardially perfused with chilled PBS and the brains removed. One hemisphere was fixed in 4% paraformaldehyde at 4 deg C for 48 hours and the other hemisphere was frozen on dry ice and stored in -80° C for biochemical experiments. Fixed brains were transferred to 30% sucrose in 0.1M phosphate buffer for at least 48 hours at 4 deg C. Brains were then serially sectioned and stained as previously described (16). Immunofluorescent images were taken by Zeiss LSM 510-META Laser Scanning Confocal Microscope at the University of Michigan Microscopy & Image Analysis Core.

Antibodies include anti-ataxin 3 clone 1H9 1:1000, anti-MJD 1:5000, anti-RTN3 R458 1:2000 (kindly provided by Riqiang Yan, Cleveland Clinic, Cleveland, OH, USA), anti-MAP2 1:2000 (M4403, Sigma), SMI32 1:2000 (NE1023, Calbiochem).

Three heterozygous SCA3 knock-in brains immunohistochemically stained for ATXN3 were systematically scored for diffuse nuclear staining, intranuclear inclusions, and extranuclear inclusions. Staining patterns indistinguishable from wild-type mice were scored as -. The presence of diffuse nuclear staining was represented by + or ++. Frequency of solitary intranuclear inclusions or extranuclear inclusions were scored by +,

++, or +++. Intranuclear versus extranuclear inclusions were further confirmed by co-immunofluorescent staining with nuclear DAPI. Examples of scoring diffuse nuclear staining and intranuclear inclusions are shown in Figure 3.6 (Chapter 3).

2.6 Motor behavior testing and fear conditioning

The examiner was blinded to the genotype in all behavioral experiments. Motor function was assessed on SCA3 knock-in mice using tests as previously reported (145), including performances on accelerating rotarod, balance beam, and locomotor activity in an open field chamber for 30 min. In chapter 3, I tested Q82/Q6 and wild-type mice ranging from 47 to 57 weeks of age. Motor performance on day 4 and open field activity were analyzed using a Student *t*-test with a Bonferroni post-hoc correction for three comparisons. In chapter 4, I tested wild-type, Q82/Q6, and Q82V/Q6 mice ranging from 53 to 61 weeks of age. I analyzed four day accelerating rotarod data by a two-way ANOVA, and I analyzed day 4 balance beam performance and open field locomotor activity by a one-way ANOVA with a Newman-Keuls multiple comparisons test.

In chapter 3, fear conditioning was performed on Q82/Q6 mice and wild-type littermates ranging from 52 to 60 weeks of age using the protocol previously described for single-day experiments (161). These experiments were performed in collaboration with Dr. Geoffrey Murphy (University of Michigan) These mice were then sacrificed and examined for aggregates in the hippocampus and amygdala.

2.7 RNA extraction, RNA sequencing, quantitative PCR, and 3' RACE

RNA was extracted from pons or half of the hindbrain of mice using TRIzol ® (Life Technologies) and further purified using the RNeasy kit with on-column DNase I digestion (Qiagen). Purified RNA was submitted to the University of Michigan

Bioinformatics Core for library generation and Illumina HiSeq RNA-sequencing. The RNA-seq data reported in chapter 3 utilized a NuGen library with 50x50bp sequencing, while chapter 4 used a TruSeq library with 100x100bp sequencing. Each sample was sequenced on at least one lane. The sequencing reads for each mouse were aligned using TopHat and the output was sorted and indexed using SAMtools to generate a BAM file. We visualized *Atxn3* transcript reads in each BAM file using Integrative Genomics Viewer (162, 163). Fragments per kilobase of exon per million fragments mapped (FPKM) reported for the full-length *Atxn3* transcript (accession NM_029705) were created by CuffLinks. We used a locally developed R script, in conjunction with CummeRbund, to output a table of all expression values (raw, externally normalized, and FPKM).

Chapter 4 presents altered transcripts from RNA-seq in a heat map format. To generate the heat map, the calculated Cuffdiff values were normalized to wild-type to determine relative fold-change for differentially expressed (DE) transcripts. Differentially expressed (DE) transcripts were identified through DEseq (DESeq.padj 0.1 cutoff, fold-change 0.8 – 1.2). For the ~150 DE transcripts of YAC-84Q mice, fold-change values relative to wild-type were generated for different genotypes and inputted into MultiExperiment Viewer to generate a heat map (<http://www.tm4.org/mev.html>).

Gene enrichment analysis was done through ToppGene (164). Cell-type expression was determined from publically-available RNA-seq data on mouse cerebral cortex (http://web.stanford.edu/group/barres_lab/brain_rnaseq.html) (165).

For quantitative RT-PCR (qRT-PCR), 1 µg of RNA was reverse-transcribed using iScript™. 0.5 µl was used with the SYBR® Green Master Mix and each reaction was

performed in duplicate. qRT-PCR was performed on the BioRad iCycler with MyIQ single color real-time PCR detection system module with the following parameters: 95°C at 3min, (95°C 10 sec, 55°C 30sec) x 40, 95°C 1 min, 55°C 1 min. The fold-change in transcript levels was calculated using the $\Delta\Delta C_t$ method (166). *Gapdh* and *ACTB* were used as controls for SCA3 knock-in mice and patient fibroblasts, respectively. For examining relative levels of *ATXN3* transcripts in SCA3 YAC mice, human *TRIP11* was used, since the YAC-15Q and YAC-84Q mice contain different copy numbers of the same integrated YAC construct, which also expresses the *TRIP11* gene. 3'RACE was performed on 2 μ g of RNA from an Q82/Q6 mouse hindbrain per the manufacturer's instructions (Life Technologies). 3' RACE products were run on an agarose gel and the 300 bp band of interest was extracted, TA-cloned (Life Technologies), and sequenced. The primers used for RT-PCR and 3'RACE are listed below.

In chapter 3, DNase I-treated RNA samples from six SCA3 fibroblast lines and one non-disease control fibroblast line were kindly provided by Dr. Guangbin Xia and Dr. Tetsuo Ashizawa (University of Florida, Gainesville, FL, USA). RNA was also isolated from three additional non-disease fibroblast lines that were graciously provided by Crystal Pacut and Dr. Eva Feldman (University of Michigan, Ann Arbor, MI, USA).

2.8 Primers

Amplicon	Forward primer (5' to 3')	Reverse primer (5' to 3')	Exp.
Atxn3 intron 9 – exon 10	TTCACGTTTGAATGTTTCAGG	ATATGAAAGGGGTCCAGGTCG	Genotype
<i>Atxn3</i> exon 10 - intron 10	GGACGTAGGAGCGACCAAG	CGAGGATCTTGGGTATCGAGT	qRT-PCR
<i>Atxn3</i> exon 10	TAGACCGACCTGGACCCCTT	CTTGGTCGCTCCTACGTCC	qRT-PCR
<i>ATXN3</i> exon 10- intron 10	GAGCACTGGGAGTGATCTAG	ATCACATGGAGCTCGTATGTC AG	qRT-PCR
<i>ATXN3</i> exon 10	GACCTATCAGGACAGAGTTCAC	CTAGATCACTCCCAAGTGCTC C	qRT-PCR
<i>Atxn3</i> exon 10-	GAGCACTGGGAGTGATCTAG	ATCACATGGAGCTCGTATGTC	qRT-PCR

exon 11		AG	
<i>Atxn3</i> exon 1 – intron 10	GACAAATAAACATGGAGTCCATCT TC	CGAGGATCTTGGGTATCGAGT	PCR
<i>ATXN3</i> exon 1 – intron 10	GACAAATAAACATGGAGTCCATCT TC	ATCACATGGAGCTCGTATGTC AG	PCR
<i>Atxn3</i> exon 1 – exon 11	GACAAATAAACATGGAGTCCATCT TC	CAAAGTGTGTGAGTAGCAAAA TGACT	PCR
<i>Atxn3</i> intron 10	TACTCGATACCCAAGATCCTCGTC	Provided by 3' RACE kit (Invitrogen)	3'RACE
<i>Gapdh</i>	CTTTGTCAAGCTCATTTCTCTG	TCTTGCTCAGTGTCTTCTG	qRT-PCR
<i>TRIP11</i>	GCCAGTCTCTGGGTCAAGTC	AATTCTGCTTCCACTTCCTCCG	qRT-PCR
<i>ACTB</i>	CGTCCACACCCGCCG	CCACCATCACGCCCTGG	qRT-PCR
<i>Acy3</i>	CTTCAACCAAGGCATGGACT	TCAAAGTCATGGTCTGTCAG	qRT-PCR
<i>Polr2a</i>	CAGGACACTGGACCGCTCAT	GCATAATATTCTCAGAGACTC CCTCA	qRT-PCR
<i>Smoc1</i>	TTCAGGAAGAAAAGATGATGGCT	ATCCATAAGGTGGGGGCTGT	qRT-PCR
<i>Agt</i>	TGTCTAGGTTGGCGCTGAAG	GATGTATACGCGGTCCCCAG	qRT-PCR
<i>Dao</i>	GTCAACACAGCCCAGAGAGT	CCAATGACTCCTGCTCCGAT	qRT-PCR
<i>Il33</i>	AGGGAGAAATCACGGCAGAA	TATTTTGCAAGGCGGGACCA	qRT-PCR

2.9 Plasmids and cell culture experiments

Non-expanded mouse *Atxn3* cDNA was amplified by PCR from a wild-type mouse, and different expanded mouse *Atxn3* cDNA were amplified from SCA3 knock-in mice. Amplified PCR products were extracted from a 1% agarose gel and TA-cloned into a pcR2.1 plasmid (Invitrogen) and subcloned into pcDNA 3.1 between BamHI and NotI sites. All constructs were ligated with T4 DNA ligase (New England BioLabs) and transformed into TOP10 cells (Invitrogen). The final constructs included those expressing nonexpanded mouse ATXN3 (Wild-type), full-length Q74 mouse ATXN3 (Q74-FL), and intron 10-containing Q71 mouse ATXN3 (Q71-int10). Plasmids were isolated with the QIAprep Spin Miniprep Kit (QIAGEN) and confirmed by sequencing before transfecting into cells.

PC12 cells were maintained at 37°C, 5% CO₂ in DMEM, 10% FBS, 1% penicillin/streptomycin/glutamine. Cells were transiently transfected with 500ng DNA in 100 µL OptiMem, using Lipofectamine PLUS Reagents, according to the manufacturer's protocol. Coverslips were coated with polyD lysine (Millipore) and incubated for 24

hours at 37°C. Cells were plated on polyD lysine-coated coverslips and transfected 24 hours later. 72 hours after transfection, cells were fixed in 4% paraformaldehyde/PBS and immunostained for ATXN3 (1H9, 1:1000). To quantify ATXN3 puncta, several fields were randomly selected using a 60x objective on an Olympus IX71 inverted microscope per transfected coverslip. The number of inclusions among nine fields was averaged for three separate experiments and graphed for each construct.

2.10 Statistical analysis

All statistics were performed in Graphpad Prism. Western blot and qRT-PCR experiments comparing two conditions were analyzed by a Student's *t*-test. For studies comparing three conditions, I performed a one-way ANOVA with the Newman-Keuls multiple comparisons test. P-values less than 0.05 were considered statistically significant. Different statistical analyses that are used are noted throughout the dissertation.

Intron 9:

...TGTAACATCAAATCACAGGTCACAACATACAGTGGTTCTGAATATAGTCATTTCTATGTC
TTTAATTCCTCAAGTCTGTGATGAAGCTGCTGTGTGACAAGGCACAGTTTCAGGTAAGTGGG
ACACAGGTAAGCAGCATCAG[**GTCGACGTTAACATGCATATAACTTCGTATAATGTAT
GCTATACGAAGTTATCTCGAGAAGTTCC TATTCTCTAGAAAGTATAGGAACTTCT
AGGATCCCCGGGTACCT**]TGAGCTCTCATTGCTTACAGACCAGACAGAGTATCAAGACA
GTATGTTTGTGCCGAGAATGAAAATGAAATAGTGAGAAAGCCAGGAGGTTGCTTGAAACG
GGATAGTCGGAGAGGGACTCCAGGGAGAACTTAGTAAATCCAGGCTTGAGTGGCAGCG
AGGGAGCCAGCCCAGGAAAGCACATTAAAGTGAGATAGTTTGTCTTATCAAAGGTGTTTTTC
CAGTGGCTTCTAACAGTGATAAAGATATATAAACCAACACTCATTGTGTAAGAATCACTAC
TAGTGAACCTTGAACAGAAAGTGCAAATACCTACCTCTTCTCTGATAATTCAAATGTGTAG
GTTTTTTGAATC
(End of intron 9)

Figure 2.1 Retained sequences in the mutant *Atn3* locus of SCA3 knock-in mice. Sequencing of a SCA3 knock-in mouse across the FRT site showed successful removal of the neomycin cassette from the SCA3 knock-in mouse, and the remaining sequences from the targeting vector (bold and in brackets) approximately 350 bp upstream of exon 10. This 110 bp sequence includes the engineered SalI and KpnI sites at the ends, a single LoxP site (red), and a single FRT site (underlined).

Chapter 3

A knock-in mouse model of Spinocerebellar Ataxia type 3 exhibits prominent aggregate pathology and aberrant splicing of the disease gene transcript

3.1 Abstract

Polyglutamine diseases, including Spinocerebellar ataxia type 3 (SCA3), are caused by CAG repeat expansions that encode abnormally long glutamine repeats in the respective disease proteins. While the mechanisms underlying neurodegeneration remain uncertain, evidence supports a proteotoxic role for mutant proteins dictated in part by the specific genetic and protein contexts. To further define pathogenic mechanisms in SCA3, we generated a mouse model in which a CAG expansion of 82 repeats was inserted into the murine locus by homologous recombination. SCA3 knock-in mice exhibit region-specific aggregate pathology marked by intranuclear accumulation of the mutant ATXN3 protein, abundant nuclear inclusions and, in select brain regions, extranuclear aggregates localized to neuritic processes. Knock-in mice also display altered splicing of the disease gene, promoting expression of an alternative isoform in which the intron immediately downstream of the CAG repeat is retained. In an independent mouse model expressing the full human *ATXN3* disease gene, expression of this alternatively spliced transcript is also enhanced. These results, together with recent

findings in other polyglutamine diseases, suggest that CAG repeat expansions can promote aberrant splicing to produce potentially more aggregate-prone isoforms of the disease proteins. This first report of a SCA3 knock-in mouse expands the repertoire of existing models of SCA3, and underscores the potential contribution of alternative splicing to disease pathogenesis in SCA3 and other polyglutamine disorders. The work of this chapter has been published in Ramani et al (151).

3.2 Introduction

Spinocerebellar ataxia type 3 (SCA3), also known as Machado-Joseph disease, is the most common dominantly inherited ataxia and one of at least nine neurodegenerative diseases caused by polyglutamine-encoding CAG repeat expansions (167). In SCA3, this expansion occurs in the *ATXN3* gene which encodes the deubiquitinase ataxin-3 (*ATXN3*) (111). Like other polyglutamine diseases, SCA3 is a disabling and ultimately fatal disorder characterized by selective degeneration in specific brain regions and age-dependent intraneuronal accumulation and aggregation of the mutant protein (2, 6). While neuronal inclusions formed by the disease protein may not be directly toxic in polyglutamine disease (37, 38), evidence supports the view that inclusions are a marker for accumulated, misfolded polyglutamine protein that is proteotoxic and contributes to neuronal dysfunction and cell loss in disease (16, 19–21, 168). Unfortunately, despite recent advances in understanding polyglutamine diseases, no preventive treatments are available for any.

Animal models have been instrumental in providing insight into polyglutamine disease pathogenesis and suggesting routes to potential therapy. Existing animal models of SCA3 have advanced the field in many ways, but all of them overexpress mutant

ATXN3 above physiological concentrations (110). While overexpression models are particularly good at recapitulating robust aggregation pathology and behavioral abnormalities, they may mask early molecular changes important to pathogenesis. Moreover, models overexpressing a single isoform of ATXN3 from cDNA do not permit investigations of the potential disease contribution of splicing changes in the mutant transcript. In contrast, “knock-in” models in which the CAG repeat expansion is inserted precisely into the endogenous murine locus have proved useful in understanding various aspects of polyglutamine disease (48, 68, 80, 81, 85–87, 142, 147, 153) including altered splicing of mutant transcripts (85, 86). For example, Sathasivam et al. recently discovered that the CAG expansion in Huntington’s disease knock-in mice promotes aberrant splicing of the Htt transcript and the production of a truncated amino-terminal fragment of the disease protein, Htt (86). Genetically precise knock-in mouse models express the mutant protein from the endogenous promoter in the proper genomic context, including all regulatory elements that influence mutant gene expression.

Knock-in mouse models have been generated for most polyglutamine diseases, but none exists for SCA3. Here, we report the first SCA3 knock-in mouse model, generated by replacing the endogenous murine CAG repeat with an 82 repeat CAG expansion. Expressing physiological levels of mutant ATXN3, the SCA3 knock-in mice exhibit robust ATXN3 accumulation both in regions known to be affected in human disease (e.g. brainstem and cerebellum) and in regions not previously described (e.g. hippocampus). SCA3 knock-in mice also display altered splicing of the mutant *Atxn3* transcript that results in the formation of a previously described alternative *ATXN3* transcript in human disease (98). We further show that CAG expansion results in similar

altered splicing in another mouse model expressing the full length human ATXN3 disease gene. In summary, the SCA3 knock-in mouse model reported here recapitulates several important molecular features of disease and should facilitate the study of early pathogenic events in this polyglutamine disease.

3.3 Results

3.3.1 Generation of the SCA3 knock-in mouse model and mutant ATXN3 expression

SCA3 is caused by CAG expansions ranging from ~60 to 87 repeats in the *ATXN3* gene (169). We inserted a CAG repeat expansion at the upper end of this disease range into the endogenous murine *Atn3* locus on a C57BL/6 background (Figure 3.1A). By homologous recombination we replaced the endogenous murine sequence CAA(CAG)₅ with (CAG)₂(CAAAAG)(CAG)₈₂ which encodes 85 glutamines interrupted by a lysine at the fourth residue (i.e. Q3KQ82), replicating the polyglutamine stretch found in human mutant ATXN3 (98). PCR across the endogenous CAG repeat confirmed successful insertion of the pathogenic expansion in heterozygous (Q82/Q6) and homozygous (Q82/Q82) SCA3 knock-in mice (Figure 3.1B). Sequencing of the intronic region upstream of the repeat expansion confirmed the removal of the neomycin cassette and the presence of the remaining FRT sequence (Figure 3.2), and sequencing of exon 10, all of intron 10 and exon 11 did not reveal any differences compared to wild-type mice other than the expansion (data not shown). CAG repeat length sizing in offspring of heterozygous Q82/Q6 mice revealed a modest tendency toward CAG repeat contraction upon maternal transmission of the mutant allele and stabilization or mild expansion upon paternal transmission (Figure 3.1C). Similar intergenerational repeat

instability has been reported in other polyglutamine disease mouse models, including a transgenic mouse model of SCA3 (40, 80, 81, 170).

Mutant ATXN3 is expressed widely throughout the SCA3 knock-in mouse, including in the brain, heart, liver, muscle and spleen (155). Western blot analysis of hindbrain lysates from one-year-old Q82/Q6 mice confirmed mutant ATXN3 expression in the brain, as well as aggregated ATXN3 protein in the stacking gel (Figure 3.1D). Electrophoresis of brain lysates from knock-in mice on low percentage (3%) SDS-PAGE further illustrated a range of high molecular weight aggregate species (Figure 3.1E). Analysis of hindbrain lysates from homozygous Q82/Q82 knock-in mice revealed exclusively mutant (expanded) ATXN3 expression with a corresponding loss of wild-type ATXN3, confirming that mutant ATXN3 is expressed from the endogenous allele (Figure 3.1F). The increased high molecular weight aggregate species are consistent with detergent-resistant aggregates previously reported in a SCA3 transgenic mouse model (16, 171). In heterozygous mice, the decreased intensity of mutant ATXN3 monomer compared to wild-type ATXN3 monomer is also consistent with the aggregation propensity of expanded polyglutamine proteins (149).

3.3.2 Neuropathological and behavioral characterization of the SCA3 knock-in mouse

To begin defining neuropathological changes in SCA3 knock-in mice, we immunostained for ATXN3 in SCA3 knock-in brain. Compared to other polyglutamine disease knock-in mouse models in which CAG expansions within the human disease range often elicit relatively modest neuropathological findings (136, 139, 140, 150), SCA3 knock-in mice display comparatively robust aggregate pathology. In heterozygous

mice, enhanced intranuclear staining for ATXN3 is present by 10 weeks in several neuronal populations, including the deep cerebellar nuclei (DCN) (Figure 3.2A), and is often accompanied by small intranuclear puncta. We do not reliably detect immunohistochemical changes in Q82/Q6 mice that are less than ~ six weeks of age. One year old heterozygous Q82/Q6 knock-in mice display more prominent intranuclear puncta, as well as more frequent solitary inclusions that are characteristic of the human disease (Figure 3.2B). Neuronal inclusions in the SCA3 knock-in mice often co-localize with p62, an ubiquitin binding protein implicated in autophagy and previously reported to localize to intranuclear inclusions in SCA3 disease brains (172–174) (Figure 3.2D, Figure 3.3).

SCA3 knock-in mice display striking regional differences in mutant ATXN3 deposition. Table 3.1 (with Figure 3.6) qualitatively report the intensity of diffuse nuclear staining and frequency of intranuclear inclusions in various brain regions in one-year-old heterozygous mice (n=4). Neurons of the hindbrain, including the DCN and several brain stem nuclei, which are known to be vulnerable targets in the human disease, show strong diffuse nuclear staining that is often accompanied by multiple intranuclear puncta and less frequently by distinct solitary large inclusions. In contrast, neurons of the forebrain, including the hippocampus, cortex, and striatum, have moderately increased diffuse nuclear staining with frequent solitary intranuclear inclusions. Despite widespread aberrant accumulation of mutant ATXN3, including in the hindbrain, one year old Q82/Q6 mice (n=9) performed equally well as age-matched wild-type mice (n=10) on various motor tasks (Figure 3.2E). Examination of cresyl-violet-stained brains of one-year-old Q82/Q6 mice (n=3) did not reveal obvious degenerative changes in any brain

regions. For example, a close examination of the DCN, a region known to be consistently affected in SCA3, did not suggest neuronal loss at one year of age (Figure 3.4).

We also observed striking extranuclear neuronal aggregates in select brain regions, summarized in Table 3.1. In one-year-old knock-in mice, for example, ubiquitin-positive extranuclear inclusions are especially abundant in the stratum radiatum of the hippocampus, which also shows frequent ubiquitin-positive intranuclear inclusions in pyramidal neurons (Figure 3.5A and B). Extranuclear inclusions are also present in the subiculum, central amygdala, and bed nucleus of the stria terminalis. Extranuclear inclusions in the hippocampus often co-localize with anti-MAP2 and SMI32 antibodies, suggesting that they reside in dendrites (Figure 3.5C). At three months of age they are detected as small puncta in the hippocampal neuropil and grow over time into large, often irregular structures by one year of age. In a two-year-old Q82/Q6 mouse, many of these large inclusions co-localized with reticulon-3 (RTN3), a potential marker for dystrophic neurites (175, 176) (Figure 3.5D). We also examined soluble lysates of SCA3 knock-in mouse hindbrain and hippocampus by western blot, but did not detect regional differences in levels of soluble, monomeric mutant ATXN3 or of high molecular weight, aggregated ATXN3 species (Figure 3.7).

The presence of robust hippocampal pathology prompted us to perform a test of fear conditioning to shock, which broadly assesses hippocampal- and amygdala-dependent memory consolidation (177). We did not observe significant differences in freezing to context or tone in one-year-old Q82/Q6 mice (n=9) compared to wild-type littermates (n=9) (Figure 3.5E). All SCA3 knock-in mice tested in this experiment were later confirmed to contain extensive extranuclear aggregates in the hippocampus and

central amygdala nucleus (not shown). In summary, SCA3 knock-in mice exhibit robust aggregate pathology throughout the brain upon physiological expression of polyglutamine-expanded ATXN3 and thus are well suited to explore the early molecular changes contributing to disease pathogenesis.

3.3.3 Alternative processing of mutant ataxin-3 transcript in SCA3

Many polyglutamine diseases and mouse models of disease are associated with transcriptional changes that may contribute to disease pathogenesis (53, 67). To identify early transcriptional and splicing changes in SCA3 knock-in mice, including potential alterations in the *Atxn3* transcript itself, we performed RNA-sequencing on a vulnerable brain region in SCA3, the pons, from 6 month old wild-type (n=7) and homozygous SCA3 knock-in mice (n=7). A full analysis of transcriptional changes will be reported later. In this study, we focus on intriguing differences noted in expression of the *Atxn3* transcript itself.

The human *ATXN3* and murine *Atxn3* genes both contain 11 exons, with the CAG repeat residing in exon 10. At least two major ATXN3 transcript variants are expressed in humans: a full length, 11 exon ATXN3 (ATXN3-11e) transcript that contains the entire ATXN3 protein coding sequence; and a 10 exon (ATXN3-10e) transcript that retains intron 10 and lacks exon 11 (98, 178). The ATXN3-11e transcript (RefSeq NM_004993) encodes the ATXN3 isoform MJD1c (107, 178), whereas the ATXN3-10e transcript (RefSeq S75313), initially identified by Kawaguchi et al. when they reported the disease mutation in SCA3 (98), encodes isoform MJD1a or MJD1b depending on a polymorphism that alters the location of the stop codon. In this study, we refer to these transcripts and corresponding protein isoforms by the number of exons (10e and 11e). We

previously reported that ATXN3-11e is normally the most abundantly expressed isoform in the brain and that the less abundant ATXN3-10e isoform is more unstable and aggregation-prone in cell models (109). The unstable, aggregation-prone nature of ATXN3-10e may reflect the presence of a carboxy-terminal hydrophobic domain that is encoded by read-through into the intron downstream of exon 10. This domain is absent from ATXN3-11e, which instead ends with a domain containing an Ubiquitin Interacting Motif (UIM).

Unexpectedly, comparison of aligned sequencing reads revealed markedly elevated reads into intron 10 of *Atxn3* in SCA3 knock-in mice, whereas few intronic reads were present in wild-type mice (Figure 3.8B). These increased reads continue ~300 bp into intron 10, ending near a putative polyadenylation site (ATTAAA) and suggesting that the transcript could terminate and become polyadenylated at this site. Indeed, 3' RACE on Q82/Q6 mouse RNA to the beginning of intron 10 revealed a ~300 bp band, which sequencing confirmed is a putative *Atxn3*-10e transcript polyadenylated at this predicted polyA site in intron 10 (Figure 3.8C). Importantly, despite the increased expression of the *Atxn3*-10e transcript, SCA3 knock-in mice still express the *Atxn3*-11e variant. RNA-sequencing reads containing exon 11 and the established *Atxn3* 3' UTR appear to be equally present in wild-type and SCA3 knock-in mice (Figure 3.8D): normalized levels (FPKMs) of predicted full-length *Atxn3*-11e transcript (accession NM_029705.3) did not differ significantly between wild-type and mutant mice (Figure 3.8E). Except for the differences noted at the exon 10/intron 10 junction, we did not observe striking or consistent changes in reads across the entire *Atxn3* gene (Figure 3.9).

To further quantify *Atxn3*-10e transcript levels in SCA3 knock-in mice, we performed quantitative PCR on reverse-transcribed RNA (qRT-PCR) from brain using primers against the exon 10/intron 10 junction. We also separately performed qRT-PCR using primers that amplify only exon 10 to estimate total (exon 10-containing) *Atxn3* transcript levels (Figure 3.10A). *Atxn3*-10e transcript levels proved to be markedly increased in 3-month-old Q82/Q6 mice compared to age-matched wild-type mice, whereas total exon 10-containing transcripts (i.e., 10e and 11e variants combined) showed a more modest upregulation in knock-in mice (Figure 3.10B). The basis for the upregulation of total *Atxn3* transcript in SCA3 knock-in mice is not clear but may reflect differences in the regulation of *Atxn3*-10e and *Atxn3*-11e transcripts since they utilize different 3'UTRs. We also cannot exclude the possibility that the manipulation of the endogenous murine *Atxn3* gene, including the presence of the FRT site, alters its expression.

To determine whether the increased levels of this alternative isoform reflect the presence of a CAG expansion, we investigated an independent SCA3 mouse model: YAC transgenic mice that express the full human *ATXN3* gene with either a normal repeat (YAC-15Q) or an expanded repeat (YAC-84Q) (159). Employing qRT-PCR with primers against *ATXN3* (Figure 3.10A), we observed significantly elevated *ATXN3*-10e transcript levels in the pons of ~5 month old YAC-84Q mice compared to age-matched YAC-15Q mice (Figure 3.10C). These results suggest that CAG repeat expansions are associated with increased production of the *ATXN3*-10e transcript. To further explore this possibility we analyzed *ATXN3* transcripts in fibroblasts derived from SCA3 patients (n=6) or non-

disease controls (n=4) (Figure 3.10D). By qRT-PCR, however, *ATXN3*-10e transcript expression levels did not differ significantly between disease and control fibroblasts.

To verify that the *ATXN3/Atxn3*-10e transcripts observed above contain the rest of the amino-terminal protein coding sequence, we performed non-quantitative PCR using primers to amplify from exon 1 to intron 10 (Figure 3.10A) on the same reverse-transcribed RNA preparations described above. We note that this PCR is non-quantitative because large GC-rich repeats (i.e. expanded CAG repeats) are poorly amplified by the polymerase. PCR amplified a single band from Q82/Q6 mice but none from wild-type mice (Figure 3.10E). Sequencing confirmed this band to be *Atxn3*-10e cDNA containing the first 10 exons followed by read through into intron 10. Thus, SCA3 knock-in mice express the full *Atxn3*-10e transcript with a CAG repeat expansion, analogous to the *ATXN3*-10e transcript in humans. Importantly, non-quantitative PCR showed that the complete *ATXN3*-10e transcript is also expressed in YAC mice expressing normal or expanded *ATXN3*, in 3 of 4 control fibroblast lines, and in all SCA3 disease fibroblast lines, including from the non-expanded allele (Figure 3.10F, G). The one control line that did not produce a detectable PCR signal (lane 3) showed reduced levels of total RNA by quantitative PCR, which may prevent detection of the less abundant *ATXN3*-10e transcript by PCR. This sample demonstrated proportionally lower levels of *ATXN3*-10e, total *ATXN3*, and *ACTB* transcripts. PCR amplification from *ATXN3* exon 7 to 11 demonstrated that *ATXN3*-11e is present in this and all other fibroblast lines (Figure 3.10G).

The expression of the *ATXN3*-10e transcript even in normal human fibroblasts suggests that the relatively larger CAG repeat length of the normal human *ATXN3* gene

(20-42 repeats) may support the production of the *ATXN3*-10e transcript. In contrast, wild-type mice, which have only 5 CAG repeats, show nearly undetectable levels of *Atxn3*-10e transcript, leading to a dramatically higher fold-change in the SCA3 knock-in mice. Tissue-specific differences could further mask CAG repeat-dependent splicing changes in SCA3 fibroblasts.

3.4 Discussion

The SCA3 knock-in mouse reported here expresses mutant ATXN3 with an expansion in the human disease range and exhibits robust accumulation and aggregation of mutant ATXN3 in the brain, detected biochemically and immunohistochemically. In addition to replicating the intranuclear accumulation and inclusions described in human disease tissue, SCA3 knock-in mice also develop extensive neuritic aggregates in select brain regions, most notably the hippocampus. SCA3 knock-in mice harboring a CAG expansion also display marked retention of intron 10 in *Atxn3* transcripts, a finding we confirmed in an independent mouse model of SCA3 expressing the full human disease gene. Based on these results, this SCA3 knock-in mouse model represents an important addition to existing models of disease that should prove particularly useful for the study of early molecular changes including mutant protein aggregation and alternative splicing.

Despite only modest expression of the mutant protein from the endogenous locus, SCA3 knock-in mice manifest relatively early signs of ATXN3 accumulation in the brain, including increased concentration in neuronal nuclei and the formation of intranuclear puncta and larger inclusions. ATXN3 accumulation is noted especially in neurons of the hindbrain known to be affected in SCA3, such as DCN and brainstem neurons (105). Nuclear localization of the mutant protein is believed to contribute to

disease pathogenesis in various polyglutamine diseases including SCA3 (50–52), and this new model could facilitate the study of factors acting early to regulate nuclear trafficking and handling of mutant ATXN3. The knock-in mouse model also should assist the dissection of posttranslational modifications occurring to mutant ATXN3 *in vivo* including proteolytic cleavage, phosphorylation, and ubiquitination, as well as their impact on disease protein behavior.

SCA3 knock-in mice also develop striking neuritic inclusions, particularly in the synapse-rich stratum radiatum of the hippocampus. The mechanisms driving the formation of these aggregates remain unclear. Deficits in trafficking and/or clearance of misfolding proteins in the distal reaches of pyramidal neurons may precipitate the formation of inclusions in subcellular compartments far removed from clearance mechanisms concentrated in the cell soma. A recent study showed that removing p62 in HD mouse models led to increased MAP2-positive HTT aggregates in the stratum radiatum that look strikingly similar to the ones shown here (179). Alternatively, neuritic aggregates could arise as a consequence of neuronal activity, which has been proposed to promote cleavage and aggregation of mutant ATXN3 at synapses (180). While the hippocampus is not considered a major disease target in SCA3, the study of the anatomically layered and easily accessible hippocampus could provide unique opportunities to study misfolded protein handling in axons and dendrites. Furthermore, an increasing number of studies report cognitive dysfunction in SCA3, which may reflect forebrain pathology (102–104). Axonal and cytoplasmic inclusions have been reported in SCA3 (106), but the extent to which they affect neuronal function is unknown. Future studies on the formation of extranuclear aggregates in SCA3 knock-in hippocampus may

provide insight into the handling of misfolded protein in neurites. Our findings also underscore the need for further pathological characterization of SCA3 disease tissue, including of the cortex and hippocampus.

The absence of behavioral deficits and overt neuropathological changes in heterozygous SCA3 knock-in mice despite prominent disease protein aggregation is perhaps not surprising given the low-level, physiological expression of the *Atxn3* disease gene. Knock-in mice with CAG repeat lengths in the human disease range, as in this study, often display mild or no behavioral deficits (80, 138, 140, 150). For example, SCA1 78Q knock-in mice manifested mild abnormalities only when homozygous for the mutant allele (80). It will be important to look for motor deficits and molecular markers of degenerative change in aged homozygous SCA3 knock-in mice, which we are in the process of generating. The absence of an overt behavioral phenotype in this and many other age-related neurodegenerative disease models highlights the point that such models are best at providing insight into pathogenic mechanisms that precede neuronal loss.

Intriguingly, SCA3 knock-in mice exhibit altered splicing of the mutant *Atxn3* transcript, mirroring the formation of a known alternative *ATXN3* transcript in humans. Increased retention of intron 10 in mutant *Atxn3* transcripts parallels the findings of Sathasivam and colleagues, who observed the retention of intron 1 in mutant *Htt* transcripts following the CAG repeat-containing exon 1 in a knock-in mouse model of HD and suggested that differential binding of splicing factors mediates aberrant splicing of the mutant transcript (86, 181). Alternatively, differences in the kinetics of transcription through an expanded repeat may shift polyadenylation site usage (182–184). Shared mechanisms across polyglutamine diseases may dictate aberrant splicing of CAG

repeat-containing transcripts, potentially producing more toxic isoforms of disease proteins in several polyglutamine disorders. We previously reported that even a non-expanded form of the ATXN3-10e variant is more aggregate-prone and less stable than the full-length isoform, suggesting that the higher hydrophobicity of the carboxy-terminus encoded by translational read-through into intron 10 increases overall aggregation propensity (109). If identified, factors that shift splicing to favor production of the full-length (i.e. 11e) ATXN3 isoform might represent targets through which to lessen mutant protein aggregation. The SCA3 knock-in mouse should facilitate studies to identify such factors.

Unfortunately, the high degree of similarity between the 10e and 11e ATXN3 isoforms raises challenges in distinguishing the two encoded proteins. We previously showed that these two isoforms have slightly different electrophoretic properties, but were unable to distinguish the ATXN3-10e isoform from ATXN3-11e isoform in ATXN3Q84-YAC mice (109). In addition, decreased solubility of the ATXN3-10e isoform may impede its detection by conventional biochemical methods. While both the ATXN3-11e and ATXN3-10e transcripts are presumably made in the human brain, their relative abundance in the SCA3 disease brain is not known. Future studies will be needed to quantify the expression of alternative ATXN3 transcripts and ATXN3 protein isoforms in human brain in order to determine their relative contribution to disease pathogenesis.

3.5 Acknowledgments

We thank members of the Paulson laboratory and Ravi Chopra for helpful comments. We are grateful to Dr. Tetsuo Ashizawa, Dr. Eva Feldman, and Dr. Riqiang Yan for providing reagents. This work utilized the Sequencing and Bioinformatics Core

Services provided by the Biomedical Research Core Facilities at the University of Michigan. This work was supported by the National Institutes of Health [RO1NS038712, RO3NS072967 to H.L.P.; F31NS083167 to B.R.; the University of Iowa Medical Scientist Training Program to G.H.]; and the University of Michigan Rackham School of Graduate Studies to B.R.

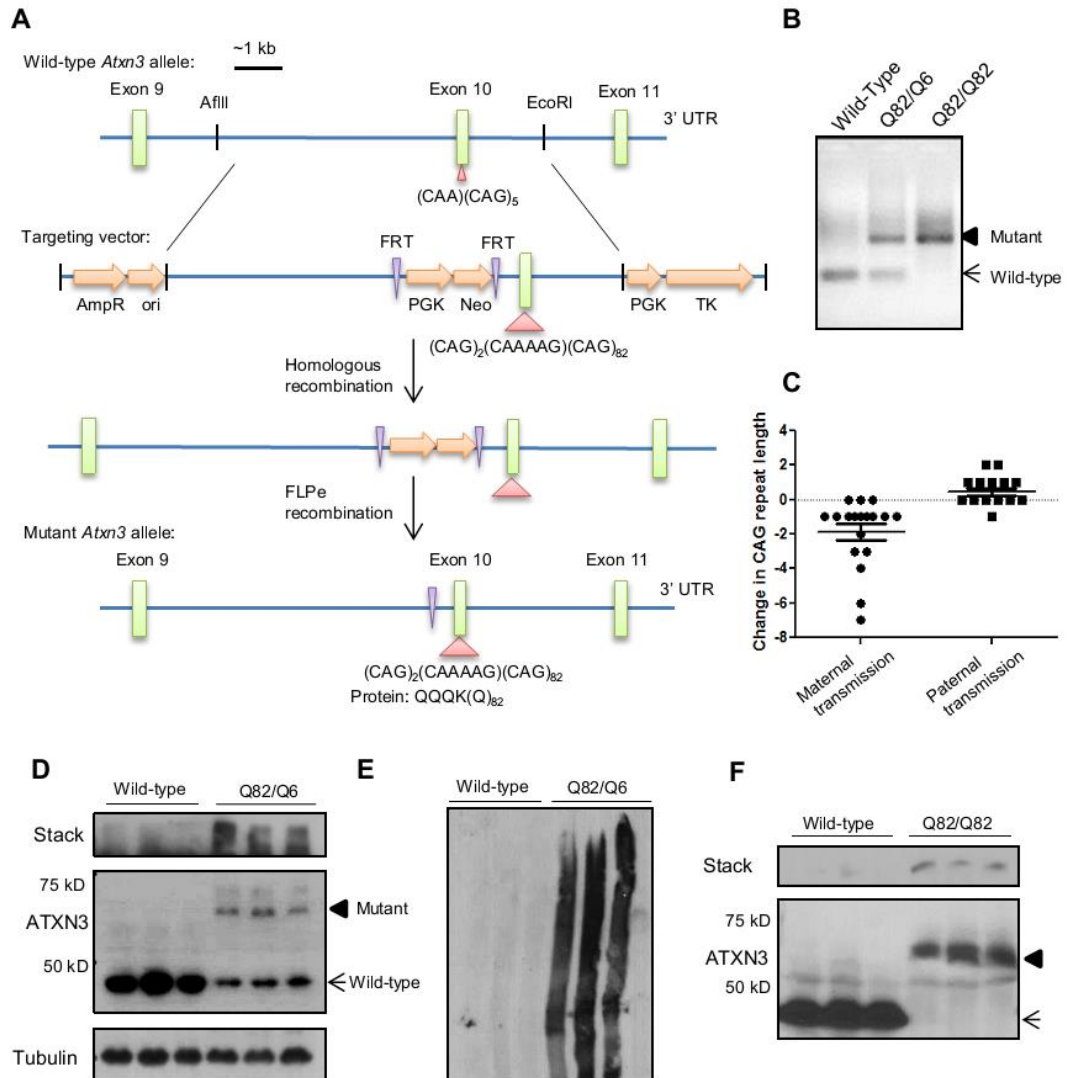


Figure 3.1 Generation of a SCA3 knock-in mouse expressing mutant ATXN3 (Q82). (A) Schematic of the generation of the SCA3 knock-in mouse in which the endogenous murine (CAA)(CAG)₅ was replaced with a human CAG expanded sequence, (CAG)₂(CAAAAG)(CAG)₈₂, by homologous recombination. The neomycin (neo) selection cassette, flanked by FRT sites, was removed by FLPe recombination. These steps were performed by Dr. Ginny Harris. (B) PCR across the CAG repeat shows the expanded repeat in heterozygous (Q82/Q6) and homozygous (Q82/Q82) SCA3 knock-in mice. (C) SCA3 knock-in mice show modest intergenerational repeat length instability with a tendency for CAG repeat contraction upon maternal transmission. (D) Western blotting shows expression of mutant ATXN3 accompanied by increased aggregates in the stacking gel in 1-year-old Q82/Q6 hindbrain lysates. (E) Electrophoresis of lysates from (D) on 3% SDS-PAGE further illustrates high molecular weight aggregates. (F) ~30-week-old homozygous Q82/Q82 mice express only mutant ATXN3 with aggregates in the stack. D and F, arrow indicates wild-type ATXN3 and arrowhead indicates mutant ATXN3.

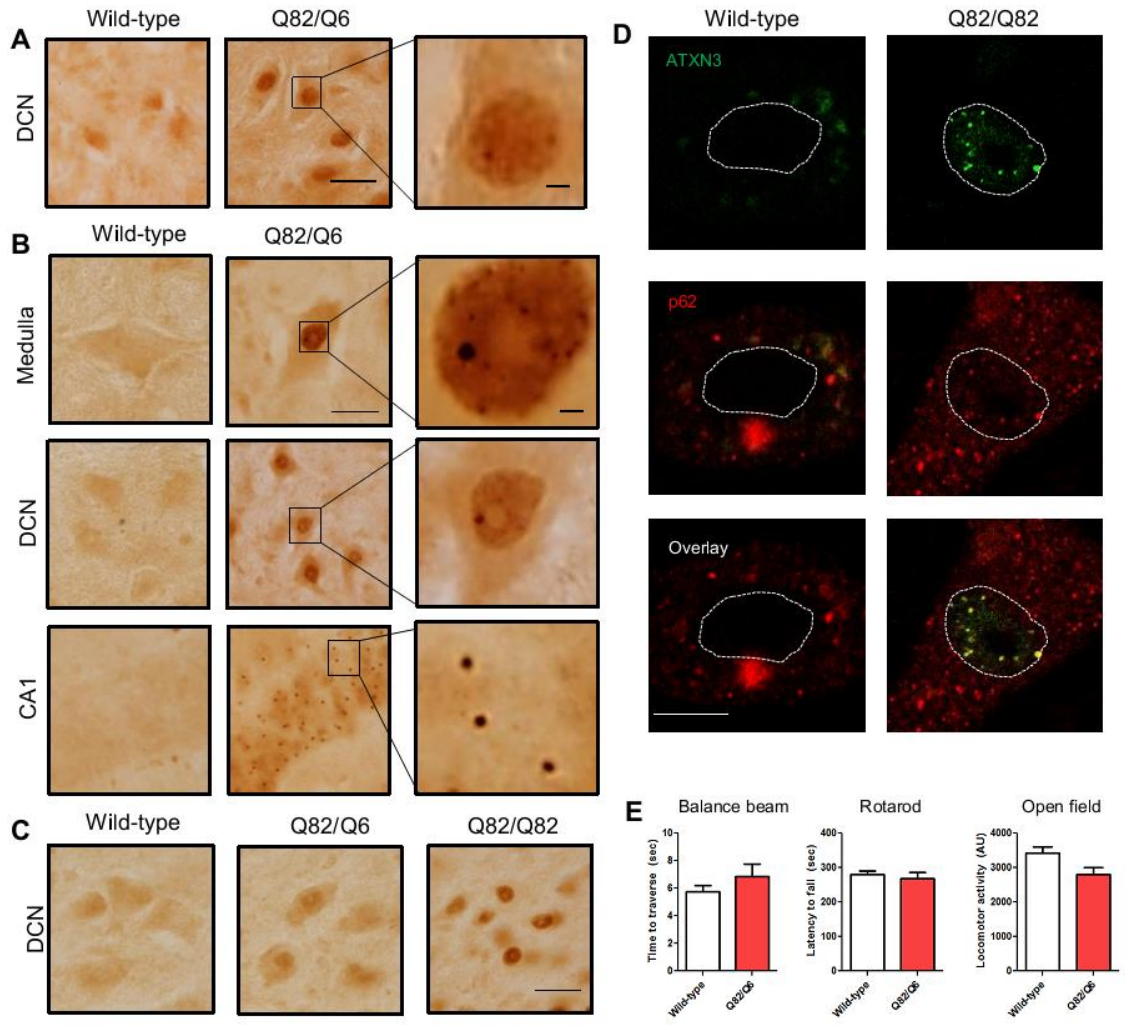


Figure 3.2 Mutant ATXN3 accumulation in the SCA3 knock-in mouse brain. (A) Immunohistochemical staining (IHC) for ATXN3 shows nuclear accumulation in the DCN of a 10-week-old Q82/Q6 mouse. Scale bar = 20 μ m, inset scale bar = 2 μ m. (B) IHC of one-year-old Q82/Q6 mice shows increased diffuse nuclear staining and intranuclear puncta/inclusions in several brain regions, including the brain stem (medulla shown), deep cerebellar nuclei (DCN), and the hippocampus (CA1 region is shown). Higher magnification insets show puncta and inclusions in nuclei. (C) Intranuclear accumulation of ATXN3 (DCN shown) is accelerated in a ~7-month-old homozygous Q82/Q82 mouse compared to a heterozygous littermate. Scale bar = 20 μ m (D) ATXN3-immunoreactive (green) intranuclear puncta and inclusions in brainstem neurons from SCA3 knock-in mice frequently co-stain with p62 (red), whereas p62 is predominantly cytoplasmic in wild-type neurons. The nuclear border is outlined by a dashed line. Scale bar = 10 μ m. (E) Performance of one-year-old Q82/Q6 (Q82/Q6) mice (n=9) did not differ from age-matched wild-type (WT) mice (n=10) on motor behavior tasks, including from left to right, 5mm balance beam, accelerating rotarod, and open field exploration. Graphs represent mean + SE.

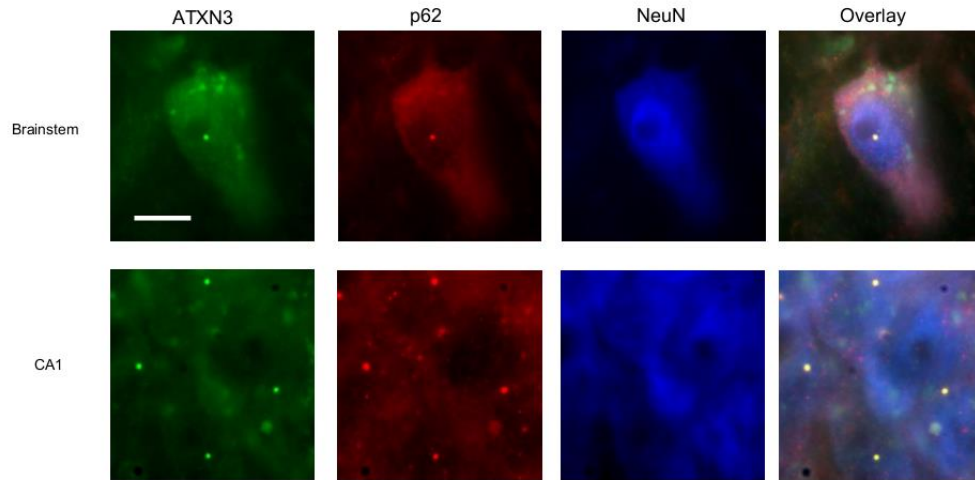


Figure 3.3 ATXN3 and p62 co-immunostaining in a heterozygous Q82/Q6 mice. Epifluorescent images showing that Atxn3 inclusions in a one-year-old Q82/Q6 mouse are immunoreactive for p62 in brainstem and hippocampal pyramidal neurons that coexpress NeuN. Scale bar = 10 μ m

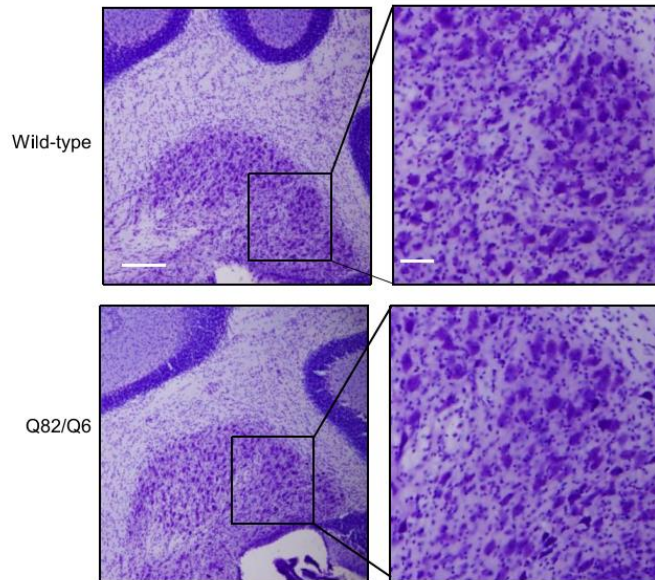


Figure 3.4 Cresyl-violet staining of Q82/Q6 brain. One-year-old Q82/Q6 mice do not show obvious degenerative changes in the DCN by cresyl violet staining. Left panels, scale bar 200 μ m. Right panel insets, scale bar = 50 μ m.

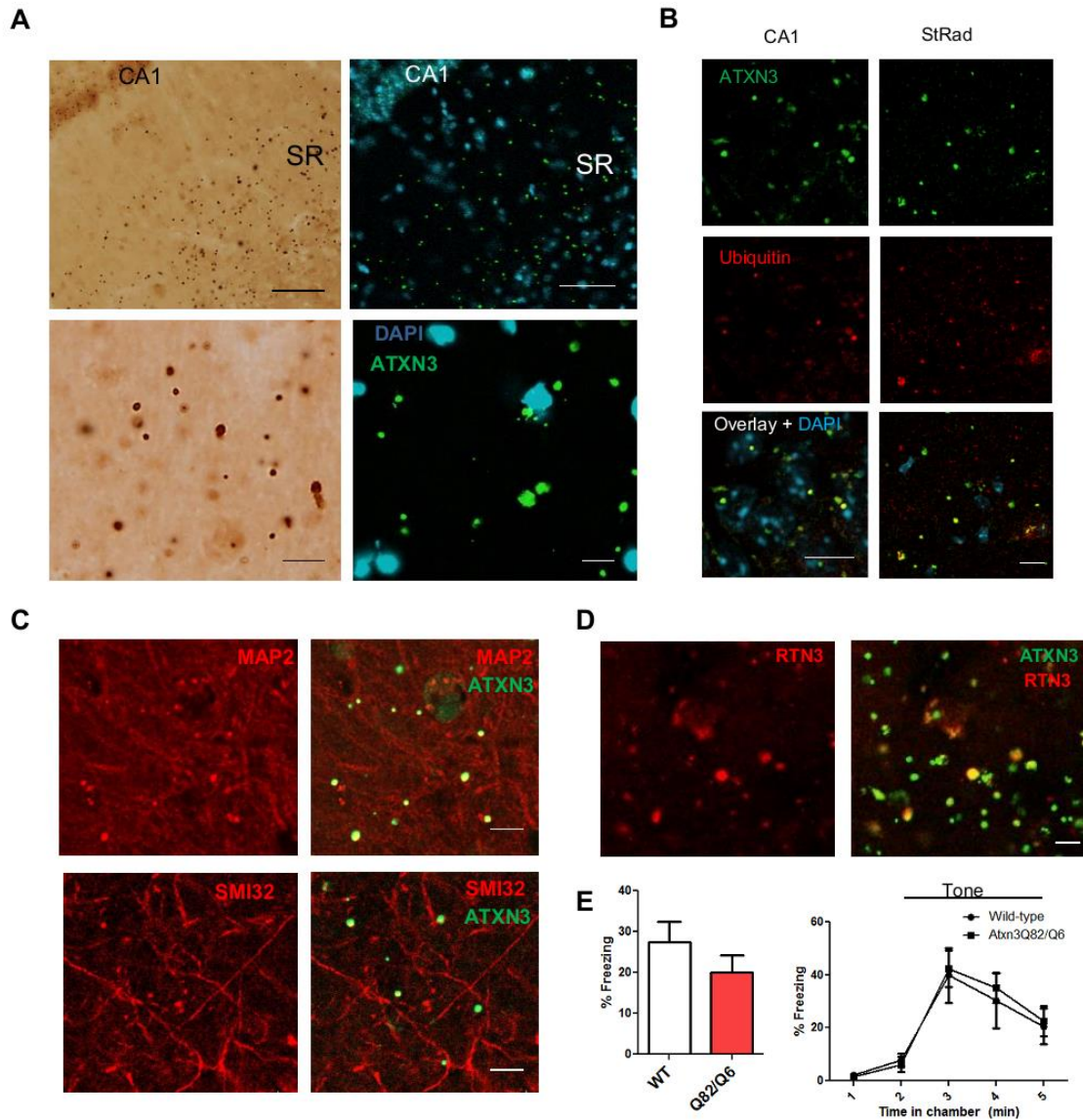


Figure 3.5 Extranuclear inclusions in the hippocampus of SCA3 knock-in mice. (A) Large extranuclear inclusions are concentrated in stratum radiatum (SR) of the hippocampus one-year-old Q82/Q82 mice. Right, immunofluorescence of a different Q82/Q82 mouse showing that inclusions do not colocalize with nuclear DAPI. Bottom panel shows magnified view of inclusions. (B) Hippocampal aggregates are often ubiquitin-positive, including both intranuclear inclusions in CA1 pyramidal neurons (left) and extranuclear inclusions in the stratum radiatum (right). (C) Extranuclear inclusions show overlap with dendritic markers MAP2 and SMI32. (D) Large Atxn3 extranuclear inclusions in the stratum radiatum of a two-year-old Q82/Q6 mouse stain for reticulon-3 (RTN3), a marker for dystrophic neurites. (E) One-year-old Q82/Q6 mice (n=9) did not differ from wild-type mice (n=9) in tests of fear conditioning, including freezing to context (left) and tone (right). Scale bars in (A) top and bottom panels are 50 μ m and 10 μ m, respectively. Scale bars in (B-D) are 10 μ m.

Region	Diffuse nuclear staining	Intranuclear inclusions	Extranuclear inclusions
Purkinje cells	-	+	-
Granular cells	+	-	-
Deep cerebellar nuclei	++	++	-
Medulla	++	++	+
Pons	++	++	+
Substantia nigra	+	+	-
Red nucleus	++	++	-
Spinal cord	++	++	+
Striatum	+	+++	+
Hippocampus	+	+++	+++
Amygdala	+	-	++
Cortex	+	+++	++
Thalamus	+	-	-

Table 3.1 Regional differences in ATXN3 accumulation in SCA3 knock-in mouse brain. One-year-old Q82/Q6 mice (n=3) were immunohistochemically stained for ATXN3. For diffuse nuclear staining, increasing + numbers indicate neurons with denser nuclear staining of Atxn3. For intranuclear and extranuclear inclusions, increasing + numbers indicate higher frequency of inclusions. Regions in knock-in mice that are indistinguishable from wild-type mice are indicated by -.

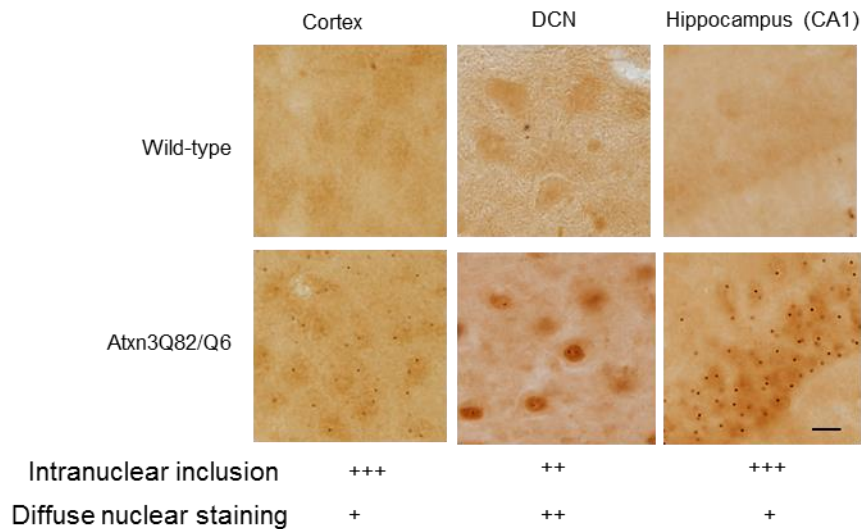


Figure 3.6 Examples of scoring ATXN3 accumulation in an immunohistochemically stained SCA3 knock-in mouse brain. Scale bar = 10µm

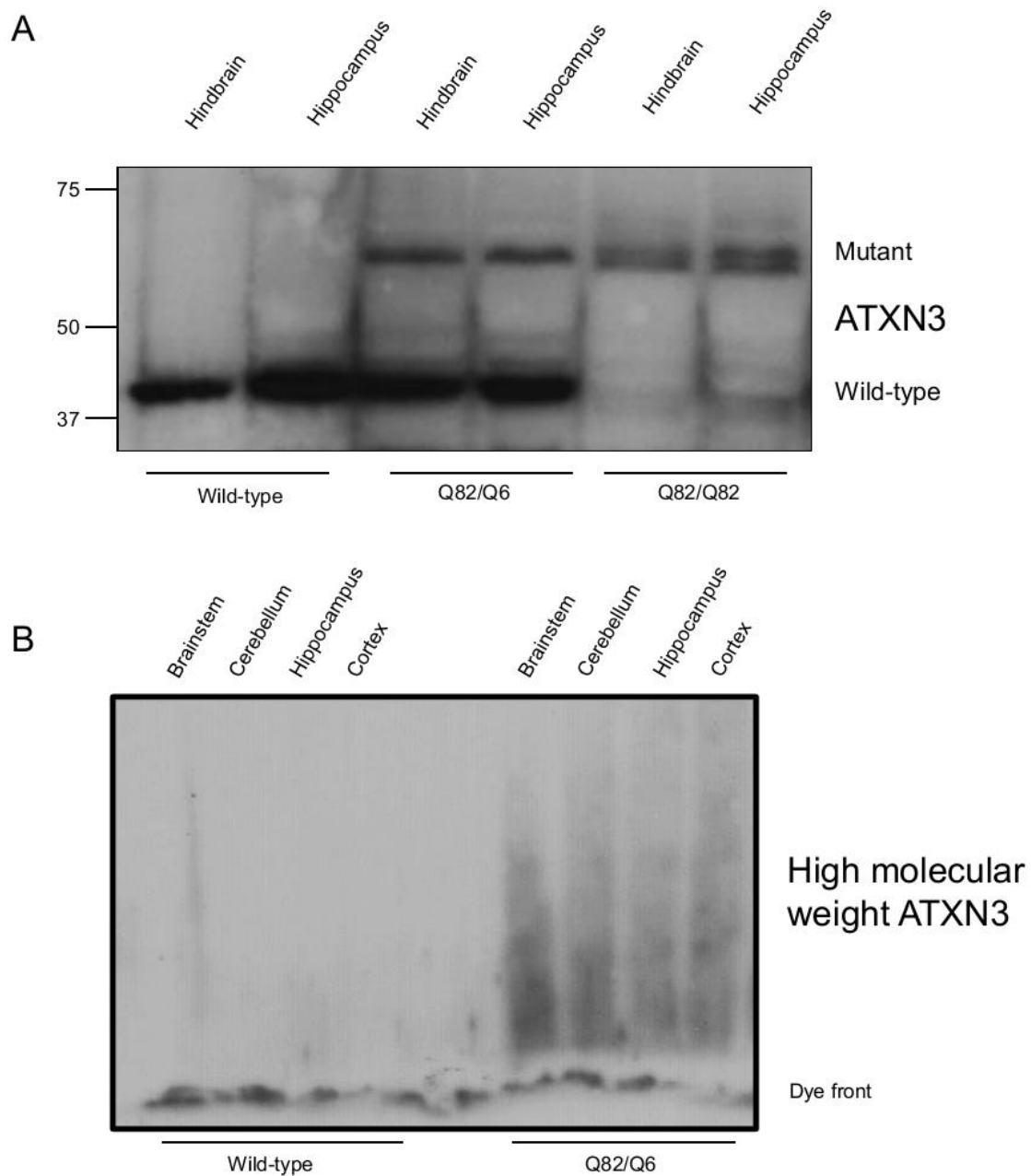


Figure 3.7 ATXN3 solubility and aggregation in different brain regions of Q82/Q6 mice. (A) 10% SDS-PAGE of soluble lysates from hindbrain and hippocampus. (B) 2% SDS-Agarose gel of soluble lysates from different brain regions in a wild-type and Q82/Q82 mouse

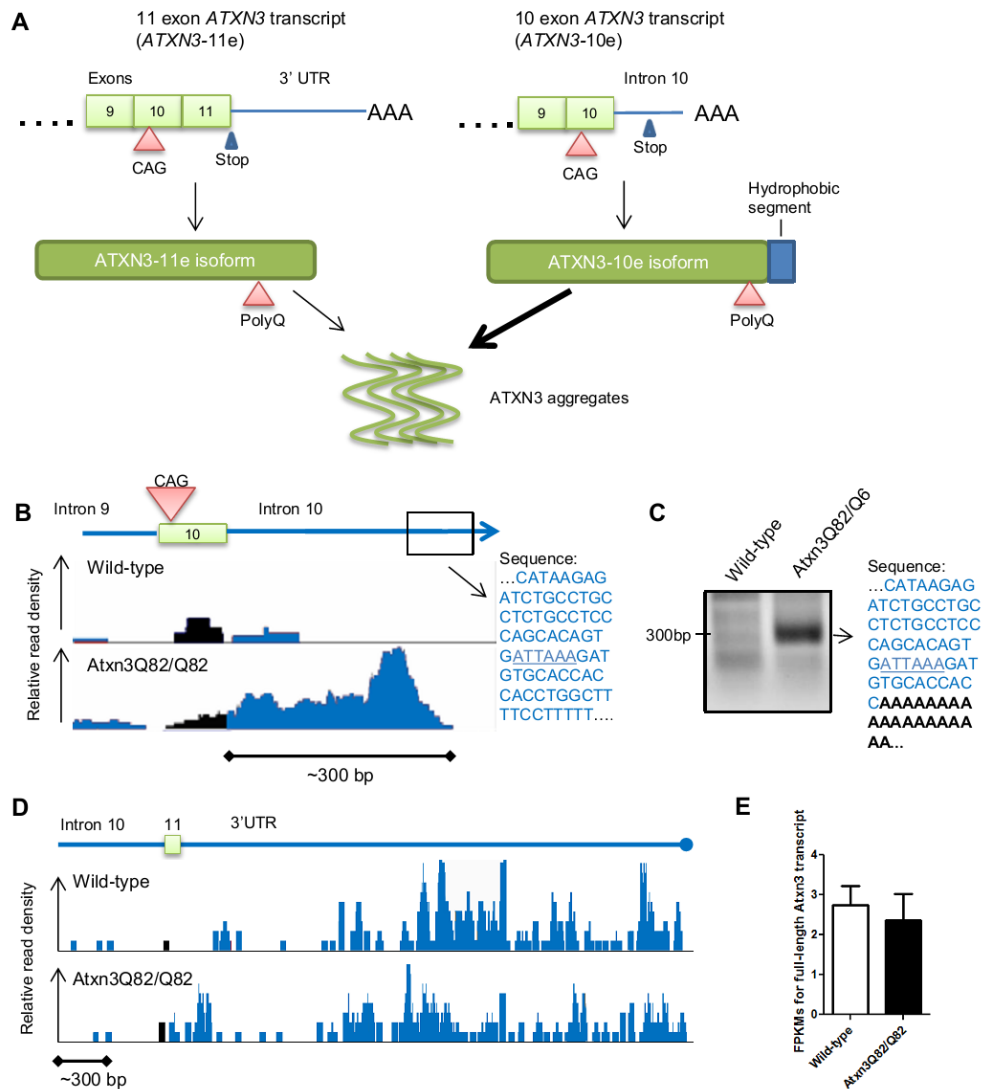


Figure 3.8 Alternative splicing of the mutant *Atxn3* transcript is enhanced in SCA3 knock-in mice. (A) Diagram of 3' alternative splicing of the human *ATXN3* transcript, showing the 10 exon-containing *ATXN3* transcript (right) generated from retention of intron 10, which encodes a hydrophobic segment that may accelerate mutant *ATXN3* aggregation. (B) RNA-sequencing on the pons of Q82/Q82 mice shows elevated reads in intron 10 following the CAG repeat-containing exon 10. Genomic sequence near the end of the reads in intron 10 (boxed) contains a putative polyadenylation (polyA) site ATTTAAA (underlined). (C) 3' RACE in a Q82/Q6 mouse amplified a 300 bp band containing this putative polyA site (underlined) followed by a polyA tail (black, bold). (D) Wild-type and homozygous Q82/Q82 mice showed similar frequency of sequencing reads in exon 11 and the 3' UTR of the SCA3 knock-in mice. (E) Levels of predicted full-length *Atxn3* transcript from the RNA-sequencing (FPKMs) do not significantly differ between wild-type (n=7) and Q82/Q82 mice (n=7). Graph represents mean plus standard deviation.

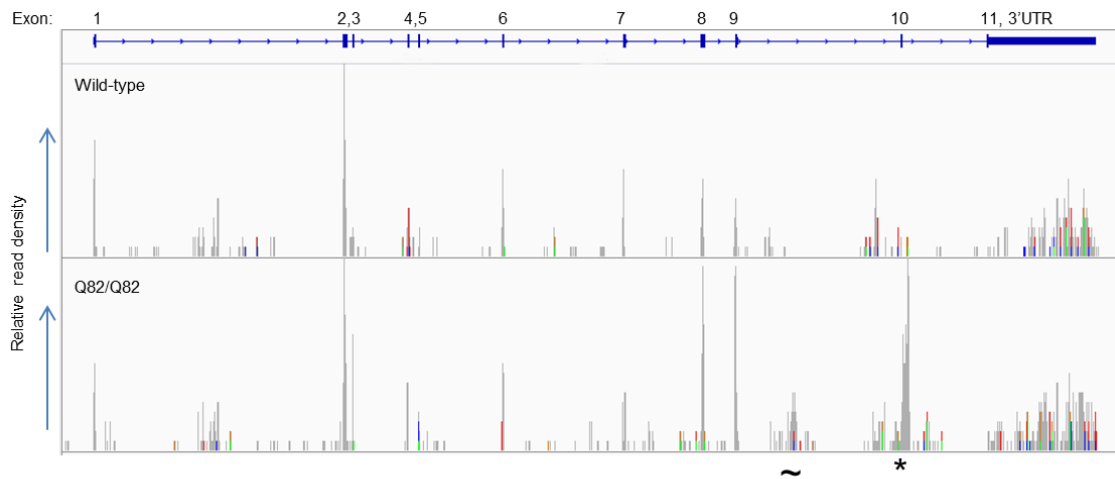


Figure 3.9 The mutant *Atxn3* transcript in SCA3 knock-in mice does not exhibit obvious abnormalities outside the exon 10-intron 10 junction. Reads across the full *Atxn3* transcript did not show consistent differences between representative wild-type and Q82/Q82 mice outside of the exon 10 – intron 10 junction (*), which shows dramatically elevated reads. The reads in intron 9 (~) do not consistently appear in other SCA3 knock-in mice.

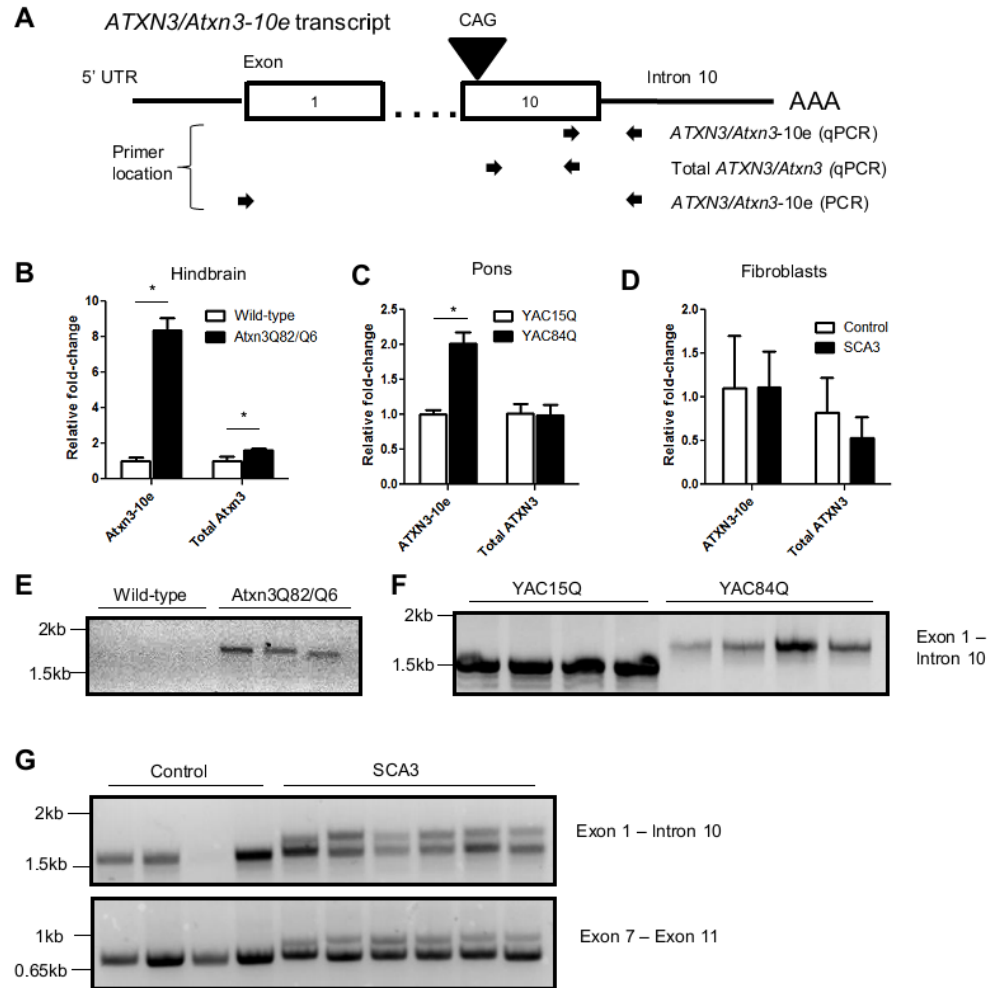


Figure 3.10 Expression of 10 exon *Atxn3/ATXN3* transcript in SCA3 mouse models and SCA3 human fibroblasts. (A) Diagram of 10 exon *ATXN3/Atxn3* (*ATXN3/Atxn3-10e*) transcript and arrows indicating location of primer pairs used for quantitative PCR (qRT-PCR) and non-quantitative PCR (PCR) on reversed-transcribed RNA. (B) *Atxn3-10e* transcript is highly upregulated (~8-fold) while total *Atxn3* transcript is only modestly upregulated (~1.5-fold) in heterozygous SCA3 knock-in mice (n=3). (C) *ATXN3-10e* transcript is also upregulated (~2-fold) in YAC mice expressing the full human *ATXN3* gene with 84 CAG repeats (YAC84Q, n=4) compared to 15 CAG repeats (YAC15Q, n=4). (D) *ATXN3-10e* transcript levels in SCA3 fibroblasts (n=6) did not significantly differ from non-disease control fibroblasts (n=4). qRT-PCR in B, C, and D were normalized to *Gapdh*, *TRIP11*, and *ACTB*, respectively. (E) PCR reveals the presence of mutant *Atxn3-10e* cDNA in SCA3 knock-in mice only. (F, G) PCR shows expanded and non-expanded *ATXN3-10e* in both YAC mouse lines, all SCA3 fibroblast lines, and three of four non-disease control fibroblast lines. Amplification of *ATXN3* exon 7 to exon 11 indicates the presence of *ATXN3-11e* in all fibroblast lines. Graphs represent the mean plus standard deviation. * p < 0.05 by an unpaired *t*-test (Mann-Whitney U).

Chapter 4

Isoform-driven aggregation of the polyglutamine disease protein ATXN3 elicits early transcriptional changes in the brain

4.1 Abstract

Polyglutamine-encoding CAG repeat expansions cause at least nine different neurodegenerative diseases, all of which are associated with aggregation of the respective disease proteins. The role of protein misfolding and aggregation in disease pathogenesis, however, remains uncertain. To address this issue, we utilized newly developed knock-in mouse models of Spinocerebellar Ataxia type 3 (SCA3) that display differential splicing of the mutant *Atxn3* disease gene transcript, resulting in different degrees of aggregation. Differential carboxy-terminal splicing markedly alters mutant ATXN3 aggregation in the brain of knock-in mice, with expression of a minor splice isoform accelerating aggregation of mutant ATXN3 and expression of a major splice isoform resulting in soluble mutant ATXN3. To determine whether transcriptional dysregulation, a common molecular feature of polyQ diseases, correlates with disease protein aggregation, we performed RNA-sequencing analysis in SCA3 knock-in mice and additional SCA3 mouse models displaying differing degrees of aggregation. In SCA3 mice, an altered

gene expression landscape correlated closely with degree of aggregation, with an unexpectedly high number of transcriptional changes predicted in oligodendrocytes. The encoded protein of one notably increased transcript, *ACY3*, was similarly increased in SCA3 disease brain, suggesting that similar transcriptional changes occur in the human disease. Finally, by utilizing Cre-recombinase's binding to a LoxP site in the mutant *Atxn3* locus, , we were simultaneously able to alter *Atxn3* splicing, increase ATXN3 solubility and reduce aggregate pathology, along with predicted gene expression changes. In summary, our findings delineate a clear relationship between mutant *Atxn3* splicing, ATXN3 aggregation, and early transcriptional changes *in vivo*. These findings support a pathogenic role for protein misfolding and aggregation in polyglutamine disease that may be critically influenced by disease gene splicing.

4.2 Introduction

Polyglutamine (polyQ) diseases are caused by abnormally long glutamine stretches encoded by CAG repeat expansions in the respective disease genes. Like many other neurodegenerative disorders, polyQ diseases are characterized by the accumulation and aggregation of misfolded disease proteins (4). In the nine known polyQ diseases including Spinocerebellar ataxia type 3 (SCA3), the clearest evidence of this process is the appearance of ubiquitin-positive neuronal inclusions containing the disease protein and other sequestered proteins (6, 100). An unresolved question, however, is the extent to which the aggregation propensity of expanded polyQ proteins, and aggregates themselves, contribute to disease pathogenesis. In multiple studies, inclusions are not correlated with toxicity and have been interpreted as protective to cells (35–38), yet factors that reduce polyQ disease protein aggregation, such as molecular chaperones,

often correlate with improved phenotypes in disease models (168, 185–187). Broadly acting cellular factors like chaperones, however, may exert beneficial effects independent of the polyQ disease protein.

One route to address the role of aggregation propensity in disease is to explore the consequences of expressing alternative disease protein isoforms that differ in aggregation. Alternative splicing of *ATXN3*, the disease gene in SCA3, can generate a diversity of *ATXN3* isoforms (108). Among these are two commonly studied isoforms: a major, full-length 11-exon containing transcript (*ATXN3*-11e, RefSeq NM_004993) (107) and a minor, 10-exon containing transcript lacking the 11th exon (*ATXN3*-10e, RefSeq S75313) (98). These two isoforms differ only in a small segment of the carboxy-terminus (Figure 4.1A). The *ATXN3*-10e transcript, which was the first reported isoform in SCA3, retains the intron following the CAG repeat-containing exon 10 and results in a more hydrophobic carboxy-terminus that likely increases *ATXN3* aggregation propensity (109). The extent to which differential expression of these two *ATXN3* isoforms contributes to disease protein aggregation and disease pathogenesis is unknown. We therefore sought to address two key questions: Does differential expression of *ATXN3* isoforms contribute to disease protein accumulation and aggregation in brain? And does the aggregation propensity of a polyQ-expanded isoform contribute to disease pathogenesis?

To address these questions, we investigated parallel SCA3 knock-in mouse models that differ in alternative splicing of the mutant *Atxn3* gene. In addition to the SCA3 knock-in mice discussed in Chapter 3 that preferentially express the aggregation-prone isoform, we isolated a variant SCA3 knock-in mouse line that predominantly expresses the full-length, major splice isoform of mutant *ATXN3* that is less prone to

aggregate. The existence of two lines expressing physiological levels of the disease gene with nearly identical polyQ expansions, yet differing in isoform expression, presented us with a rare opportunity to compare the effect of expressing different ATXN3 isoforms on disease protein aggregation and its downstream consequences. Because transcriptional dysregulation is a common feature of polyQ diseases and likely contributes to disease processes (53), we carried out comparative transcriptional profiling in the nervous system of these knock-in lines and other SCA3 mouse models to identify molecular correlates of ATXN3 aggregation. Our findings shed light both on the role of alternative splicing in disease protein aggregation and on the potential contribution of aggregation to transcriptional dysregulation in SCA3 and perhaps other polyQ disorders.

4.3 Results

4.3.1 Distinct SCA3 knock-in lines express different mutant *Atxn3* transcripts

Alternative mutant *Atxn3* transcripts expressed in distinct SCA3 knock-in mouse lines. For the current study we used SCA3 knock-in mice generated by homologous recombination, in which the endogenous *Atxn3* exon 10 was replaced with a mutant exon 10 harboring an expanded (82) CAG repeat (Chapter 3). We reported that SCA3 knock-in (Q82) mice robustly express the *Atxn3*-10e transcript and exhibit low levels of soluble mutant ATXN3, with a correspondingly high burden of aggregated mutant ATXN3 in the brain. In generating the SCA3 knock-in colony, we serendipitously identified a knock-in mouse variant that expresses comparatively high levels of soluble mutant ATXN3 despite having a nearly identical CAG repeat expansion. This more soluble ATXN3 phenotype segregated with the mutant allele and was maintained in subsequent generations, allowing

us to selectively breed a “variant” SCA3 knock-in line (Q82V mice) that could be studied in parallel to Q82 mice.

Western blot analysis (Figure 4.1B) demonstrated that heterozygous Q82V/Q6 mice express higher levels of soluble mutant ATXN3 in brain than do heterozygous Q82/Q6 mice. As in other polyQ disease models (80, 81), repeat expansion lengths vary slightly from animal to animal in both lines due to mild repeat instability, but these subtle differences in repeat length did not correlate with or explain this difference in solubility. To explore the molecular basis of this difference, we performed non-quantitative PCR on reverse-transcribed RNA (RT-PCR) to examine different *Atxn3* isoform transcripts in the brain. The aggregation-prone ATXN3-10e isoform was expressed in Q82/Q6 mice, as reported in Chapter 3, but not in Q82V/Q6 or wild-type mice (Figure 4.1C). In contrast, the full-length *Atxn3*-11e isoform was readily detected in Q82V/Q6 mice but not in Q82/Q6 mice (Figure 4.1C). Quantitative PCR on the same samples confirmed higher levels of *Atxn3*-10e transcript in Q82/Q6 mice (Figure 4.1D).

To determine if the two SCA3 knock-in lines express mutant *Atxn3* transcripts at similar endogenous levels, we calculated transcript levels using RNA-sequencing (RNA-seq) reads from the pons of wild-type, Q82/Q6, and Q82V/Q6 mice. Total *Atxn3* transcripts are elevated ~2-fold in Q82/Q6 mice, whereas *Atxn3*-11e transcript levels are equal across genotypes (Figure 4.1E), suggesting that Q82/Q6 mice express mutant *Atxn3*-11e transcript in addition to mutant *Atxn3*-10e transcript. These results indicate approximately physiological expression of different mutant *Atxn3* transcripts in SCA3 knock-in lines with the Q82 line expressing more ATXN3.

We have not yet identified a genetic difference that delineates the two different SCA3 knock-in mouse lines. Sequencing of ~8,000 base pairs in homozygous Q82/Q82 and Q82V/Q82V mice showed no differences in the sequenced regions, which spanned most of intron 9 including the FRT site, and all of *Atxn3* exon 10, intron 10 and exon 11. In both lines we confirmed the presence of a LoxP site immediately upstream of the FRT site, included in the original targeting construct. Later in this study we exploit this LoxP site to convert Q82 mice to a phenotype similar to that of Q82V mice. We also cloned and sequenced the mutant *Atxn3*-10e and *Atxn3*-11e cDNA expressed in the respective homozygous SCA3 knock-in mice, and found no sequence differences apart from the alternatively spliced exons preferentially expressed in the two lines (not shown).

In summary, we isolated two distinct SCA3 knock-in lines that differentially express, from the endogenous *Atxn3* locus, mutant *Atxn3* transcripts encoding two ATXN3 isoforms with alternative carboxy-termini predicted to differ in solubility (Figure 4.2). These mice provide an ideal opportunity to investigate the pathophysiological consequences of altered mutant ATXN3 isoform expression on disease protein accumulation and aggregation.

4.3.2 ATXN3 accumulation in neuronal nuclei and aggregation differs in the two SCA3 knock-in lines

To determine if endogenous expression of the different isoforms leads to differences in ATXN3 accumulation in the nervous system, we performed immunohistochemical staining (IHC) for ATXN3 on one-year-old SCA3 knock-in brains. Q82/Q6 mice show robust intranuclear ATXN3 accumulation, both diffuse and punctate, as well as larger inclusions in neurons, both intranuclear and extranuclear. In contrast,

ATXN3 immunostaining in Q82V/Q6 mice showed no aggregate pathology and was indistinguishable from that of wild-type mice (Figure 4.3A). To identify biochemical differences in aggregation, we immunoprecipitated ATXN3 from both lines, resolved the eluted immunoprecipitates on polyacrylamide gradient gels, and immunoblotted for ATXN3. Compared to Q82V/Q6 mice, Q82/Q6 mice showed increased levels of high molecular weight ATXN3 species with correspondingly lower levels of soluble ATXN3 monomer (Figure 4.3B).

As reported in Chapter 3, aggregation-positive Q82/Q6 mice do not develop motor abnormalities. Conceivably, the higher levels of soluble mutant ATXN3 in Q82V mice could accelerate a behavioral phenotype. Thus, we assessed motor performance in aged (53-60 week old) SCA3 knock-in mice from both lines. Neither Q82/Q6 nor Q82V/Q6 mice showed deficits on any motor tasks compared to wild-type mice (Figure 4.3 C-F). Q82/Q6 mice tend to be slightly smaller than wild-type or Q82V/Q6 mice (Figure 4.3E and F), but otherwise appear healthy.

To exclude the possibility that the increased ATXN3 aggregation in Q82/Q6 mice is driven primarily by its ~2-fold increase in overall *Atn3* transcript levels, we generated homozygous Q82V/Q82V mice containing two mutant alleles. These mice show an even higher level of soluble mutant ATXN3 (Figure 4.4A) yet still relatively little ATXN3 accumulation and aggregation in the brain. Even at one year of age, Q82V/Q82V mice show minimal ATXN3 diffuse nuclear accumulation and ATXN3 puncta by IHC compared to age-matched Q82/Q6 mice (Figure 4.4B). An exception is that, upon aging, Q82V/Q82V mice begin to exhibit large extranuclear aggregates in the hippocampus, reminiscent of the hippocampal aggregate in heterozygous Q82/Q6 mice. Blinded scoring

of aggregate pathology in the pons and hippocampus of SCA3 knock-in mice confirmed robust ATXN3 aggregation in Q82/Q6 mice, some in Q82V/Q82V mice, and none in Q82V/Q6 mice (Figure 4.4C).

In further confirming the differing aggregation propensities of the different SCA3 knock-in lines, IHC of a ~8-week-old Q82/Q82 mouse showed enhanced nuclear accumulation of ATXN3 in the DCN, while a Q82V/Q82V showed no nuclear accumulation (Figure 4.4D). These differences in accumulation correlated with differing relative expression of *Atn3-10e* in the same mice (Figure 4.4E). Together, these results establish that expression of the mutant ATXN3-10e isoform is associated with increased ATXN3 aggregation and nuclear accumulation compared to equivalent expression of the alternative mutant isoform, ATXN3-11e. These differences may arise from the differing predicted solubility of ATXN3 isoforms (Figure 4.2). Therefore, alternative splicing of the ATXN3 disease allele may influence disease protein aggregation.

4.3.3 Transcriptional alterations are associated with ATXN3 nuclear accumulation and aggregation in SCA3 mouse models

Transcriptional dysregulation is a frequent feature of polyQ diseases (188, 189), and transcriptional profiling readily detects early perturbations in gene expression elicited by abnormal disease proteins. Accordingly, we performed RNA-seq on a vulnerable brain region in SCA3, the pons, in both knock-in lines as well as in an unrelated mouse model of SCA3 to determine whether ATXN3's propensity to accumulate and aggregate correlated with specific transcriptional changes. A list of the genotypes used for RNA-seq and the relative abundance of ATXN3 aggregates in the pons of the various lines are shown in Figure 4.5A. In addition to analyzing wild-type mice, heterozygous Q82, and

both heterozygous and homozygous Q82V mice, we also examined two transgenic lines that overexpress the full human ATXN3 gene with either a normal (15Q) or pathogenic (84Q) CAG repeat, the YAC-15Q and YAC-84Q lines (159). YAC-84Q mice show robust ATXN3 accumulation and aggregation throughout the brain, including in the pons, while YAC-15Q mice overexpress normal human ATXN3 without aggregation or intranuclear accumulation (159).

The three tested aggregation-positive lines (YAC-84Q, Q82/Q6, and Q82V/Q82V mice) exhibited more than 200 differentially expressed (DE) transcripts compared to wild-type mice, whereas the aggregation-negative lines (YAC-15Q and Q82V/Q6 mice) exhibited fewer than 100. Thus, the presence of aggregate-prone ATXN3 generally correlated with increased transcriptional changes (Figure 4.5B).

YAC-84Q mice have the most robust aggregation profile among tested genotypes. To determine the extent to which altered transcripts in YAC-84Q mice are shared with other SCA3 mice, we generated a heat map of the differentially expressed transcripts of YAC-84Q using fold-change values relative to wild-type, and we compared their expression across all tested genotypes. The greatest number of transcriptional changes was shared with Q82/Q6 mice which, like YAC-84Q mice, have a high aggregate burden. A significant subset of changes was also shared with Q82V/Q82V mice, which manifest aggregates albeit fewer than the other two lines. In contrast, aggregation-negative YAC-15Q and Q82V/Q6 mice shared relatively few changes with YAC-84Q mice and were most similar to wild type mice (Figure 4.5C).

To explore the trends in transcriptional changes, we graphed the number of shared transcripts between the different mutant ATXN3-expressing lines (Figure 4.5D). Only

seven changed transcripts, all but one downregulated, were shared across all four mutant ATXN3-expressing lines; none of these genes were altered in YAC-15Q mice. These seven may represent transcripts altered by polyQ-expanded ATXN3 expression independent of aggregation. A comparison of transcriptional changes shared by all three aggregation-positive genotypes revealed a balance of 21 upregulated and 18 downregulated genes, suggesting that ATXN3 aggregation may drive upregulation of certain transcripts.

Among the differentially expressed transcripts shared between any two genotypes, YAC-84Q and Q82/Q6 mice share the most: 56 upregulated and 33 downregulated transcripts. Based on predicted cell type expression patterns (165), differentially expressed transcripts are preferentially expressed in oligodendrocytes (Figure 4.5E). Consistent with this observation, gene enrichment analysis of these 89 transcripts identified categories associated with myelination and oligodendrocyte development (Figure 4.6).

An unanswered question in SCA3 and other polyQ diseases is the extent to which disease pathogenesis is associated with loss of function of the mutant protein. To address this, we performed a separate RNA-seq experiment on the pons of Q82/Q82 mice and ATXN3 knockout (ATXN3-KO) mice at ~9 weeks of age. A heat map of the same list of transcripts from Figure 4.5C, the differentially expressed transcripts of YAC-84Q mice, showed a similar transcriptional signature in Q82/Q82 mice, but not in ATXN3-KO mice (Figure 4.7A). A Venn diagram of the differentially expressed transcripts showed that a much larger number of transcripts are altered in Q82/Q82 mice than in ATXN3-KO mice: 570 versus 91 transcripts, respectively (Figure 4.7B). This Venn diagram reveals

that 22 altered transcripts are shared between Q82/Q82 and ATXN3-KO mice, representing a small number of transcripts that could be altered due to loss of ATXN3 function. In contrast, a higher number of DE transcripts, 59, are shared between Q82/Q82, Q82/Q6, and YAC-84Q mice (Figure 4.7C). Together, these results indicate that majority of transcriptional changes in aggregate-containing mice do not represent changes due to loss of ATXN3 function. These findings further support the view that aggregation in SCA3, and perhaps other polyQ diseases, drives molecular changes through toxic gain-of-function mechanisms.

We validated a subset of robustly altered transcripts in an independent set of Q82/Q6 mice to ensure reproducibility and to identify transcripts that might serve as biomarkers correlating with disease protein aggregation. qRT-PCR on pontine tissue from six month old Q82/Q6 and Q82V/Q6 mice confirmed selective upregulation of *Acy3* and *Smoc1* and selective downregulation of *Agt* and *Dao* in Q82/Q6 mice; *Il33*, as predicted by RNA-seq, was reduced in both Q82/Q6 and Q82V/Q6 mice (Figure 4.8A). Only one tested transcript, *Polr2a*, was not confirmed as significantly altered.

Because of the robust change in *Acy3* associated with ATXN3 aggregation in mouse models, we analyzed ACY3 at the protein level. Western blotting for ACY3 in hindbrain lysates confirmed that the ACY3 protein is selectively upregulated in Q82/Q6 mice (Figure 4.8B). Importantly, ACY3 protein levels are also significantly increased in SCA3 human brainstem compared to Alzheimer Disease (AD) brainstem controls (Figure 4.8C), suggesting that altered transcripts in SCA3 mice may predict congruent changes in human disease. In summary, the propensity of ATXN3 to accumulate in neuronal nuclei and form aggregates in the pons correlates with specific robust transcriptional changes.

4.3.4 Cre-recombinase expression in Q82 mice alters *Atxn3* splicing and attendant aggregation

The molecular basis for differential splicing in the two knock-in lines may center on the LoxP site located ~300 bp upstream of exon 10, because we can partially convert the *Atxn3* splicing pattern of Q82/Q6 mice to that of Q82V/Q6 mice (Figure 4.9A). We expressed Cre-recombinase in Q82/Q6 mice under control of the Nestin promoter (Q82/Q6+Cre) to drive Cre expression in the brain and elicit alterations in *Atxn3* splicing. Q82/Q6+Cre mice show reduced levels of *Atxn3*-10e transcript by RT-PCR and qRT-PCR (Figure 4.9A and B). Consistent with this change, Q82/Q6+Cre mice also showed detectable *Atxn3*-11e transcript by RT-PCR, similar to Q82V mice (Figure 4.9A). Consistent with this change in splice isoform expression, we observed reduced levels of high molecular weight, aggregated ATXN3 and increased soluble monomeric ATXN3 in two month old Q82/Q6+Cre mice (Figure 4.9C). Finally, of the four robustly dysregulated transcripts confirmed in Q82/Q6 mice (Figure 4.8), qRT-PCR showed that three of these four (*Acy3*, *Smoc1*, and *Agt*) were significantly corrected towards wild-type levels in Q82/Q6+Cre mice (Figure 4.9D). These experiments provide converging evidence for an association between ATXN3-10e isoform expression, mutant ATXN3 aggregation, and selective transcriptional changes presumably linked to ATXN3 aggregation.

4.4 Discussion

Our comparison of SCA3 knock-in mice differentially expressing the two most disease-relevant ATXN3 splice isoforms illustrates that isoform expression can profoundly influence polyQ disease protein accumulation and aggregation. Comparison

of transcriptional changes in both knock-in lines and in independent transgenic lines expressing normal or expanded human ATXN3 further showed that the presence of aggregated ATXN3 correlates with transcriptional changes in the nervous system. While attention in the polyQ disease field has focused on neurons, many altered brain transcripts in aggregate-positive mice are known to be enriched in oligodendrocytes. Among these is *ACY3*, which encodes an aminoacylase that is predicted to hydrolyze N-acetylaspartate (NAA) into acetate and aspartate, and this upregulation may contribute to the decreased level of NAA reported in SCA3 brain (190). The contribution of nonneuronal cells to disease pathogenesis in SCA3 and other polyQ disorders warrants further study.

The expression of two major mutant ATXN3 isoforms studied here, identical except for their extreme carboxy-termini, leads to marked differences in ATXN3 accumulation and aggregation *in vivo*. Just as expressing polyQ fragments of full-length disease proteins can accelerate disease pathogenesis (23, 26), even a single exon difference in polyQ disease protein isoforms can markedly alter disease protein accumulation in the brain. Furthermore, our findings indicate that the diffuse nuclear accumulation of mutant ATXN3 is associated with its aggregation propensity. Importantly, an expanded polyQ tract in the disease range is *not* sufficient to drive ATXN3 into the nucleus *in vivo*. These results further underscore the importance of protein context in the polyQ diseases to influence disease pathogenesis.

The relatively low-level of expression from the endogenous *Atn3* locus in the knock-in mice may have aided our ability to capture relatively subtle differences in ATXN3 isoform solubility. The human and mouse ATXN3 isoforms are predicted to show differences in solubility based on their amino acid composition (Figure 4.2).

However, overexpression of the mutant mouse ATXN3 in cell culture did not reveal dramatic differences in puncta and inclusion formation between the two different isoforms with similar polyQ lengths (Figure 4.10).

Efforts to identify the presumed genetic difference that drives differential *Atxn3* splicing in the Q82 and Q82V lines are ongoing. Intriguingly, both the SCA3 knock-in lines were generated from one founder mouse. This founder was crossed with a FLPe transgenic mouse, generating two F1 (FLPe-expressing) SCA3 knock-in mice that were further bred with wild-type mice to generate F2 mice harboring the CAG expansion in *Atxn3* with the Neo cassette removed (Figure 4.11A). We retrospectively examined protein and brain from these two F1 mice and found no differences in solubility between the two lines (Figure 4.11B). Moreover, RT-PCR revealed *Atxn3*-10e and *Atxn3*-11e transcripts at similar levels in both mice (Figure 4.11C). These results, together, suggest that the Q82 and Q82V lines appeared subsequent to the removal of the Neo cassette. We have not yet examined F2 mice to test this hypothesis.

The close segregation of this difference with the mutant *Atxn3* allele, persisting even in homozygous mice, implies a *cis*-acting factor. To rule out a potentially protective *trans*-acting factor in the Q82V line that can rescue ATXN3 aggregation, we generated a “hybrid” homozygous Q82V/Q82 mouse. IHC of this mouse at ~12 weeks did not show increased or decreased nuclear ATXN3 or inclusion formation in the brainstem or hippocampus (Figure 4.11D). Western blotting of this mouse also segregated two distinct mutant ATXN3 bands with differing intensities (Figure 4.11E), further supporting the possibility that the knock-in lines differ with respect to a *cis*-acting element at the *Atxn3* gene. However, sequestration of the more soluble ATXN3 species by the aggregation-

prone ATXN3 species generated by the Q82 mouse may confound this interpretation. These findings are preliminary and must be repeated, but still exclude the possibility that a *trans*-acting factor in the Q82V line rescues ATXN3 aggregation. We are currently performing whole genome sequencing to identify possible mutations that explain the differences between the two lines.

The ability of coexpressed Cre-recombinase to partially convert the splicing pattern of Q82 mice to that of Q82V mice further supports the view that the different molecular phenotypes of the two lines directly reflect different ATXN3 isoform expression. We speculate that Cre-recombinase may act by binding the single LoxP sequence, potentially altering kinetics of *Atxn3* transcription, thereby affecting splicing (183). The ability of Cre-recombinase to drive these phenomena indicates that the Q82 mice resemble a “conditional” mouse in which aggregation could be manipulated in different cell-types. One could exploit this to address the extent to which ATXN3 aggregation drives transcriptional changes in neurons versus non-neuronal cells through cell-autonomous mechanisms.

Although the reduced solubility of the polyQ expanded disease protein likely contributes to disease pathogenesis, isolating the disease protein species responsible for this toxicity *in vivo* remains an active area of pursuit. The aggregation propensity of disease protein drives the formation of intranuclear puncta/inclusions and biochemically insoluble aggregate species associated with disease. These easily visualized structures themselves may not be directly toxic and do not exclude the pathogenic role of monomeric or oligomeric polyQ protein species upstream in the aggregation cascade that are more difficult to detect (11, 42, 46). We suggest that the inclusions and aggregates *in*

in vivo represent disease biomarkers that reflect the overall increased presence of abnormal disease protein, including both toxic and non-toxic conformers. Ongoing studies aim to identify levels of polyQ disease protein conformers *in vivo* that best predict toxicity. At present, therapies to reduce the aggregate burden should remain a viable approach, provided that therapies primarily do so by improving disease protein folding or clearance.

Our findings support the notion that transcriptional alterations reflect disease-associated processes imposed by disease protein accumulation and aggregation. Accordingly, only SCA3 mouse models showing signs of aggregation also shared robust transcriptional changes. In contrast, high levels of soluble, expanded ATXN3 in Q82V mice were not sufficient to drive the early transcriptional changes seen in ATXN3 aggregate-positive mice, and overexpression of nonexpanded ATXN3 in YAC-15Q mice caused almost no transcriptional perturbation. Moreover, ATXN3-KO mice did not show much overlap with ATXN3 aggregation-associated transcriptional profiles. Studies from models of HD and SCA3 have shown that treatments that improve disease phenotypes correlate with corrected transcriptional changes (191–193). Our findings are particularly novel in establishing that, for mutant ATXN3 isoforms harboring the same polyQ repeat length, the propensity for ATXN3 to accumulate and aggregate most directly correlates with an altered transcriptional signature *in vivo*. These transcriptional changes conceivably occur alongside or may even directly connect with pathways that drive toxicity. However, a lack of neurotoxic readouts in these SCA3 mouse models limits conclusions we can draw about causal links between disease protein aggregation, transcriptional changes, and toxicity. The future identification of neuropathological

abnormalities that coincide with disease protein aggregation in the SCA3 mouse models would be informative.

Increasing evidence supports glial contributions to polyQ disease (194). In SCA7, for example, mutant ATXN7 drives dysfunction of Bergmann glia that ultimately drives Purkinje neuron dysfunction and death (195, 196). Recently, a HD knock-in mouse model was reported to exhibit early myelination defects potentially precipitated by altered oligodendrocyte differentiation (148). Another recent study showed that expressing mutant HTT in oligodendrocytes alone is sufficient to induce demyelination and behavioral abnormalities in mice (197). Oligodendrocyte dysfunction is also featured in ALS (198), in which the expression of aggregation-prone mutant SOD1 in oligodendrocyte progenitors contributes to disease onset in a mouse model (199). Our analysis of transcriptional changes in SCA3 mouse models showed that the majority of altered transcripts are most highly expressed in oligodendrocytes, but the process that driving this is unclear. The transcriptional profile probably does not reflect changes in oligodendrocyte number since the identified oligodendrocyte-associated transcripts in SCA3 mice include large portions of elevated and reduced transcripts. Although we did not observe clear nuclear ATXN3 accumulation or aggregation in oligodendrocytes by immunofluorescence, small ATXN3 oligomers and microaggregates may drive transcriptional changes cell-autonomously.

While oligodendrocyte pathology has not been closely studied in SCA3, the human disease exhibits clear white matter abnormalities. Magnetic resonance imaging (MRI) of SCA3 brains have shown significant reduction in pontine white matter that correlates with clinical disease severity (200, 201). Outside the CNS, cytoplasmic

ATXN3 aggregates have been detected in Schwann cells of SCA3 disease tissue (202), and YAC-84Q mice exhibit diminished myelination of the sciatic nerve (159). SCA3 knock-in mice may not practically allow examination of demyelination in the pons, where myelinated fibers are particularly heterogeneous and difficult to quantify, but further analysis of aged YAC-84Q and homozygous Q82 mice may help establish functional consequences of dysregulated oligodendrocyte transcripts.

4.5 Acknowledgements

We thank members of the Paulson lab and Dr. Roger Albin for helpful discussion on the manuscript. This work utilized core services provided by the University of Michigan DNA sequencing core. This work was supported by the National Institutes of Health [RO1NS038712, RO3NS072967 to H.L.P.; F31NS083167 to B.R.; the University of Iowa Medical Scientist Training Program to G.H.]; and the University of Michigan Rackham School of Graduate Studies to B.R.

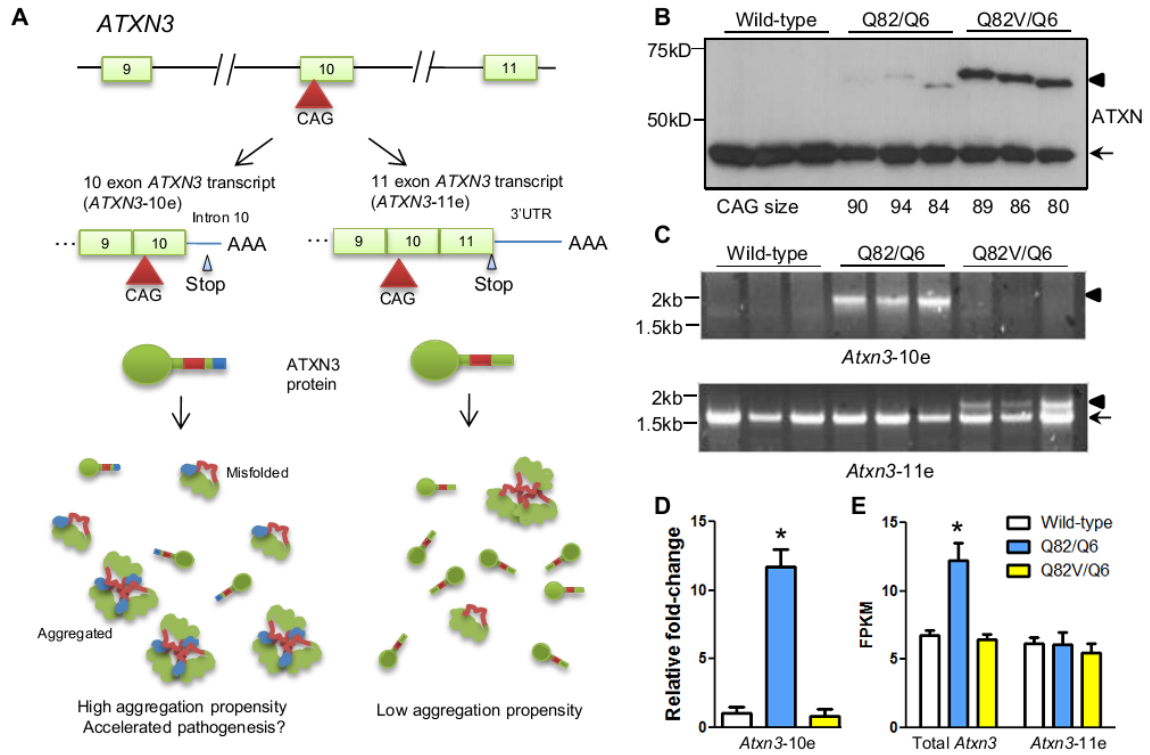
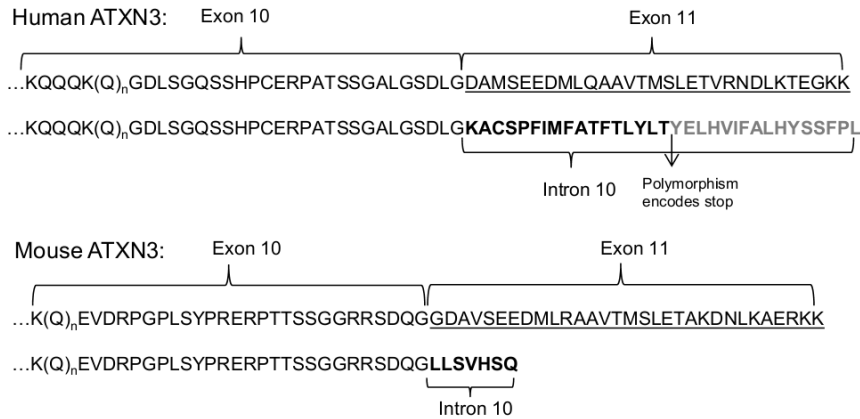


Figure 4.1 SCA3 knock-in lines express different *Atxn3* transcripts. (A) The human *ATXN3* gene expressed at least two different transcripts: a full-length *ATXN3* transcript with 11 exons (*ATXN3-11e*, right) and alternate transcript generated by retaining intron 10 (*ATXN3-10e*, left), which encodes a different carboxy-terminus that makes it more aggregation-prone. This chapter shows that the *Atxn3-10e* transcript in SCA3 knock-in mice is associated with accelerated disease protein aggregation in the brain and may accelerate pathogenesis. (B) Western blot analysis of brain shows that “variant” SCA3 knock-in mice (Q82V/Q6) express high soluble levels of mutant ATXN3 compared to our previously reported Q82/Q6 mice despite harboring similar CAG repeat lengths. (C) Non-quantitative RT-PCR amplified mutant *Atxn3-10e* cDNA in only Q82/Q6 mice and full-length mutant *Atxn3* cDNA only in Q82V/Q6 mice. (D) Quantitative RT-PCR (qRT-PCR, left) with primers specific to *Atxn3-10e* confirmed enhanced relative expression in Q82/Q6 mice (E) Calculated transcript levels from RNA-seq reads (FPKM, right) of the pons showed ~2-fold increase in total *Atxn3* in Q82/Q6 mice compared to wild-type or Q82V/Q6 mice, but equal *Atxn3-11e* between all genotypes. Arrows: wild-type ATXN3; arrowhead: mutant ATXN3. * $p < 0.05$



The grand average of hydropathicity (GRAVY)

<http://www.gravy-calculator.de/>

More positive value indicates higher hydropathicity

Human ATXN3-11e
GRAVY: -0.70415512465374

Human ATXN3-10e
GRAVY: -0.55686813186813

Mouse ATXN3-11e
GRAVY: -0.6769014084507

Mouse ATXN3-10e
GRAVY: -0.64471299093656

Mouse ATXN3 exon 11 (GDAVSEEDMLRAAVTMSLETAKDNLKAERKK)
GRAVY: -0.75483870967742

Mouse ATXN3 intron 10 (LLSVHSQ)
GRAVY: 0.5

Figure 4.2. Human and murine ATXN3-10e isoforms are predicted to have greater hydrophobicity. Protein sequences encoded from *ATXN3/Atxn3* Exon 10/11 and Exon 10/intron 10 are shown above. Calculating the grand average of hydropathicity (GRAVY) for the full-length protein or differentially encoded segment showed a higher positive value for 10e isoforms, reflecting a higher amount of hydrophobic amino acids.

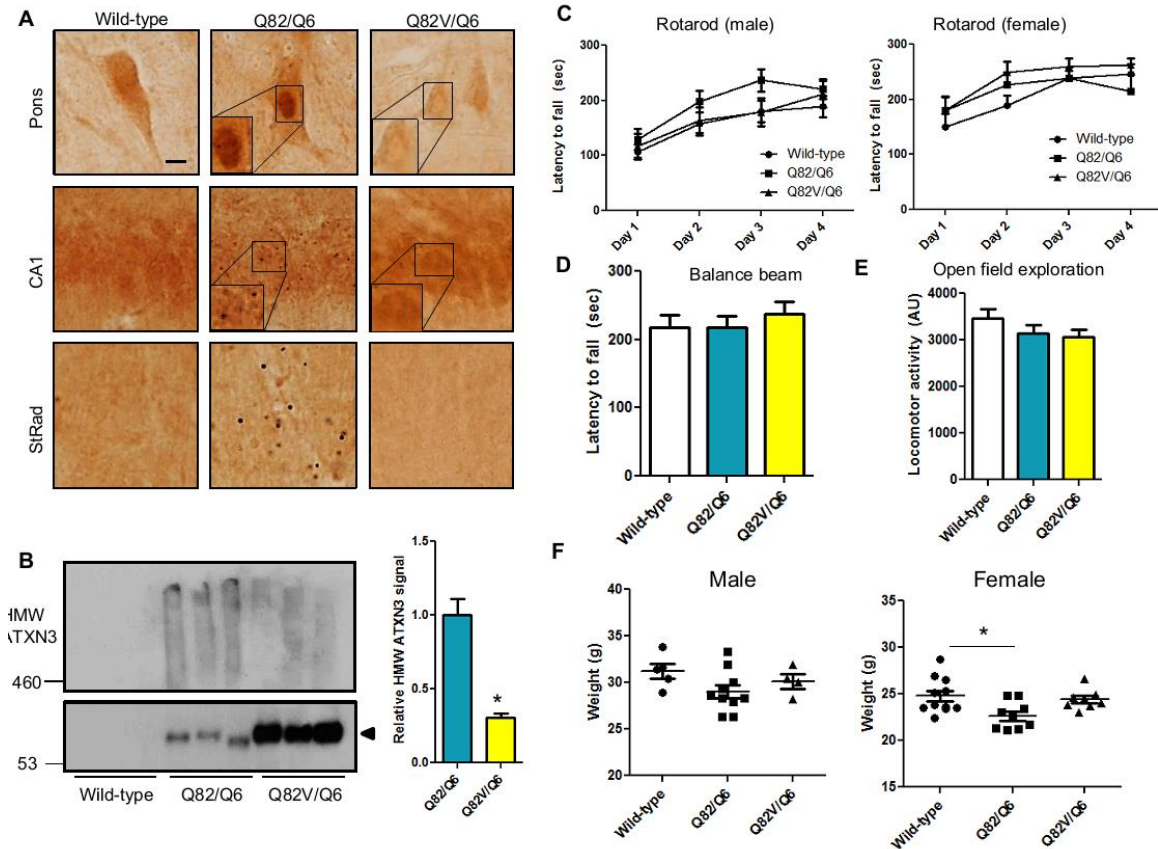


Figure 4.3 ATXN3 aggregation is increased in SCA3 knock-in mice expressing *Atxn3-10e*. (A) Immunohistochemical staining (IHC) for ATXN3 in ~1-year-old brains shows prominent nuclear accumulation and intraneuronal inclusions throughout the brain in Q82/Q6 mice, including in the pons, deep cerebellar nuclei (DCN), in hippocampus (CA1 and stratum radiatum, StRad), but not in Q82V/Q6 mice. Scale bar = 10mm. (B) ATXN3 immunoprecipitated from brain lysates, resolved on a polyacrylamide gradient gel and probed for ATXN3, show reduced high molecular weight (HMW) ATXN3 species in Q82V/Q6 mice compared to Q82/Q6 mice with a corresponding increase in soluble ATXN3 (arrowhead). Quantification of the HMW ATXN3 is shown on the right. (C-F) 53 to 60-week-old mice showed no differences in motor performance on rotarod (C), balance beam (D), or open field (E). Genotypes included wild-type (n=19), Q82/Q6 (n=19), and Q82V/Q6 (n=18) mice. Female Q82/Q6 mice showed a slightly reduced weight (F). Graphs represent the mean \pm SD (B) or SEM (C-F) * $p < 0.05$.

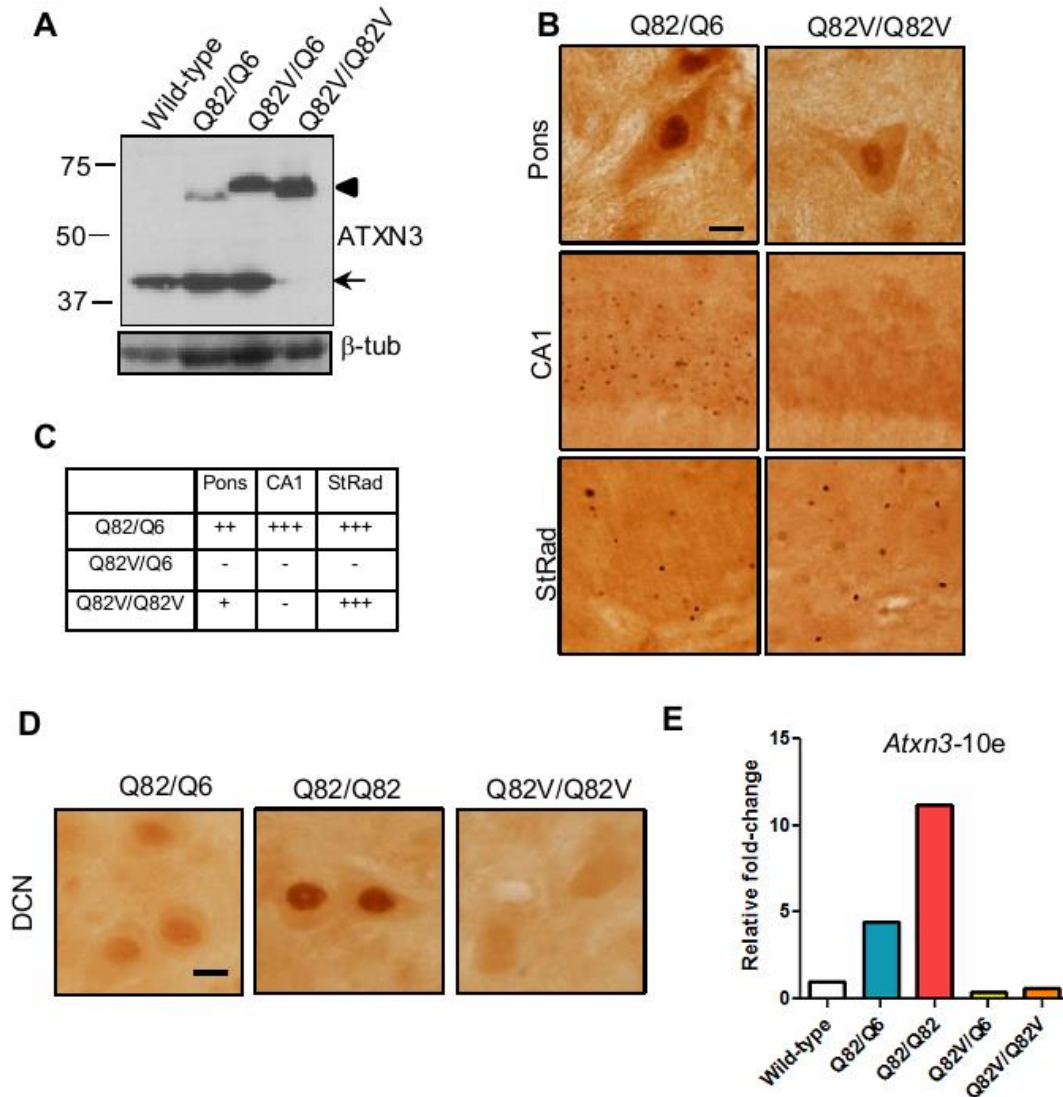


Figure 4.4. ATXN3 aggregation remains low in homozygous variant SCA3 knock-in mice. (A) Western blot analysis of Q82V/Q82V mouse brain show higher levels of soluble mutant ATXN3 (arrowhead) compared to a Q82/Q6 mouse. Arrow: wild-type ATXN3. (B) IHC of ATXN3 in a ~48-week-old homozygous Q82V/Q82V still show markedly reduced nuclear accumulation and inclusion formation in the brainstem and hippocampus compared to an age-matched Q82/Q6 mouse. Q82V/Q82V mice contain large extranuclear inclusions in the hippocampus similar to Q82/Q6 mice. Scale bar = 10µm (C) Table summarizing the aggregate amount scored in different regions of n=3 SCA3 knock-in mice at ~48 weeks of age. (D) IHC for ATXN3 mice shows further enhanced nuclear ATXN3 in the DCN of a ~8-week-old Q82/Q82 mouse and no apparent nuclear accumulation in an age-matched Q82V/Q82V mouse. (E) qRT-PCR of hindbrain RNA of the mice from (D) showed ATXN3 nuclear accumulation correlated with relative *Atxn3-10e* expression.

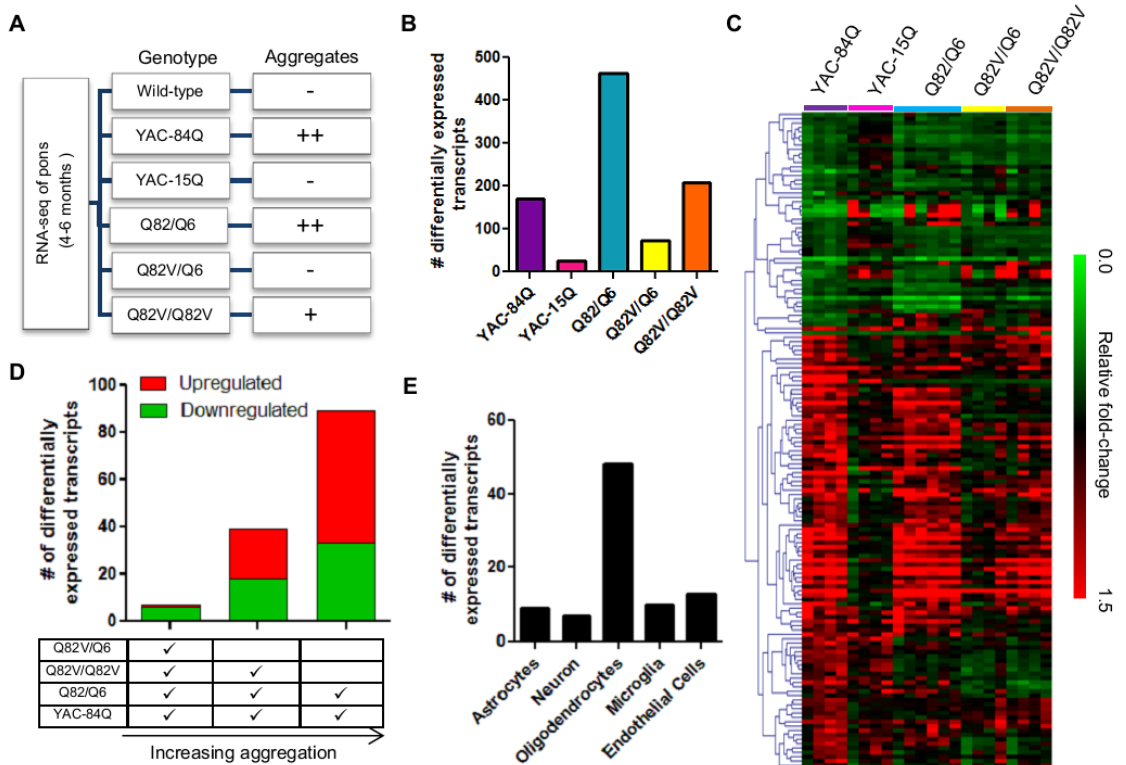


Figure 4.5. Increased aggregation-propensity of ATXN3 associates with robust distinct transcriptional changes in the pons. (A) Summary of the genotypes used for RNA-seq and the relative amount of ATXN3 aggregation in the brain of each mouse, including transgenic SCA3 YAC mice expressing ATXN3 from full-length *ATXN3* gene with 15 (YAC-Q15) or 84 (YAC-Q84) CAG repeats. Transcripts differentially expressed (DE) from wild-type were obtained from DESeq. (B) Mice containing ATXN3 aggregates (Q82/Q6, Q82V/Q82V, and YAC-Q84) exhibit a higher number of DE transcripts than mice with little or no aggregates (Q82V/Q6 and YAC-Q15). (C) Clustered heat map of the ~100 most significant DE transcripts in YACQ84 mice parallel the changes in Q82/Q6, and to a lesser extent, in Q82V/Q6 mice. (D) Graphing shared DE transcripts between different genotypes shows an increasing amount of upregulated transcripts associated with mice with increasing ATXN3 aggregation. (E) DE transcripts shared in Q82/Q6 and YAC-Q84 mice are expressed in several cell-types in the brain, but are predominantly enriched in oligodendrocyte-lineage cells.

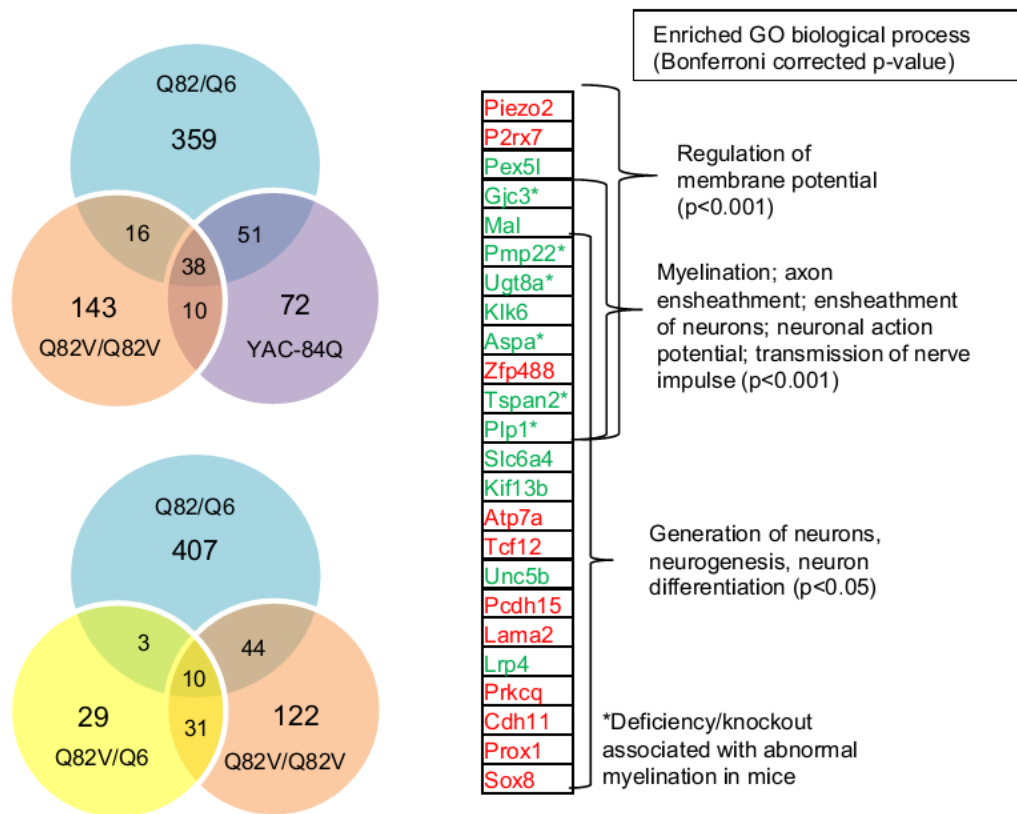


Figure 4.6 Transcripts associated with ATXN3 aggregation are enriched in biological processes linked to oligodendrocytes. Left, Venn diagram showing DE transcripts shared between different genotypes. Q82/Q6 and YAC-84Q mice share the highest number transcripts among these comparisons. These transcripts were subjected to gene enrichment analysis, shown right. Both upregulated (red) and downregulated (green) transcripts were associated with indicated pathways.

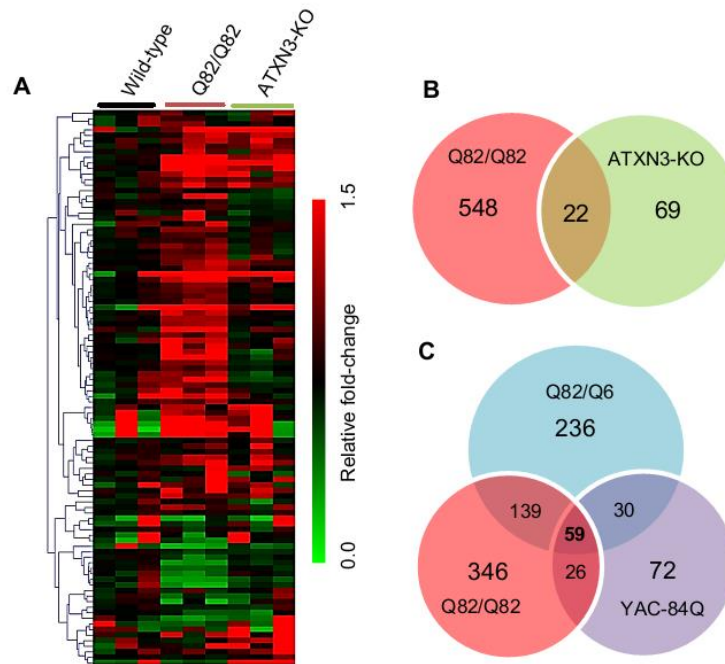


Figure 4.7 Transcriptional alterations in Q82/Q82 mice are minimally associated with ATXN3 loss of function. (A) Heat map of the same transcripts from Figure 4.4C shows similar alterations in pontine RNA-seq of 9-week-old Q82/Q82 mice (n=3), but not in ATXN3 knockout (ATXN3-KO) mice (n=3). (B) Venn diagram showing a large number of DE transcripts in Q82/Q82 with 22 transcripts shared with ATXN-KO mice. (C) Q82/Q82 mice share a larger number of altered transcripts (59) with Q82/Q6 and YAC-84Q mice.

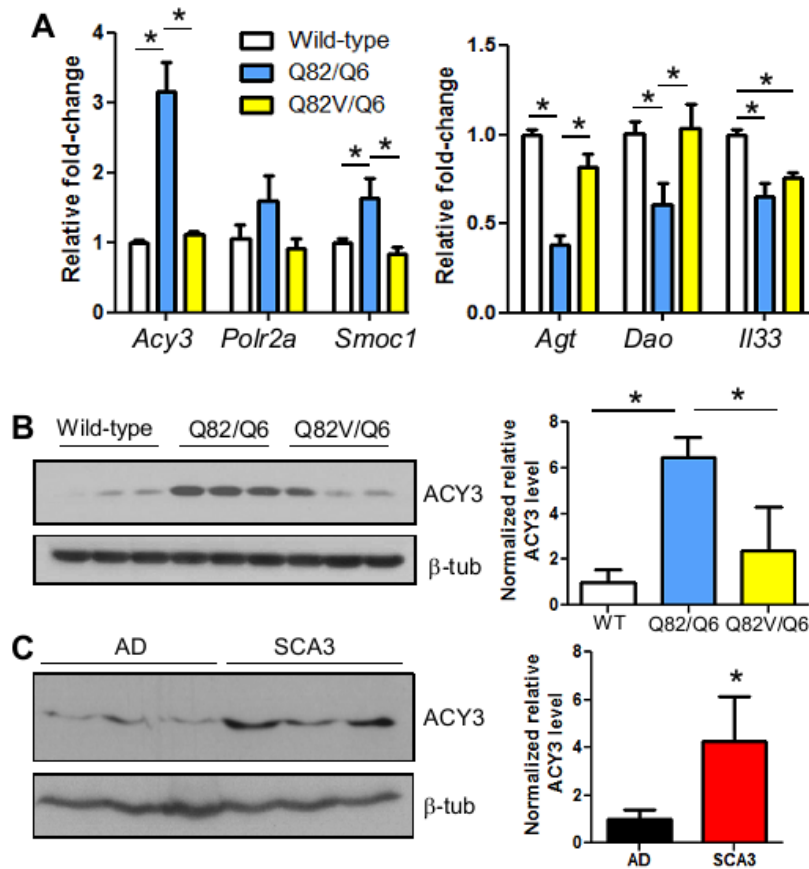


Figure 4.8. Validation of altered transcripts in Q82 versus Q82V SCA3 knock-in mice. (A) qRT-PCR of several DE transcripts including some upregulated (left: *Acy3*, *Polr2a*, and *Smoc1*) and downregulated (right: *Agt*, *Dao*, and *Il33*) in ~6-month-old SCA3 knock-in mice (n=5). (B) Western blot of ACY3 in ~1-year-old SCA3 knock-in mice hindbrain and with quantification shown on the right. (C) Western blot of ACY3 in Alzheimer disease (AD) and SCA3 brainstem lysates with quantification shown on the right. Graphs represent the mean \pm SD, *p < 0.05.

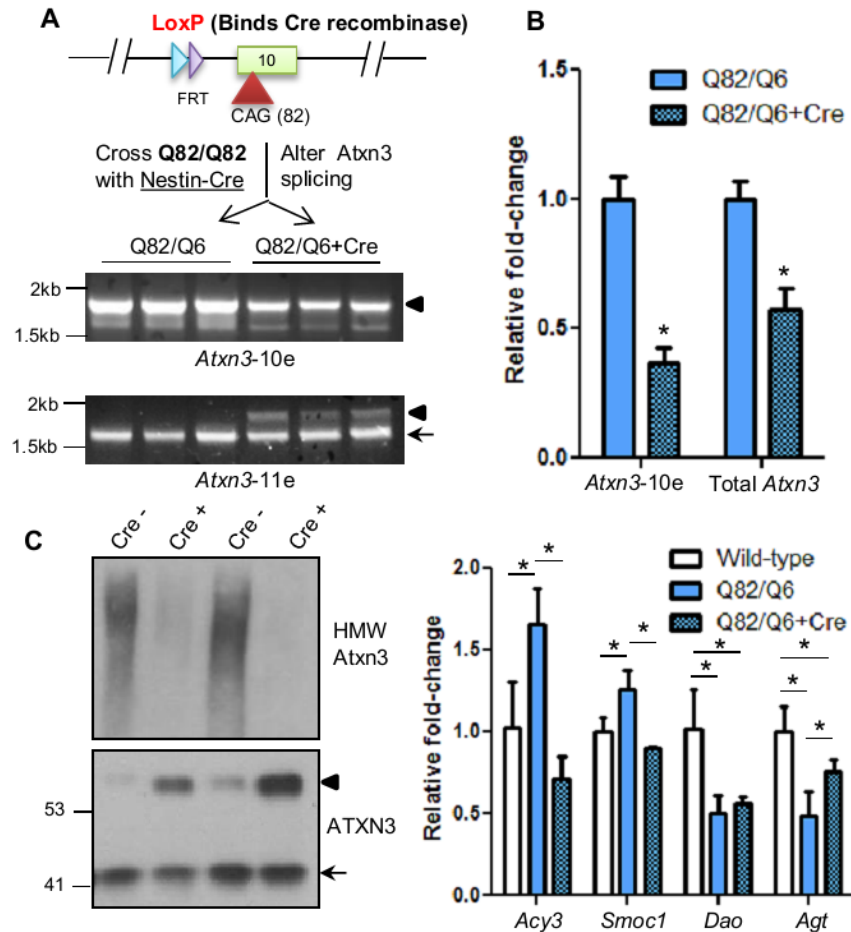


Figure 4.9. Expression of Cre recombinase in the brain of Q82/Q6 mice reduces *Atxn3-10e* expression, ATXN3 aggregation, and transcriptional changes. (A) Schematic of Q82 knock-in locus showing a single LoxP site in intron 9 that can bind Cre recombinase. Below, RT-PCR of the pons showed reduced *Atxn3-10e* expression and recovery of *Atxn3-11e* signal in Q82/Q6 mice expressing Cre-recombinase under the Nestin promoter (Q82/Q6+Cre). (B) qRT-PCR of the same samples showed significant reduction *Atxn3-10e* and total (exon 10-containing) *Atxn3* transcript in Q82/Q6+Cre mice (n=3). (C) Western blotting of brain lysates IP-ed for Atxn3 and resolved on a 3-12% Tris-Acetate gel showed reduced aggregation of ATXN3 in Q82/Q6+Cre mice relative to Q82/Q6 mice that coincided with increased soluble monomeric mutant ATXN3. (D) qRT-PCR on pons of ~2-month-old Q82/Q6+Cre mice (n=3) showed correction toward wild-type levels of three of four tested transcripts (*Acy3*, *Smoc1*, and *Agt*) relative to Q82/Q6 littermates (n=3). Graphs represent the mean +/- SD. *p < 0.05 by one-way ANOVA.

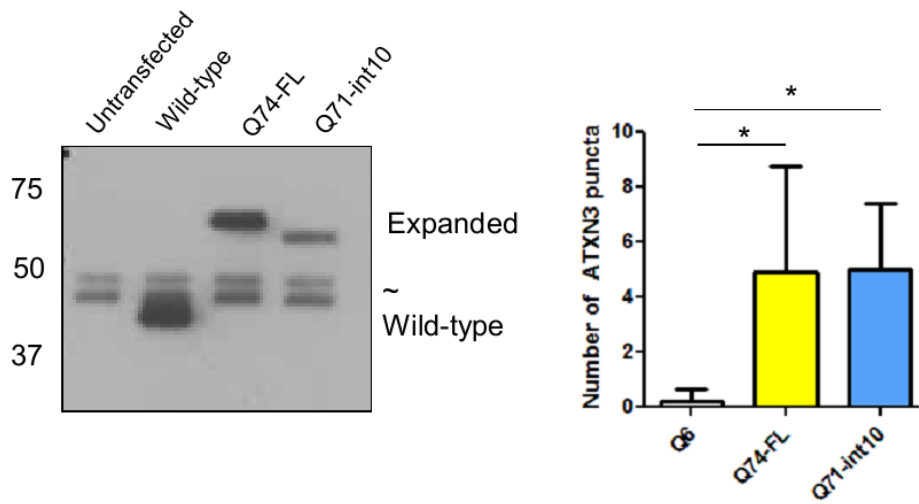


Figure 4.10. Overexpressing mutant ATXN3 isoforms in cell culture did not show differences in puncta formation. Left, western blot of *Atn3* from pcDNA 3.1 shows expression of nonexpanded ATXN3 (Wild-type), mouse Q74 ATXN3-11e (Q74-FL), and mouse Q71 ATXN3-10e (Q71-int10) in HEK293 cells. Right, average number of puncta and inclusions per field following 72 h expression of *Atn3* constructs in PC12 cells (n=3 experiments).

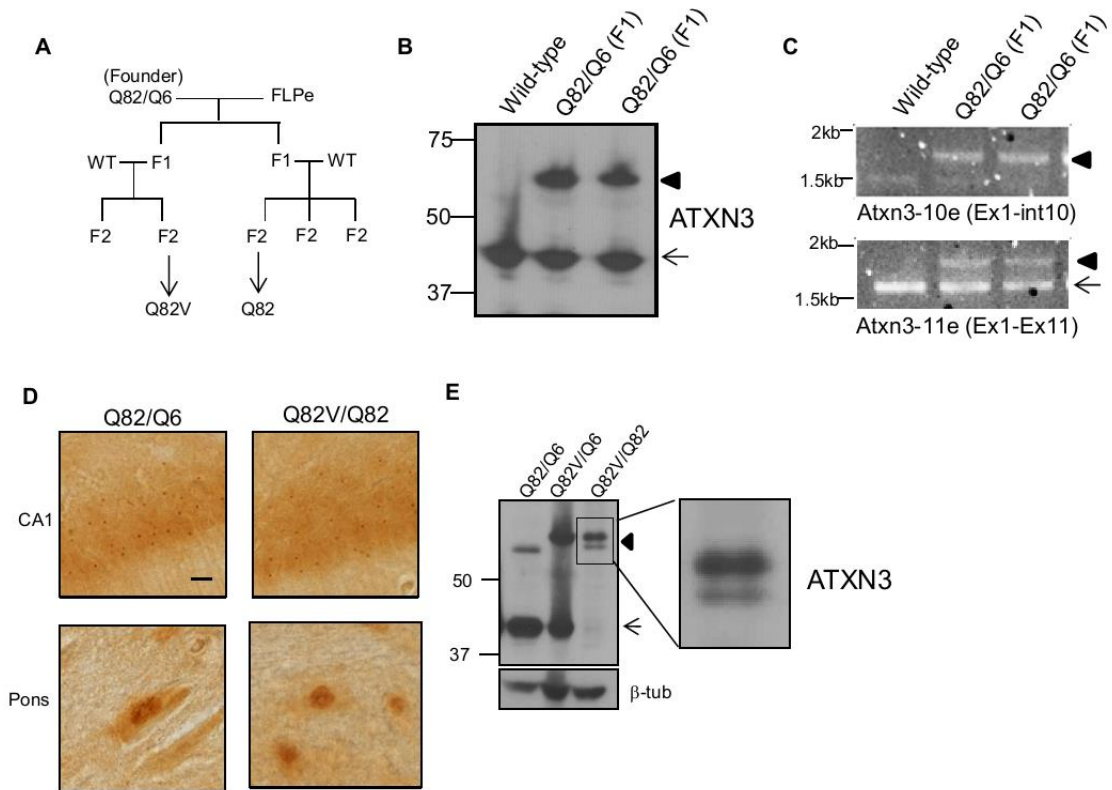


Figure 4.11 Identifying the origin and heritability of the different mutant *Atxn3* phenotypes in SCA3 knock-in mice. (A) Simplified pedigree of the SCA3 knock-in lines, which were generated by breeding the founder with a FLPe transgenic mouse. (B, C) F1 (FLPe expressing) SCA3 knock-in mice did not show differences in mutant *Atxn3* solubility and show expression of both mutant *Atxn3* transcripts by RT-PCR. (D) Preliminary experiments showed that generating a hybrid Q82V/Q82 mouse did not markedly increase or decrease ATXN 3 aggregation relative to an age-matched Q82/Q6 mouse (~12 weeks). (E) Western blot of the Q82V/Q82 separated two distinct ATXN3 bands with different intensities. Arrow: wild-type ATXN3. Arrowhead: mutant ATXN3

Chapter 5

Conclusions and future directions

The results described in this dissertation lead to four main conclusions. Firstly, the Q82 SCA3 knock-in mouse model represents a significant new disease model for the field that exhibits key molecular features of disease, including robust disease protein aggregation and alternative splicing of the mutant transcript. Secondly, alternative splicing of *ATXN3* can markedly affect mutant ATXN3 aggregation in the brain. Thirdly, the aggregation of mutant ATXN3 correlates with an early and robust transcriptional signature in the brain. And finally, the altered transcriptional profile of SCA3 mice containing ATXN3 aggregates alerts us to the potential involvement of oligodendrocytes in disease pathogenesis. Together, the main findings of this thesis suggest that the misfolding tendency of polyQ disease protein is a, if not the, driving force in disease. Nevertheless, substantial gaps remain in our understanding of SCA3 and the polyQ diseases as we strive for new therapies. In this section I outline some of the opportunities moving forward from this work.

5.1 Diverse uses of the SCA3 knock-in mice and extended characterization

No SCA3 knock-in mouse had been reported before 2014. By the end of 2015, the field will likely have three SCA3 knock-in mice: our two SCA3 knock-in mouse lines,

one of which is already published (151), and a chimeric exon 10/11 SCA3 knock-in mouse model reported by Switonski et al.(152). Our published Q82 SCA3 knock-in line is already available to the public through Jackson Laboratories. We plan to publish the Q82 variant line described in chapter 4 shortly. Scientists will be able to utilize one or more of these knock-in mice to explore early molecular changes, alterations to native interactors, and the potential contribution of loss of function effects to SCA3 disease pathogenesis. Among the available SCA3 knock-in mice, the Q82 line shows the most early and robust mutant ATXN3 aggregation throughout the CNS and will likely be the most useful for studying disease processes.

Future characterization of behavioral and neuropathological changes in the Q82 and Q82V lines could establish the detrimental effects of mutant ATXN3 expression and aggregation. I found no differences between one-year-old heterozygous knock-in lines on motor testing, but homozygous knock-in mice at one year of age or older may further exhibit the consequences ATXN3 aggregation. I would predict that aged Q82/Q82 mice will weigh significantly less than age-matched wild-type and Q82V/Q82V mice, but may not exhibit robust differences on motor performance. However, homozygous mice should be further tested for other neuropathological changes including neuronal loss, gliosis, decreased neurotransmitter binding, synaptic/electrophysiological changes, or other subtle deficits that would indicate neuronal dysfunction or degeneration. In the end, however, the strength of the SCA3 knock-in probably lies not in studies of motor behavior or neurodegeneration, but in studies of early molecular and cellular changes in disease.

Delineating the genetics between the SCA3 knock-in lines remains a high priority. My analysis of the pedigree of these knock-in lines suggests that the differences likely appeared during the removal of the Neo cassette using the FLP/FRT system, but PCR and Sanger sequencing of this region did not show any differences in this region. I have submitted tail DNA from a Q82/Q82 and a Q82V/Q82V mouse for whole genome sequencing to broadly assess the full *Atxn3* locus. Identifying a critical genetic difference between the knock-in lines could inform aspects of splicing biology, including *cis*- and *trans*-acting factors that underlie *Atxn3* splicing. Moreover, scientists would appreciate a report of how gene manipulation in biological models can deviate from expectations, especially since these techniques are pervasively used. To my knowledge, genetic aberrations driven by the FLP/FRT have not been documented.

Expressing Cre recombinase in the Q82 line intriguingly substantiates my conclusions by recapitulating features of the Q82V line, but the mechanism that drive this phenomenon is unknown. I could not identify another nearby LoxP site that might recombine with the LoxP site in intron 9. My working hypothesis is that Cre recombinase simply binds the LoxP in intron 9 to alter the kinetics of RNA polymerase action at that junction, which could influence splicing (183). Cre recombinase binding to LoxP may reduce mis-splicing of *Atxn3* by extending the time for splicing machinery to efficiently join exon 10 and 11. To test if Cre recombinase can reversibly alter splicing of *Atxn3*, one could transiently express Cre recombinase in Q82 mice under a tamoxifen-inducible promoter and test levels of *Atxn3*-10e transcript before and after the clearance of Cre recombinase.

Cre recombinase-driven differences in splicing and ATXN3 aggregation in our Q82 line may serendipitously help future study of ATXN3 aggregation in different cell types. Directing Cre recombinase to specific cell-types by driving expression under different promoters could be a novel way to assess both neuronal and non-neuronal contributions to disease. Studies in SBMA, HD, and SCA7 have provided evidence for non-cell-autonomous effects of the polyQ disease protein (194, 196, 203), but this is unexplored in SCA3. Our Q82 knock-in mouse would have the added benefit of testing the effects of ATXN3 aggregation *in vivo* without overexpression or complete deletion of the mutant protein. A study of this type is unprecedented in the polyQ disease field.

A final note on the utility of SCA3 knock-in mice is its ability to test new gene-editing technologies for study and therapy. Nucleases engineered to specifically edit genomes have recently emerged as a powerful way to specifically modify genes *in vivo* (204). While these techniques are in their infancy, they could easily expand as a novel type of gene therapy that could apply to the polyQ disease (205). Since the goal of such a therapy would be to target the endogenous disease gene, polyQ disease knock-in mice would be ideal to test the effects of altering the disease gene *in vivo*. The modifications could include altering or removing the CAG repeat expansion or simply ablating disease gene expression. SCA3 is in a favorable position among polyQ diseases to silence *ATXN3* as a therapy, since *ATXN3* knockout mice do not exhibit deleterious features. Therefore, SCA3 knock-in mice could be at the forefront in testing advanced genome editing therapies in polyQ disease.

5.2 ATXN3 isoforms and protein context in polyQ disease

The work of this dissertation is the first to show the striking extent to which altering disease protein isoforms can affect disease protein aggregation *in vivo*. Even a subtle difference between ATXN3 isoforms, differing by only one exon, markedly affects ATXN3 aggregation in the brain. The influence of different disease protein isoforms could pertain to other polyQ diseases. HD knock-in mice show retention of intron 1 following the CAG repeat-containing exon 1, resulting in the expression of a highly aggregation-prone exon 1 fragment (86). In SCA6, a downstream cistron within *CACNA1A* can drive the production of a C-terminal polyQ-containing fragment that may drive SCA6 pathogenesis (206). Our findings further argue for the exploration of even subtle differences in polyQ protein isoforms that could potentially influence disease. Alternative splicing of the disease gene has been reported for all other polyQ diseases, including SCA1 (207), SCA2 (208), SCA6 (209), SCA7 (210), SCA17 (211), SBMA (212), and DRPLA (213). Scientific understanding of the role of protein context in polyQ diseases would benefit from the exploration of even subtle differences exhibited by alternative isoforms of the disease protein.

Future studies in SCA3 are needed to establish the relative contribution of the expression of human ATXN3-10e isoform *in vivo*. One way to address this is through YAC-84Q mice, which express both the *ATXN3*-10e and -11e transcripts. The Paulson lab and their collaborators together have shown that RNA interference targeting the 3'UTR of the *ATXN3* transcript dramatically reduces *ATXN3* aggregation in YAC-Q84 mice (214, 215). This silencing strategy presumably knocks down the *ATXN3*-11e isoform which contains the 3'UTR, and this was shown to abrogate *ATXN3* expression

and aggregation. However, whether the expression of the mutant *ATXN3*-10e remains after siRNA treatment is uncertain. Selectively targeting the *ATXN3*-10e transcript with siRNA or promoting splicing to the full-length transcript with anti-sense oligonucleotides may also reduce *ATXN3* aggregation in YAC-84Q mice, further establishing a pathogenic contribution of *ATXN3*-10e isoform.

To explore different splice isoforms of *SCA3*, a recently developed human embryonic stem cell line (hESCs) containing a CAG expansion in *ATXN3* may prove to be useful. This cell line, which is already being studied in the Paulson lab, can be differentiated into neurons and expresses mutant *ATXN3* at physiological levels (not shown). Based on the results presented in this thesis, I expect that these cells will be found to express both *ATXN3*-10e and -11e transcripts. Moreover, hESCs can be modified by gene-editing (216) to directly test the consequences of altering the disease gene. For example, gene editing can be used to drive the selective expression of different *ATXN3* transcripts (i.e. -10e vs. -11e) at physiological levels in differentiated neurons to examine their respective effects on aggregation and disease-relevant cellular pathways.

The factors driving the mis-splicing of *ATXN3* and other polyQ disease genes are unknown. The enhanced expression of *Atxn3*-10e transcript in Q82 mice first suggested a CAG-repeat-length-dependent process, supported with data from *SCA3* YAC mice (Chapter 3), but its absence in Q82V mice argues that the presence of an expanded CAG repeat is not sufficient. CAG-dependent mis-splicing of other polyQ disease genes has not yet been shown to converge on a common role of CAG expansions in affecting splicing. Sathasivam and colleagues identified SRSF6 as a putative splicing factor that preferentially binds to CAG expansions (86). Testing SRSF6's binding to disease repeats

in the differentially spliced SCA3 knock-in lines may reveal differences that suggest a SRSF6-dependent mechanism. However a higher priority is identifying the cis-acting genetic differences between these two lines. As more information on alternative splicing of different polyQ disease genes becomes available, we may begin to uncover common elements that regulate splicing and their roles in disease.

5.3 Disease protein aggregation in polyQ disease pathogenesis

Along with the finding that alternative splicing can modify disease protein aggregation *in vivo*, the work in this dissertation sheds light on the pathogenic role of aggregation. Studies have increasingly shifted away from using aggregation as a readout for the pathogenic disease process with the understandable concern that the presence of non-toxic aggregates, or possibly even protective aggregates, may confound the results. Nonetheless, my view is that prominent aggregates and intraneuronal inclusions still serve as important biomarkers of the abnormal process of mutant protein accumulation with toxic properties. My findings indirectly suggest that the aggregation propensity of polyQ-expanded ATXN3 drives disease. However, this raises two issues that relate to investigating aggregation and toxicity in disease models.

The first issue is the difficulty of establishing a causal relationship between aggregation and disease pathogenesis in an animal model that lacks robust behavioral or degenerative phenotypes. In this dissertation, I infer pathogenicity of aggregates from the altered transcriptional profiles of the SCA3 knock-in mice. My reasoning is that a higher number of transcriptional changes most likely reflects the presence of a stressful stimulus that perturbs the transcriptional network. Consistent with this, aggregate-containing SCA3 mice showed a greater number of altered transcripts than YAC-Q15

overexpressing nonexpanded ATXN3, Q82V/Q6 mice with non-aggregated mutant ATXN3, or ATXN3-KO mice, suggesting that the misfolding tendency of ATXN3 stresses cells in some manner. These findings complement a large body of literature discussed in Chapter 1 that supports a clear association between aggregation and toxicity. The strength of my work here is in investigating this association under physiological conditions and without overexpression of other cellular factors, but this comes at a cost of easily accessible toxic phenotypes. Future studies examining other early molecular changes, such as electrophysiological (217), neurometabolic (190), cytoarchitectural (i.e. morphology of subcellular structures) , or subtle white matter abnormalities, could further elucidate the role of aggregation in disease pathogenesis in the SCA3 knock-in mice. Furthermore, establishing additional early readouts of toxicity would also help in the future assessment of treatment efficacies in mouse models of disease.

The second issue is the importance of identifying the toxic polyQ species or conformers that lead to neurodegeneration. One challenge is that a sufficient concentration of misfolded mutant polyQ protein monomers may aggregate to form both toxic and non-toxic polyQ protein species, thus adding difficulty to dissociating the relative contributions of each polyQ protein species to toxicity. To partially address this, Miller et al developed an antibody, 3B5H10, specific to misfolded conformations of polyQ monomer that predicted toxicity in cell culture (42, 46). It would be interesting to see if this or other conformer-specific antibodies show differences in reactivity between Q82 and Q82V lines to provide an additional correlate of toxicity. Antibodies or methods specific to toxic polyQ conformers *in vivo* that serve as better predictive markers or pathogenesis could replace aggregate burden and inclusion formation as disease markers.

With aggregation as a central mediator of disease, my findings support continued efforts to target factors that influence disease protein aggregation. For example, I have already discussed how alternative isoforms and proteolytic processing of the disease protein can affect aggregation and pathogenesis. Various post-translational modifications also can play important roles in aggregation, as reviewed by Pennuto et al (218), including ubiquitination, SUMOylation, phosphorylation, acetylation, palmitoylation, and transglutamination. An improved understanding of the proteostasis network has led to insights on quality control factors that can help refold or clear the mutant polyQ disease protein (168). In addition to Hsp70, different Hsp40 proteins are recognized as potent suppressors of mutant polyQ disease protein aggregation that may prove beneficial (219). Lastly, induction of autophagy has been supported as a viable therapeutic option to clear aggregates in the nervous system (220). With the increasing identification of key modifiers of aggregation, major efforts are taking place to identify pharmacological compounds that can act through these pathways. These therapies include protease (calpain) inhibitors (221), chaperone activators (222), and autophagy inducers (220). Moreover, future studies may reveal novel factors that can influence disease protein aggregation.

5.4 Understanding transcriptional changes in polyQ disease

The importance of nuclear localization in driving polyQ disease toxicity in different disease models supports transcriptional dysregulation as a major contributor to disease pathogenesis. This possibility is supported by a large body of evidence in HD and other polyQ diseases that have demonstrated detrimental effects of altered activity of specific transcription factors and the corresponding changes in expression of their

downstream targets. This has led to increased efforts to use gene expression profiling via microarray and RNA-seq, which sensitively and rapidly provide vast amounts of transcriptional data, to identify pathways that lead to toxicity. However, despite significant technological advances in transcriptional profiling and its analysis, this strategy still poses an immense challenge for several reasons.

When presented with extensive transcriptional data from disease models or tissue, several factors complicate the interpretation of altered transcripts and their role in disease pathogenesis. An altered transcript in a disease model may fall under at least one of these categories: 1) The transcriptional change is directly detrimental, 2) it represents a neutral marker of a detrimental disease process, 3) it correlates with the presence of the disease mutation, but is unrelated to the disease process, or 4) it is a protective response to the disease process. Furthermore, when expression profiles are obtained from brain tissue, other factors must be considered: altered transcripts may reflect cell-autonomous mechanisms elicited by effects of the disease protein in that cell, non-cell autonomous responses to changes in another cell, or an epiphenomenon caused by changes in cellular composition of the analyzed tissue, as occurs with neuronal loss or gliosis. Finally, the cascade of events leading to an observed change in gene expression can be extremely complex and indirect, with potentially dozens of intermediate changes set forth by disruption of major cellular components.

Nevertheless, a tissue-based gene expression profile provides a broad signature that can serve as a useful and sensitive biomarker of disease progression in mouse models. By analyzing multiple SCA3 mouse models in our RNA-seq datasets, we were able to focus attention on a specific candidate transcript associated with mutant ATXN3

aggregation, ACY3, and validate the observed changes in human disease tissue. A transcriptional profile of SCA3 human disease tissue, or of iPSCs or hESCs with the disease mutation, would be invaluable in assessing the validity of the SCA3 mouse models. Future therapeutic studies that target ATXN3 levels or aggregation in YAC-84Q or Q82 SCA3 knock-in mice can assess several transcripts, including ACY3, to determine if therapies are effective. Furthermore, transcriptional alterations, as I have shown in my work, can also easily be assessed presymptomatically. Therefore, testing a focused set of transcripts by qRT-PCR would be a time- and cost-effective way to assess disease progression in these mouse models.

Ongoing analysis of our RNA-seq data could help distill information about the SCA3 disease network in the brain to identify critical altered factors. The analytical process remains challenging, but continues to evolve with increasingly available data and improved computational technology. Researchers are more commonly integrating vast databases of information on transcriptional alterations, protein-protein interactors, functional biological pathways, metabolic pathways and more, to develop a complex disease network (223). Gene co-expression analyses are now increasingly used to sort transcriptional data and identify major transcriptional networks and their “hubs” in disease, which may represent critical transcription factors (224, 225). For example, our collaboration with the Guan group at the University of Michigan will make use of unique algorithms (226) that examine co-expression to generate a transcriptional network in different SCA3 mouse models to extract information on central factors that drive transcriptional perturbation in SCA3. The altered transcripts or factors themselves may

not necessarily play direct pathogenic roles, but this information can provide important clues to the disease process in the nervous system elicited by aggregation.

Substantial gaps still exist in our understanding of the transcriptome, including its diversity and dynamic regulation in different cell types. These gaps include a poor understanding of the differences in alternative splicing across the transcriptome which could provide clues to disease processes and its effects in RNA-associated pathways(227); such differences can be further explored in our RNA-seq data. In addition, while scientists have focused on coding transcripts in SCA3, the vast majority of our transcriptome is non-coding (228). Our RNA-seq data could provide a unique look into some non-coding RNAs that may be dysregulated in disease. Unfortunately, because our RNAseq selected for polyadenylated transcripts, we cannot directly examine microRNAs. Future studies should examine the microRNAs altered in disease in a directed manner, as their regulation can crucially influence aging and degenerative processes (229, 230). Our data can potentially be mined for alterations in polyadenylated long non-coding RNAs (lncRNAs). The study of lncRNAs is on the rise in neurodegenerative disease, with few reports in polyQ disease emerging over the last few years (231–234), but is unexplored in SCA3.

5.5 Oligodendrocytes and glial contributions to polyQ disease

A central goal for researchers studying neurological disease is to improve neuronal function, since neuronal activity and action directly dictate behavior/cognition. Accordingly, attention in polyQ diseases and most other neurodegenerative disorders has been on neurons and their dysfunction. However, a large body of evidence now supports the importance of non-neuronal cells in nervous system function and specific diseases

(235). Even beyond primary glial loss as a cause of neurological disease, as in multiple sclerosis, glial dysfunction can play critical roles in neurodegenerative disease and ultimately affect neuronal function. Therefore, an improved understanding of non-neuronal dysfunction can lead to better insight into polyQ disease pathogenesis.

White matter dysfunction may contribute to disease symptoms in SCA3 but requires further exploration. Our analysis of RNA-seq data in SCA3 mouse models implicates a robust transcriptional response by oligodendrocytes, the primary myelin-producing cell of the CNS. Previous studies using MRI of SCA3 brain have revealed consistent and prominent white matter abnormalities that correlate with symptoms (200, 201), but these have not been as well characterized neuropathologically. The polyQ research field would benefit from improved white matter characterization in disease and disease mouse models to begin uncovering the consequences of myelin dysfunction.

A primary step to understanding oligodendrocyte dysfunction is to determine the factors that drive transcriptional changes in the SCA3 knock-in mice. Two main questions arise from our profiling data in SCA3 mice: 1) Are the transcriptional changes driven in oligodendrocytes cell-autonomously and 2) do the transcriptional changes depend on mutant ATXN3's nuclear localization? A recent study by Huang et al showed that mutant HTT alters MYRF, a myelin-associated transcription factor, to alter transcription directly in oligodendrocytes (197). However, immunostaining for Olig2 or CC1, markers of oligodendrocytes, did not show clear colocalization with ATXN3 or its aggregates in SCA3 knock-in mouse brain. Based on cell-type specific RNA-seq expression data of mouse cortex (165), ATXN3 is expressed in oligodendrocytes. While we do not detect ATXN3 in oligodendrocytes by immunostaining, oligomers or

microaggregates of ATXN3 that cannot be easily visualized may still contribute to cell-autonomous changes in oligodendrocytes. As discussed earlier, one could express Cre-recombinase via an *Olig2* promoter in the Q82 line to reduce ATXN3 aggregation in oligodendrocytes to determine if alteration of *Acy3* and other oligodendrocyte-associated transcripts are normalized. Alternatively, generating a novel mouse model of SCA3 that allows cell-type specific deletion of the mutant gene may prove worthwhile to delineate the contribution of ATXN3 aggregation in different cell types of the nervous system, as well as cell-autonomous and non-cell-autonomous contributions to neuronal dysfunction. Finally, transcriptional profiling of mouse brain with aggregation-prone mutant ATXN3 prevented from entering the nucleus by adding an NES (52) may provide information on the nuclear dependence of mutant ATXN3 on eliciting transcriptional changes.

5.6 Concluding remarks

The polyQ diseases and related neurodegenerative diseases pose a significant burden worldwide without any available disease-modifying therapies. Disease protein misfolding and aggregation has been recognized as a central feature of the polyQ diseases nearly since their discovery, and for almost as long has been a major point of debate. My work in this dissertation helps cement a central role for mutant ATXN3 aggregation in SCA3 pathogenesis, and this concept likely applies to other polyQ diseases. Dissecting polyQ disease pathways has proved to be complicated and challenging. Building relevant disease models is a crucial step towards understanding disease and moving towards therapies. In this regard, mouse models of disease, and in particular knock-in mouse models that express endogenous levels of disease proteins, will continue to be important tools for exploring disease pathogenesis. My dissertation work in uncovering the

characteristics of novel SCA3 knock-in mouse models is a major step for future studies that will utilize these mice to explore disease pathways.

Considering the incomplete understanding of these disease processes and the desperate need for therapies for polyQ disease, a simple and direct strategy targeting the mutant disease protein and its misfolding tendency remains the most sensible avenue for therapy. Importantly, my work argues that the effectiveness of such strategies can be tested in mouse models that do not exhibit a motor phenotype. Along with disease protein aggregation, early transcriptional changes and other markers can help assess treatment efficacy in preclinical trials. My work and the works of others further support pre-symptomatic administration of polyQ disease-modifying therapies, including those that reduce disease protein aggregation, to prevent or delay onset of disease. An effective treatment for polyQ disease would help a large number of people and would also serve as an important proof-of-concept to open doors to treatments for other proteinopathies.

References

1. La Spada, A., Wilson, E., Lubahn, D., Harding, A. and Fischbeck, K. (1991) Androgen receptor gene mutations in X-linked spinal and bulbar muscular atrophy. *Nature*, **352**, 77–79.
2. Seidel, K., Siswanto, S., Brunt, E.R.P., den Dunnen, W., Korf, H.-W. and Rüb, U. (2012) Brain pathology of spinocerebellar ataxias. *Acta Neuropathol.*, **124**, 1–21.
3. Iizuka, R., Hirayama, K. and Maehara, K. (1984) Dentato-rubro-pallido-luysian atrophy : a clinico-pathological study. *J Neurol Neurosurg Psychiatry*, **47**, 1288–1298.
4. Ross, C.A. and Poirier, M.A. (2004) Protein aggregation and neurodegenerative disease. *Nat. Med.*, **10**, S10–S17.
5. DiFiglia, M., Sapp, E., Chase, K., Davies, S.W., Bates, G.P., Vonsattel, J.P. and Aronin, N. (1997) Aggregation of Huntingtin in Neuronal Intranuclear Inclusions and Dystrophic Neurites in Brain. *Science (80-.)*, **277**, 1990–1993.
6. Paulson, H.L., Perez, M.K., Trotter, Y., Trojanowski, J.Q., Subramony, S.H., Das, S.S., Vig, P., Mandel, J., Fischbeck, K.H. and Pittman, R.N. (1997) Expanded Polyglutamine Protein in Spinocerebellar Ataxia Type 3. *Neuron*, **19**, 333–344.
7. Chai, Y., Koppenhafer, S.L., Shoemith, S.J., Perez, M.K. and Paulson, H.L. (1999) Evidence for proteasome involvement in polyglutamine disease: localization to nuclear inclusions in SCA3/MJD and suppression of polyglutamine aggregation in vitro. *Hum. Mol. Genet.*, **8**, 673–682.
8. Cummings, C.J., Mancini, M., Antalffy, B., DeFranco, D.B., Orr, H.T. and Zoghbi, H.Y. (1998) Chaperone suppression of aggregation and altered subcellular proteasome localization imply protein misfolding in SCA1. *Nat. Genet.*, **19**, 148–154.
9. Maciel, P., Gaspar, C., DeStefano, A., Silveira, I., Coutinho, P., Radvany, J., Dawson, D., Sudarsky, L., Guimarães, J. and Loureiro, J. (1995) Correlation between CAG repeat length and clinical features in Machado-Joseph disease. *Am. J. Hum. Genet.*, **57**, 54–61.
10. Andrew, S.E., Goldberg, Y.P., Kremer, B., Telenius, H., Theilmann, J., Adam, S., Starr, E., Squitieri, F., Lin, B. and Kalchman, M.A. (1993) The relationship between trinucleotide (CAG) repeat length and clinical features of Huntington's disease. *Nat. Genet.*, **4**, 398–403.
11. Legleiter, J., Mitchell, E., Lotz, G.P., Sapp, E., Ng, C., DiFiglia, M., Thompson, L.M. and Muchowski, P.J. (2010) Mutant huntingtin fragments form oligomers in a polyglutamine length-dependent manner in vitro and in vivo. *J. Biol. Chem.*, **285**, 14777–14790.
12. Miller, V.M., Nelson, R.F., Gouvion, C.M., Williams, A., Rodriguez-Lebron, E., Harper, S.Q., Davidson, B.L., Rebagliati, M.R. and Paulson, H.L. (2005) CHIP

- suppresses polyglutamine aggregation and toxicity in vitro and in vivo. *J. Neurosci.*, **25**, 9152–9161.
13. Muchowski, P.J., Schaffar, G., Sittler, A., Wanker, E.E., Hayer-Hartl, M.K. and Hartl, F.U. (2000) Hsp70 and hsp40 chaperones can inhibit self-assembly of polyglutamine proteins into amyloid-like fibrils. *Proc. Natl. Acad. Sci. U. S. A.*, **97**, 7841–7846.
 14. Tam, S., Geller, R., Spiess, C. and Frydman, J. (2006) The chaperonin TRiC controls polyglutamine aggregation and toxicity through subunit-specific interactions. *Nat. Cell Biol.*, **8**, 1155–1162.
 15. Satyal, S.H., Schmidt, E., Kitagawa, K., Sondheimer, N., Lindquist, S., Kramer, J.M. and Morimoto, R.I. (2000) Polyglutamine aggregates alter protein folding homeostasis in *Caenorhabditis elegans*. *Proc. Natl. Acad. Sci. U. S. A.*, **97**, 5750–5755.
 16. Williams, A.J., Knutson, T.M., Colomer Gould, V.F. and Paulson, H.L. (2009) In vivo suppression of polyglutamine neurotoxicity by C-terminus of Hsp70-interacting protein (CHIP) supports an aggregation model of pathogenesis. *Neurobiol. Dis.*, **33**, 342–353.
 17. Warrick, J.M., Chan, H.Y., Gray-Board, G.L., Chai, Y., Paulson, H.L. and Bonini, N.M. (1999) Suppression of polyglutamine-mediated neurodegeneration in *Drosophila* by the molecular chaperone HSP70. *Nat. Genet.*, **23**, 425–428.
 18. Adachi, H., Katsuno, M., Minamiyama, M., Sang, C., Pagoulatos, G., Angelidis, C., Kusakabe, M., Yoshiki, A., Kobayashi, Y., Doyu, M., et al. (2003) Heat shock protein 70 chaperone overexpression ameliorates phenotypes of the spinal and bulbar muscular atrophy transgenic mouse model by reducing nuclear-localized mutant androgen receptor protein. *J. Neurosci.*, **23**, 2203–2211.
 19. Labbadia, J., Novoselov, S.S., Bett, J.S., Weiss, A., Paganetti, P., Bates, G.P. and Cheetham, M.E. (2012) Suppression of protein aggregation by chaperone modification of high molecular weight complexes. *Brain*, **135**, 1180–1196.
 20. Malik, B., Nirmalanathan, N., Gray, A.L., La Spada, A.R., Hanna, M.G. and Greensmith, L. (2013) Co-induction of the heat shock response ameliorates disease progression in a mouse model of human spinal and bulbar muscular atrophy: implications for therapy. *Brain*, **136**, 926–943.
 21. Sontag, E.M., Lotz, G.P., Agrawal, N., Tran, A., Aron, R., Yang, G., Necula, M., Lau, A., Finkbeiner, S., Glabe, C., et al. (2012) Methylene blue modulates huntingtin aggregation intermediates and is protective in Huntington's disease models. *J. Neurosci.*, **32**, 11109–11119.
 22. Al-Ramahi, I., Lam, Y.C., Chen, H.K., De Gouyon, B., Zhang, M., Pérez, A.M., Branco, J., De Haro, M., Patterson, C., Zoghbi, H.Y., et al. (2006) CHIP protects from the neurotoxicity of expanded and wild-type ataxin-1 and promotes their ubiquitination and degradation. *J. Biol. Chem.*, **281**, 26714–26724.
 23. Ikeda, H., Yamaguchi, M., Sugai, S., Aze, Y., Narumiya, S. and Kakizuka, A. (1996) Expanded polyglutamine in the Machado-Joseph disease protein induces cell death in vitro and in vivo. *Nature*, **381**, 196–202.
 24. Martindale, D., Hackam, A., Wiczorek, A., Ellerby, L., Wellington, C., McCutcheon, K., Singaraja, R., Kazemi-Esfarjani, P., Devon, R., Kim, S., et al.

- (1998) Length of huntingtin and its polyglutamine tract influences localization and frequency of intracellular aggregates. *Nat. Genet.*, **18**, 231–236.
25. Zoghbi, H.Y. and Orr, H.T. (1999) Polyglutamine diseases: Protein cleavage and aggregation. *Curr. Opin. Neurobiol.*, **9**, 566–570.
 26. Mangiarini, L., Sathasivam, K., Seller, M., Cozens, B., Harper, A., Hetherington, C., Lawton, M., Trotter, Y., Lehrach, H., Davies, S.W., et al. (1996) Exon I of the HD gene with an expanded CAG repeat is sufficient to cause a progressive neurological phenotype in transgenic mice. *Cell*, **87**, 493–506.
 27. Haacke, A., Hartl, F.U. and Breuer, P. (2007) Calpain inhibition is sufficient to suppress aggregation of polyglutamine-expanded ataxin-3. *J. Biol. Chem.*, **282**, 18851–18856.
 28. Berke, S.J.S., Schmied, F.A.F., Brunt, E.R., Ellerby, L.M. and Paulson, H.L. (2004) Caspase-mediated proteolysis of the polyglutamine disease protein ataxin-3. *J. Neurochem.*, **89**, 908–918.
 29. Wellington, C.L., Ellerby, L.M., Hackam, A.S., Margolis, R.L., Trifiro, M.A., Singaraja, R., McCutcheon, K., Salvesen, G.S., Propp, S.S., Bromm, M., et al. (1998) Caspase cleavage of gene products associated with triplet expansion disorders generates truncated fragments containing the polyglutamine tract. *J. Biol. Chem.*, **273**, 9158–9167.
 30. Wellington, C.L., Ellerby, L.M., Gutekunst, C.-A., Rogers, D., Warby, S., Graham, R.K., Loubser, O., van Raamsdonk, J., Singaraja, R., Yang, Y.-Z., et al. (2002) Caspase cleavage of mutant huntingtin precedes neurodegeneration in Huntington's disease. *J. Neurosci.*, **22**, 7862–7872.
 31. Gafni, J. and Ellerby, L.M. (2002) Calpain Activation in Huntington's Disease. *In Vitro*, **22**, 4842–4849.
 32. Simões, A.T., Gonçalves, N., Koeppen, A., Déglon, N., Kügler, S., Duarte, C.B. and Pereira de Almeida, L. (2012) Calpastatin-mediated inhibition of calpains in the mouse brain prevents mutant ataxin 3 proteolysis, nuclear localization and aggregation, relieving Machado-Joseph disease. *Brain*, **135**, 2428–39.
 33. Hübener, J., Weber, J.J., Richter, C., Honold, L., Weiss, A., Murad, F., Breuer, P., Wüllner, U., Bellstedt, P., Paquet-Durand, F., et al. (2013) Calpain-mediated ataxin-3 cleavage in the molecular pathogenesis of spinocerebellar ataxia type 3 (SCA3). *Hum. Mol. Genet.*, **22**, 508–518.
 34. Todd, T.W. and Lim, J. (2013) Aggregation formation in the polyglutamine diseases: protection at a cost? *Mol. Cells*, **36**, 185–194.
 35. Kuemmerle, S., Gutekunst, C.A., Klein, A.M., Li, X.J., Li, S.H., Beal, M.F., Hersch, S.M. and Ferrante, R.J. (1999) Huntingtin aggregates may not predict neuronal death in Huntington's disease. *Ann. Neurol.*, **46**, 842–849.
 36. Gutekunst, C.A., Li, S.H., Yi, H., Mulroy, J.S., Kuemmerle, S., Jones, R., Rye, D., Ferrante, R.J., Hersch, S.M. and Li, X.J. (1999) Nuclear and neuropil aggregates in Huntington's disease: relationship to neuropathology. *J. Neurosci.*, **19**, 2522–2534.
 37. Saudou, F., Finkbeiner, S., Devys, D. and Greenberg, M.E. (1998) Huntingtin acts in the nucleus to induce apoptosis but death does not correlate with the formation of intranuclear inclusions. *Cell*, **95**, 55–66.

38. Arrasate, M., Mitra, S., Schweitzer, E.S., Segal, M.R. and Finkbeiner, S. (2004) Inclusion body formation reduces levels of mutant huntingtin and the risk of neuronal death. *Nature*, **431**, 805–810.
39. Slow, E.J., Graham, R.K., Osmand, A.P., Devon, R.S., Lu, G., Deng, Y., Pearson, J., Vaid, K., Bissada, N., Wetzel, R., et al. (2005) Absence of behavioral abnormalities and neurodegeneration in vivo despite widespread neuronal huntingtin inclusions. *Proc. Natl. Acad. Sci. U. S. A.*, **102**, 11402–11407.
40. Silva-Fernandes, A., Costa, M.D.C., Duarte-Silva, S., Oliveira, P., Botelho, C.M., Martins, L., Mariz, J.A., Ferreira, T., Ribeiro, F., Correia-Neves, M., et al. (2010) Motor uncoordination and neuropathology in a transgenic mouse model of Machado-Joseph disease lacking intranuclear inclusions and ataxin-3 cleavage products. *Neurobiol. Dis.*, **40**, 163–176.
41. Chafekar, S.M., Wisén, S., Thompson, A.D., Echeverria, A., Walter, G.M., Evans, C.G., Makley, L.N., Gestwicki, J.E. and Duennwald, M.L. (2012) Pharmacological tuning of heat shock protein 70 modulates polyglutamine toxicity and aggregation. *ACS Chem. Biol.*, **7**, 1556–1564.
42. Nucifora, L.G., Burke, K.A., Feng, X., Arbez, N., Zhu, S., Miller, J., Yang, G., Ratovitski, T., Delannoy, M., Muchowski, P.J., et al. (2012) Identification of novel potentially toxic oligomers formed in vitro from mammalian-derived expanded huntingtin exon-1 protein. *J. Biol. Chem.*, **287**, 16017–16028.
43. Hoffner, G. and Djian, P. (2014) Monomeric, oligomeric and polymeric proteins in huntington disease and other diseases of polyglutamine expansion. *Brain Sci.*, **4**, 91–122.
44. Nagai, Y., Inui, T., Popiel, H.A., Fujikake, N., Hasegawa, K., Urade, Y., Goto, Y., Naiki, H. and Toda, T. (2007) A toxic monomeric conformer of the polyglutamine protein. *Nat. Struct. Mol. Biol.*, **14**, 332–340.
45. Legleiter, J., Lotz, G.P., Miller, J., Ko, J., Ng, C., Williams, G.L., Finkbeiner, S., Patterson, P.H. and Muchowski, P.J. (2009) Monoclonal antibodies recognize distinct conformational epitopes formed by polyglutamine in a mutant huntingtin fragment. *J. Biol. Chem.*, **284**, 21647–21658.
46. Miller, J., Arrasate, M., Brooks, E., Libeu, C.P., Legleiter, J., Hatters, D., Curtis, J., Cheung, K., Krishnan, P., Mitra, S., et al. (2012) Identifying polyglutamine protein species in situ that best predict neurodegeneration. *Nat. Chem. Biol.*, **8**, 318–318.
47. Doi, H., Adachi, H., Katsuno, M., Minamiyama, M., Matsumoto, S., Kondo, N., Miyazaki, Y., Iida, M., Tohnai, G., Qiang, Q., et al. (2013) p62/SQSTM1 differentially removes the toxic mutant androgen receptor via autophagy and inclusion formation in a spinal and bulbar muscular atrophy mouse model. *J. Neurosci.*, **33**, 7710–27.
48. Yu, Z., Dadgar, N., Albertelli, M., Gruis, K., Jordan, C., Robins, D.M. and Lieberman, A.P. (2006) Androgen-dependent pathology demonstrates myopathic contribution to the Kennedy disease phenotype in a mouse knock-in model. *J. Clin. Invest.*, **116**, 2663–2672.
49. Montie, H.I., Cho, M.S., Holder, L., Liu, Y., Tsvetkov, A.S., Finkbeiner, S. and Merry, D.E. (2009) Cytoplasmic retention of polyglutamine-expanded androgen receptor ameliorates disease via autophagy in a mouse model of spinal and bulbar muscular atrophy. *Hum. Mol. Genet.*, **18**, 1937–1950.

50. Peters, M.F., Jr, F.C.N., Kushi, J., Seaman, H.C., Cooper, J.K., Herring, W.J., Dawson, V.L., Dawson, T.M. and Ross, C.A. (1999) Nuclear Targeting of Mutant Huntingtin Increased Toxicity. *Mol. Cell. Neurosci.*, **128**, 121–128.
51. Klement, I.A., Skinner, P.J., Kaytor, M.D., Yi, H., Hersch, S.M., Clark, H.B., Zoghbi, H.Y. and Orr, H.T. (1998) Ataxin-1 Nuclear Localization and Aggregation : Role in Polyglutamine-Induced Disease in SCA1 Transgenic Mice. **95**, 41–53.
52. Bichelmeier, U., Schmidt, T., Hübener, J., Boy, J., Rüttiger, L., Häbig, K., Poths, S., Bonin, M., Knipper, M., Schmidt, W.J., et al. (2007) Nuclear localization of ataxin-3 is required for the manifestation of symptoms in SCA3: in vivo evidence. *J. Neurosci.*, **27**, 7418–7428.
53. Takahashi, T., Katada, S. and Onodera, O. (2010) Polyglutamine diseases: where does toxicity come from? what is toxicity? where are we going? *J. Mol. Cell Biol.*, **2**, 180–191.
54. Mohan, R.D., Abmayr, S.M. and Workman, J.L. (2014) The expanding role for chromatin and transcription in polyglutamine disease. *Curr. Opin. Genet. Dev.*, **26**, 96–104.
55. Cong, S.Y., Pepers, B.A., Evert, B.O., Rubinsztein, D.C., Roos, R.C., Van Ommen, G.J.B. and Dorsman, J.C. (2005) Mutant huntingtin represses CBP, but not p300, by binding and protein degradation. *Mol. Cell. Neurosci.*, **30**, 12–23.
56. Steffan, J.S., Kazantsev, A.G., Spasic-Boskovic, O., Greenwald, M., Zhu, Y.Z., Gohler, H., Wanker, E.E., Bates, G.P., Housman, D.E. and Thompson, L.M. (2000) The Huntington's disease protein interacts with p53 and CREB-binding protein and represses transcription. *Proc. Natl. Acad. Sci. U. S. A.*, **97**, 6763–6768.
57. Dunah, A.W., Jeong, H., Griffin, A., Kim, Y.-M., Standaert, D.G., Hersch, S.M., Mouradian, M.M., Young, A.B., Tanese, N. and Krainc, D. (2002) Sp1 and TAFII130 transcriptional activity disrupted in early Huntington's disease. *Science*, **296**, 2238–2243.
58. Zuccato, C., Tartari, M., Crotti, A., Goffredo, D., Valenza, M., Conti, L., Cataudella, T., Leavitt, B.R., Hayden, M.R., Timmusk, T., et al. (2003) Huntingtin interacts with REST/NRSF to modulate the transcription of NRSE-controlled neuronal genes. *Nat. Genet.*, **35**, 76–83.
59. Poletti, A. (2004) The polyglutamine tract of androgen receptor: From functions to dysfunctions in motor neurons. *Front. Neuroendocrinol.*, **25**, 1–26.
60. Nedelsky, N.B., Pennuto, M., Smith, R.B., Palazzolo, I., Moore, J., Nie, Z., Neale, G. and Taylor, J.P. (2010) Native Functions of the Androgen Receptor Are Essential to Pathogenesis in a Drosophila Model of Spinobulbar Muscular Atrophy. *Neuron*, **67**, 936–952.
61. Lim, J., Crespo-Barreto, J., Jafar-Nejad, P., Bowman, A.B., Richman, R., Hill, D.E., Orr, H.T. and Zoghbi, H.Y. (2008) Opposing effects of polyglutamine expansion on native protein complexes contribute to SCA1. *Nature*, **452**, 713–718.
62. Fryer, J.D., Yu, P., Kang, H., Mandel-Brehm, C., Carter, A.N., Crespo-Barreto, J., Gao, Y., Flora, A., Shaw, C., Orr, H.T., et al. (2011) Exercise and Genetic Rescue of SCA1 via the Transcriptional Repressor Capicua. *Science (80-)*, **334**, 690–693.
63. McMahon, S.J., Pray-Grant, M.G., Schieltz, D., Yates, J.R. and Grant, P. a (2005) Polyglutamine-expanded spinocerebellar ataxia-7 protein disrupts normal SAGA

- and SLIK histone acetyltransferase activity. *Proc. Natl. Acad. Sci. U. S. A.*, **102**, 8478–8482.
64. Friedman, M.J., Shah, A.G., Fang, Z.-H., Ward, E.G., Warren, S.T., Li, S. and Li, X.-J. (2007) Polyglutamine domain modulates the TBP-TFIIB interaction: implications for its normal function and neurodegeneration. *Nat. Neurosci.*, **10**, 1519–1528.
 65. Friedman, M.J., Wang, C.E., Li, X.J. and Li, S. (2008) Polyglutamine expansion reduces the association of TATA-binding protein with DNA and induces DNA binding-independent neurotoxicity. *J. Biol. Chem.*, **283**, 8283–8290.
 66. Courtney, E., Kornfeld, S., Janitz, K. and Janitz, M. (2010) Transcriptome profiling in neurodegenerative disease. *J. Neurosci. Methods*, **193**, 189–202.
 67. Seredenina, T. and Luthi-Carter, R. (2012) What have we learned from gene expression profiles in Huntington’s disease? *Neurobiol. Dis.*, **45**, 83–98.
 68. Yang, S., Huang, S., Gaertig, M. a, Li, X.-J. and Li, S. (2014) Age-Dependent Decrease in Chaperone Activity Impairs MANF Expression, Leading to Purkinje Cell Degeneration in Inducible SCA17 Mice. *Neuron*, **81**, 349–365.
 69. Gatchel, J.R., Watase, K., Thaller, C., Carson, J.P., Jafar-Nejad, P., Shaw, C., Zu, T., Orr, H.T. and Zoghbi, H.Y. (2008) The insulin-like growth factor pathway is altered in spinocerebellar ataxia type 1 and type 7. *Proc. Natl. Acad. Sci. U. S. A.*, **105**, 1291–6.
 70. Suzuki, K., Zhou, J., Sato, T., Takao, K., Miyagawa, T., Oyake, M., Yamada, M., Takahashi, H., Takahashi, Y., Goto, J., et al. (2012) DRPLA transgenic mouse substrains carrying single copy of full-length mutant human DRPLA gene with variable sizes of expanded CAG repeats exhibit CAG repeat length- and age-dependent changes in behavioral abnormalities and gene expression profiles. *Neurobiol. Dis.*, **46**, 336–350.
 71. Halievski, K., Mo, K., Westwood, J.T. and Monks, D. a. (2015) Transcriptional Profile of Muscle following Acute Induction of Symptoms in a Mouse Model of Kennedy’s Disease/Spinobulbar Muscular Atrophy. *PLoS One*, **10**, e0118120.
 72. Chua, J.P., Reddy, S.L., Yu, Z., Giorgetti, E., Montie, H.L., Mukherjee, S., Higgins, J., Mceachin, R.C., Robins, D.M., Merry, D.E., et al. (2015) Disrupting SUMOylation enhances transcriptional function and ameliorates polyglutamine androgen receptor – mediated disease. *J. Clin. Invest.*, **125**, 831–845.
 73. Cha, J.J. (2007) Transcriptional Signatures in Huntington’s Disease. *Prog Neurobiol.*, **83**, 228–248.
 74. Kuhn, A., Goldstein, D.R., Hodges, A., Strand, A.D., Sengstag, T., Kooperberg, C., Becanovic, K., Pouladi, M. a., Sathasivam, K., Cha, J.H.J., et al. (2007) Mutant huntingtin’s effects on striatal gene expression in mice recapitulate changes observed in human Huntington’s disease brain and do not differ with mutant huntingtin length or wild-type huntingtin dosage. *Hum. Mol. Genet.*, **16**, 1845–1861.
 75. Scherzinger, E., Sittler, A., Schweiger, K., Heiser, V., Lurz, R., Hasenbank, R., Bates, G.P., Lehrach, H. and Wanker, E.E. (1999) Self-assembly of polyglutamine-containing huntingtin fragments into amyloid-like fibrils: implications for Huntington’s disease pathology. *Proc. Natl. Acad. Sci. U. S. A.*, **96**, 4604–4609.
 76. Yang, S.-H., Cheng, P.-H., Banta, H., Piotrowska-Nitsche, K., Yang, J.-J., Cheng, E.C.H., Snyder, B., Larkin, K., Liu, J., Orkin, J., et al. (2008) Towards a transgenic model of Huntington’s disease in a non-human primate. *Nature*, **453**, 921–924.

77. Saute, J.A.M., de Castilhos, R.M., Monte, T.L., Schumacher-Schuh, A.F., Donis, K.C., D'Ávila, R., Souza, G.N., Russo, A.D., Furtado, G.V., Gheno, T.C., et al. (2014) A randomized, phase 2 clinical trial of lithium carbonate in Machado-Joseph disease. *Mov. Disord.*, **29**, 568–573.
78. Sampaio, C., Borowsky, B. and Reilmann, R. (2014) Clinical Trials in Huntington ' s Disease : Interventions in Early Clinical Development and Newer Methodological Approaches Therapeutic Interventions in Clinical Development. *Mov. Disord.*, **29**, 1419–1428.
79. Fischbeck, K.H. (2012) Developing treatment for spinal and bulbar muscular atrophy. *Prog. Neurobiol.*, **99**, 257–261.
80. Lorenzetti, D., Watase, K., Xu, B., Matzuk, M.M., Orr, H.T. and Zoghbi, H.Y. (2000) Repeat instability and motor incoordination in mice with a targeted expanded CAG repeat in the Sca1 locus. *Hum. Mol. Genet.*, **9**, 779–785.
81. Ishiguro, H., Yamada, K., Sawada, H., Nishii, K., Ichino, N., Sawada, M., Kurosawa, Y., Matsushita, N., Kobayashi, K., Goto, J., et al. (2001) Repeat Instability Occurs in Mouse Knock-In for a Mutant Huntington ' s Disease Gene. **297**, 289–297.
82. Wheeler, V.C., Auerbach, W., White, J.K., Srinidhi, J., Auerbach, A., Ryan, A., Duyao, M.P., Vrbanc, V., Weaver, M., Gusella, J.F., et al. (1999) Length-dependent gametic CAG repeat instability in the Huntington ' s disease knock-in mouse. *Hum. Mol. Genet.*, **8**, 115–122.
83. Dragileva, E., Hendricks, A., Teed, A., Gillis, T., Lopez, E.T., Friedberg, E.C., Kucherlapati, R., Edelman, W., Lunetta, K.L., MacDonald, M.E., et al. (2009) Intergenerational and striatal CAG repeat instability in Huntington ' s disease knock-in mice involve different DNA repair genes. *Neurobiol. Dis.*, **33**, 37–47.
84. Kovalenko, M., Dragileva, E., St Claire, J., Gillis, T., Guide, J.R., New, J., Dong, H., Kucherlapati, R., Kucherlapati, M.H., Ehrlich, M.E., et al. (2012) Msh2 acts in medium-spiny striatal neurons as an enhancer of CAG instability and mutant huntingtin phenotypes in Huntington ' s disease knock-in mice. *PLoS One*, **7**, e44273.
85. Watase, K., Barrett, C.F., Miyazaki, T., Ishiguro, T., Ishikawa, K., Hu, Y., Unno, T., Sun, Y., Kasai, S., Watanabe, M., et al. (2008) Spinocerebellar ataxia type 6 knockin mice develop a progressive neuronal dysfunction with age-dependent accumulation of mutant CaV2.1 channels. *Proc. Natl. Acad. Sci. U. S. A.*, **105**, 11987–11992.
86. Sathasivam, K., Neueder, A., Gipson, T.A., Landles, C., Benjamin, A.C., Housman, D.E. and Bates, G.P. (2013) Aberrant splicing of HTT generates the pathogenic exon 1 protein in Huntington disease. *Proc. Natl. Acad. Sci. U. S. A.*, **110**, 2366–2370.
87. Lam, Y.C., Bowman, A.B., Jafar-Nejad, P., Lim, J., Richman, R., Fryer, J.D., Hyun, E.D., Duvick, L. a, Orr, H.T., Botas, J., et al. (2006) ATAXIN-1 interacts with the repressor Capicua in its native complex to cause SCA1 neuropathology. *Cell*, **127**, 1335–1347.
88. Ju, H., Kokubu, H., Todd, T.W., Kahle, J.J., Kim, S., Richman, R., Chirala, K., Orr, H.T., Zoghbi, H.Y. and Lim, J. (2013) Polyglutamine disease toxicity is regulated by Nemo-like kinase in spinocerebellar ataxia type 1. *J. Neurosci.*, **33**, 9328–9336.
89. Chort, A., Alves, S., Marinello, M., Dufresnois, B., Dornbierer, J.-G., Tesson, C., Latouche, M., Baker, D.P., Barkats, M., El Hachimi, K.H., et al. (2013) Interferon β

- induces clearance of mutant ataxin 7 and improves locomotion in SCA7 knock-in mice. *Brain*, **136**, 1732–1745.
90. Renier, K.J., Troxell-Smith, S.M., Johansen, J.A., Katsuno, M., Adachi, H., Sobue, G., Chua, J.P., Sun Kim, H., Lieberman, A.P., Breedlove, S.M., et al. (2014) Antiandrogen flutamide protects male mice from androgen-dependent toxicity in three models of spinal bulbar muscular atrophy. *Endocrinology*, **155**, 2624–2634.
 91. Keiser, M.S., Boudreau, R.L. and Davidson, B.L. (2014) Broad therapeutic benefit after RNAi expression vector delivery to deep cerebellar nuclei: implications for spinocerebellar ataxia type 1 therapy. *Mol. Ther.*, **22**, 588–95.
 92. Lieberman, A.P., Yu, Z., Murray, S., Peralta, R., Low, A., Guo, S., Yu, X.X., Cortes, C.J., Bennett, C.F., Monia, B.P., et al. (2014) Peripheral Androgen Receptor Gene Suppression Rescues Disease in Mouse Models of Spinal and Bulbar Muscular Atrophy. *Cell Rep.*, **7**, 774–784.
 93. Nakano, K., Dawson, D. and Spence, A. (1972) Machado disease. A hereditary ataxia in Portuguese emigrants to Massachusetts. *Neurology*, **22**, 49–55.
 94. Woods, B. and Schaumburg, H. (1972) Nigro-spino-dentatal degeneration with nuclear ophthalmoplegia. A unique and partially treatable clinico-pathological entity. *J Neurol Sci*, **17**, 149–166.
 95. Rosenberg, R., Nyhan, W. and Bay, C. (1976) Autosomal dominant striatonigral degeneration: a clinical, pathological, and biochemical study of a new genetic disorder. *Trans Am Neurol Assoc.*, **101**, 78–80.
 96. Romanul, F.C., Fowler, H.L., Radvany, J., Feldman, R.G. and Feingold, M. (1977) Azorean Disease of the Nervous System. *N. Engl. J. Med.*, **296**, 1505–1508.
 97. Coutinho, P. and Andrade, C. (1978) Autosomal dominant system degeneration in Portuguese families of the Azores Islands. A new genetic disorder involving cerebellar, pyramidal, extrapyramidal and spinal cord motor functions. *Neurology*, **28**, 703–709.
 98. Kawaguchi, Y., Okamoto, T., Taniwaki, M., Aizawa, M., Inoue, M., Katayama, S., Kawakami, H., Nakamura, S., Nishimura, M., Akiguchi, I., et al. (1994) CAG expansions in a novel gene for Machado-Joseph disease at chromosome 14q32.1. *Nat. Genet.*, **8**, 221–228.
 99. Schöls, L., Bauer, P., Schmidt, T., Schulte, T. and Riess, O. (2004) Review Autosomal dominant cerebellar ataxias : clinical features , genetics , and pathogenesis. *Lancet Neurol*, **3**, 291–304.
 100. Riess, O., Rüb, U., Pastore, A., Bauer, P. and Schöls, L. (2008) SCA3: neurological features, pathogenesis and animal models. *Cerebellum*, **7**, 125–137.
 101. D’Abreu, A., França, M.C., Paulson, H.L. and Lopes-Cendes, I. (2010) Caring for Machado-Joseph disease: current understanding and how to help patients. *Parkinsonism Relat. Disord.*, **16**, 2–7.
 102. Lopes, T.M., D’Abreu, A., França, M.C., Yasuda, C.L., Betting, L.E., Samara, A.B., Castellano, G., Somazz, J.C., Balthazar, M.L.F., Lopes-Cendes, I., et al. (2013) Widespread neuronal damage and cognitive dysfunction in spinocerebellar ataxia type 3. *J. Neurol.*, **260**, 2370–2379.
 103. Roeske, S., Filla, I., Heim, S., Amunts, K., Helmstaedter, C., Wüllner, U., Wagner, M., Klockgether, T. and Minnerop, M. (2013) Progressive cognitive dysfunction in spinocerebellar ataxia type 3. *Mov. Disord.*, **28**, 1435–1438.

104. Feng, L., Chen, D.B., Hou, L., Huang, L.H., Lu, S.Y., Liang, X.L. and Li, X.H. (2014) Cognitive Impairment in Native Chinese with Spinocerebellar Ataxia Type 3. *Eur. Neurol.*, **71**, 262–270.
105. Rüb, U., Schöls, L., Paulson, H., Auburger, G., Kermer, P., Jen, J.C., Seidel, K., Korf, H.-W. and Deller, T. (2013) Clinical features, neurogenetics and neuropathology of the polyglutamine spinocerebellar ataxias type 1, 2, 3, 6 and 7. *Prog. Neurobiol.*, **104**, 38–66.
106. Seidel, K., den Dunnen, W.F. a, Schultz, C., Paulson, H., Frank, S., de Vos, R. a, Brunt, E.R., Deller, T., Kampinga, H.H. and Rüb, U. (2010) Axonal inclusions in spinocerebellar ataxia type 3. *Acta Neuropathol.*, **120**, 449–460.
107. Goto, J., Watanabe, M., Ichikawa, Y., Yee, S.B., Ihara, N., Endo, K., Igarashi, S., Takiyama, Y., Gaspar, C., Maciel, P., et al. (1997) Machado-Joseph disease gene products carrying different carboxyl termini. *Neurosci. Res.*, **28**, 373–377.
108. Bettencourt, C., Santos, C., Montiel, R., Costa, M.D.C., Cruz-Morales, P., Santos, L.R., Simões, N., Kay, T., Vasconcelos, J., Maciel, P., et al. (2010) Increased transcript diversity: novel splicing variants of Machado-Joseph disease gene (ATXN3). *Neurogenetics*, **11**, 193–202.
109. Harris, G.M., Dodelzon, K., Gong, L., Gonzalez-Alegre, P. and Paulson, H.L. (2010) Splice isoforms of the polyglutamine disease protein ataxin-3 exhibit similar enzymatic yet different aggregation properties. *PLoS One*, **5**, e13695.
110. Colomer Gould, V.F. (2012) Mouse models of spinocerebellar ataxia type 3 (Machado-Joseph disease). *Neurotherapeutics*, **9**, 285–296.
111. Burnett, B., Li, F. and Pittman, R.N. (2003) The polyglutamine neurodegenerative protein ataxin-3 binds polyubiquitylated proteins and has ubiquitin protease activity. *Hum. Mol. Genet.*, **12**, 3195–205.
112. Winborn, B.J., Travis, S.M., Todi, S. V, Scaglione, K.M., Xu, P., Williams, A.J., Cohen, R.E., Peng, J. and Paulson, H.L. (2008) The deubiquitinating enzyme ataxin-3, a polyglutamine disease protein, edits Lys63 linkages in mixed linkage ubiquitin chains. *J. Biol. Chem.*, **283**, 26436–43.
113. Schmitt, I., Linden, M., Khazneh, H., Evert, B.O., Breuer, P., Klockgether, T. and Wuellner, U. (2007) Inactivation of the mouse *Atxn3* (ataxin-3) gene increases protein ubiquitination. *Biochem. Biophys. Res. Commun.*, **362**, 734–739.
114. Scaglione, K.M., Zavodszky, E., Todi, S. V, Patury, S., Xu, P., Rodríguez-Lebrón, E., Fischer, S., Konen, J., Djarmati, A., Peng, J., et al. (2011) Ube2w and ataxin-3 coordinately regulate the ubiquitin ligase CHIP. *Mol. Cell*, **43**, 599–612.
115. Warrick, J.M., Morabito, L.M., Bilen, J., Gordesky-Gold, B., Faust, L.Z., Paulson, H.L. and Bonini, N.M. (2005) Ataxin-3 suppresses polyglutamine neurodegeneration in *Drosophila* by a ubiquitin-associated mechanism. *Mol. Cell*, **18**, 37–48.
116. Alves, S., Régulier, E., Nascimento-Ferreira, I., Hassig, R., Dufour, N., Koeppen, A., Carvalho, A.L., Simões, S., de Lima, M.C.P., Brouillet, E., et al. (2008) Striatal and nigral pathology in a lentiviral rat model of Machado-Joseph disease. *Hum. Mol. Genet.*, **17**, 2071–83.
117. Hübener, J. and Riess, O. (2010) Polyglutamine-induced neurodegeneration in SCA3 is not mitigated by non-expanded ataxin-3: conclusions from double-transgenic mouse models. *Neurobiol. Dis.*, **38**, 116–24.

118. Zeng, L., Tallaksen-Greene, S.J., Wang, B., Albin, R.L. and Paulson, H.L. (2013) The de-ubiquitinating enzyme ataxin-3 does not modulate disease progression in a knock-in mouse model of Huntington disease. *J Huntingtons Dis.*, **2**, 201–215.
119. Macedo-ribeiro, S., Cortes, L., Maciel, P. and Carvalho, A.L. (2009) Nucleocytoplasmic Shuttling Activity of Ataxin-3. *PLoS One*, **4**, e5834.
120. Reina, C.P., Zhong, X. and Pittman, R.N. (2010) Proteotoxic stress increases nuclear localization of ataxin-3. *Hum. Mol. Genet.*, **19**, 235–249.
121. Li, F., Macfarlan, T., Pittman, R.N. and Chakravarti, D. (2002) Ataxin-3 is a histone-binding protein with two independent transcriptional corepressor activities. *J. Biol. Chem.*, **277**, 45004–45012.
122. Evert, B.O., Araujo, J., Vieira-Saecker, A.M., de Vos, R. a I., Harendza, S., Klockgether, T. and Wüllner, U. (2006) Ataxin-3 represses transcription via chromatin binding, interaction with histone deacetylase 3, and histone deacetylation. *J. Neurosci.*, **26**, 11474–11486.
123. Araujo, J., Breuer, P., Dieringer, S., Krauss, S., Dorn, S., Zimmermann, K., Pfeifer, A., Klockgether, T., Wuellner, U. and Evert, B.O. (2011) FOXO4-dependent upregulation of superoxide dismutase-2 in response to oxidative stress is impaired in spinocerebellar ataxia type 3. *Hum. Mol. Genet.*, **20**, 2928–41.
124. Ward, J.M. and La Spada, A.R. (2015) Ataxin-3, DNA Damage Repair, and SCA3 Cerebellar Degeneration: On the Path to Parsimony? *PLOS Genet.*, **11**, e1004937.
125. Wang, G., Sawai, N., Kotliarova, S., Kanazawa, I. and Nukina, N. (2000) Ataxin-3, the MJD1 gene product, interacts with the two human homologs of yeast DNA repair protein RAD23, HHR23A and HHR23B. *Hum. Mol. Genet.*, **9**, 1795–1803.
126. Doss-pepe, E.W., Stenroos, E.S., Johnson, W.G. and Madura, K. (2003) Ataxin-3 Interactions with Rad23 and Valosin-Containing Protein and Its Associations with Ubiquitin Chains and the Proteasome Are Consistent with a Role in Ubiquitin-Mediated Proteolysis. **23**, 6469–6483.
127. Blount, J.R., Tsou, W.-L., Ristic, G., Burr, A.A., Ouyang, M., Galante, H., Scaglione, K.M. and Todi, S. V (2014) Ubiquitin-binding site 2 of ataxin-3 prevents its proteasomal degradation by interacting with Rad23. *Nat. Commun.*, **5**, 1–10.
128. Chatterjee, A., Saha, S., Chakraborty, A., Silva-Fernandes, A., Mandal, S.M., Neves-Carvalho, A., Liu, Y., Pandita, R.K., Hegde, M.L., Hegde, P.M., et al. (2015) The Role of the Mammalian DNA End-processing Enzyme Polynucleotide Kinase 3'-Phosphatase in Spinocerebellar Ataxia Type 3 Pathogenesis. *PLOS Genet.*, **11**, e1004749.
129. Gao, R., Liu, Y., Silva-Fernandes, A., Fang, X., Paulucci-Holthauzen, A., Chatterjee, A., Zhang, H.L., Matsuura, T., Choudhary, S., Ashizawa, T., et al. (2015) Inactivation of PNKP by Mutant ATXN3 Triggers Apoptosis by Activating the DNA Damage-Response Pathway in SCA3. *PLOS Genet.*, **11**, e1004834.
130. Lu, X., Mattis, V.B., Wang, N., Al-ramahi, I., Berg, N. Van Den, Fratantoni, S.A., Waldvogel, H., Greiner, E., Osmand, A., Elzein, K., et al. (2014) Targeting ATM ameliorates mutant Huntingtin toxicity in cell and animal models of Huntington ' s disease. *Sci. Transl. Med.*, **6**, 1–12.
131. Giuliano, P., de Cristofaro, T., Affaitati, A., Pizzulo, G.M., Feliciello, A., Criscuolo, C., De Michele, G., Filla, A., Avvedimento, E. V. and Varrone, S. (2003) DNA

- damage induced by polyglutamine-expanded proteins. *Hum. Mol. Genet.*, **12**, 2301–2309.
132. Fujita, K., Nakamura, Y., Oka, T., Ito, H., Tamura, T., Tagawa, K., Sasabe, T., Katsuta, A., Motoki, K., Shiwaku, H., et al. (2013) A functional deficiency of TERA/VCP/p97 contributes to impaired DNA repair in multiple polyglutamine diseases. *Nat. Commun.*, **4**, 1816.
 133. Xiao, H., Yu, Z., Wu, Y., Nan, J., Merry, D.E., Sekiguchi, J.M., Ferguson, D.O., Lieberman, A.P. and Dressler, G.R. (2012) A polyglutamine expansion disease protein sequesters PTIP to attenuate DNA repair and increase genomic instability. *Hum. Mol. Genet.*, **21**, 4225–4236.
 134. White, J., Auerbach, W., Duyao, M.P., Vonsattel, J.-P., Gusella, J.F., Joyner, A.L. and MacDonald, M.E. (1997) Huntingtin is required for neurogenesis and is not impaired by the Huntington's disease CAG expansion. *Nature*, **17**, 404–410.
 135. Levine, M., Klapstein, G.J., Koppel, A., Gruen, E., Cepeda, C., Vargas, M.E., Jokel, E.S., Carpenter, E.M., Zanjani, H., Hurst, R.S., et al. (1999) Enhanced sensitivity to N-methyl-D-aspartate receptor activation in transgenic and knockin mouse models of Huntington's disease. *J Neurosci Res*, **58**, 515–32.
 136. Shelbourne, P.F., Killeen, N., Hevner, R.F., Johnston, H.M., Tecott, L., Lewandoski, M., Ennis, M., Ramirez, L., Li, Z., Iannicola, C., et al. (1999) Huntington's disease CAG expansion at the murine Hdh locus is unstable and associated with behavioural abnormalities in mice. *Hum. Mol. Genet.*, **8**, 763–774.
 137. Sawada, H., Ishiguro, H., Nishii, K., Yamada, K., Tsuchida, K., Takahashi, H., Goto, J., Kanazawa, I. and Nagatsu, T. (2007) Characterization of neuron-specific huntingtin aggregates in human huntingtin knock-in mice. *Neurosci. Res.*, **57**, 559–573.
 138. Lin, C., Tallaksen-greene, S., Chien, W., Cearley, J.A., Jackson, W.S., Crouse, A.B., Ren, S., Li, X., Albin, R.L. and Detloff, P.J. (2001) Neurological abnormalities in a knock-in mouse model of Huntington's disease. *Hum. Mol. Genet.*, **10**, 137–144.
 139. Menalled, L.B., Sison, J.D., Wu, Y., Olivieri, M., Li, X., Li, H. and Zeitlin, S. (2002) Early Motor Dysfunction and Striosomal Distribution of Huntingtin Microaggregates in Huntington's Disease Knock-In Mice. *Hum. Mol. Genet.*, **22**, 8266–8276.
 140. Wheeler, V.C., White, J.K., Gutekunst, C., Vrbanc, V., Weaver, M., Li, X., Li, S., Yi, H., Vonsattel, J., Gusella, J.F., et al. (2000) Long glutamine tracts cause nuclear localization of a novel form of huntingtin in medium spiny striatal neurons in Hdh Q92 and Hdh Q111 knock-in mice. *Hum. Mol. Genet.*, **9**, 503–514.
 141. Brooks, S., Higgs, G., Jones, L. and Dunnett, S.B. (2012) Longitudinal analysis of the behavioural phenotype in HdhQ92 Huntington's disease knock-in mice. *Brain Res. Bull.*, **88**, 148–155.
 142. Menalled, L.B., Sison, J.D., Dragatsis, I., Zeitlin, S. and Chesselet, M.-F. (2003) Time course of early motor and neuropathological anomalies in a knock-in mouse model of Huntington's disease with 140 CAG repeats. *J. Comp. Neurol.*, **465**, 11–26.
 143. Menalled, L.B., Kudwa, A.E., Miller, S., Fitzpatrick, J., Watson-Johnson, J., Keating, N., Ruiz, M., Mushlin, R., Alosio, W., McConnell, K., et al. (2012)

- Comprehensive behavioral and molecular characterization of a new knock-in mouse model of Huntington's disease: zQ175. *PLoS One*, **7**, e49838.
144. Zheng, S., Ghitani, N., Blackburn, J.S., Liu, J.-P. and Zeitlin, S.O. (2012) A series of N-terminal epitope tagged Hdh knock-in alleles expressing normal and mutant huntingtin: their application to understanding the effect of increasing the length of normal Huntingtin's polyglutamine stretch on CAG140 mouse model pathogenesis. *Mol. Brain*, **5**, 28.
 145. Heng, M.Y., Tallaksen-Greene, S.J., Detloff, P.J. and Albin, R.L. (2007) Longitudinal evaluation of the Hdh(CAG)150 knock-in murine model of Huntington's disease. *J. Neurosci.*, **27**, 8989–8998.
 146. Tallaksen-Greene, S.J., Crouse, a B., Hunter, J.M., Detloff, P.J. and Albin, R.L. (2005) Neuronal intranuclear inclusions and neuropil aggregates in HdhCAG(150) knockin mice. *Neuroscience*, **131**, 843–852.
 147. Heng, M.Y., Duong, D.K., Albin, R.L., Tallaksen-Greene, S.J., Hunter, J.M., Lesort, M.J., Osmand, A., Paulson, H.L. and Detloff, P.J. (2010) Early autophagic response in a novel knock-in model of Huntington disease. *Hum. Mol. Genet.*, **19**, 3702–3720.
 148. Jin, J., Peng, Q., Hou, Z., Jiang, M., Wang, X., Langseth, a. J., Tao, M., Barker, P.B., Mori, S., Bergles, D.E., et al. (2015) Early white matter abnormalities, progressive brain pathology and motor deficits in a novel knock-in mouse model of Huntington's disease. *Hum. Mol. Genet.*, **24**, 2508–2527.
 149. Watase, K., Weeber, E.J., Xu, B., Antalffy, B., Yuva-Paylor, L., Hashimoto, K., Kano, M., Atkinson, R., Sun, Y., Armstrong, D.L., et al. (2002) A long CAG repeat in the mouse Scn1 locus replicates SCA1 features and reveals the impact of protein solubility on selective neurodegeneration. *Neuron*, **34**, 905–919.
 150. Damrath, E., Heck, M. V, Gispert, S., Azizov, M., Nowock, J., Seifried, C., Rüb, U., Walter, M. and Auburger, G. (2012) ATXN2-CAG42 sequesters PABPC1 into insolubility and induces FBXW8 in cerebellum of old ataxic knock-in mice. *PLoS Genet.*, **8**, e1002920.
 151. Ramani, B., Harris, G.M., Huang, R., Seki, T., Murphy, G.G., Costa, M.D.C., Fischer, S., Saunders, T.L., Xia, G., McEachin, R.C., et al. (2015) A knockin mouse model of spinocerebellar ataxia type 3 exhibits prominent aggregate pathology and aberrant splicing of the disease gene transcript. *Hum. Mol. Genet.*, **24**, 1211–1224.
 152. Switonski, P.M., Szlachcic, W.J., Krzyzosiak, W.J. and Figiel, M. (2015) A new humanized ataxin-3 knock-in mouse model combines the genetic features, pathogenesis of neurons and glia and late disease onset of SCA3/MJD. *Neurobiol. Dis.*, **73**, 174–188.
 153. Yoo, S.Y., Pennesi, M.E., Weeber, E.J., Xu, B., Atkinson, R., Chen, S., Armstrong, D.L., Wu, S.M., Sweatt, J.D. and Zoghbi, H.Y. (2003) SCA7 knockin mice model human SCA7 and reveal gradual accumulation of mutant ataxin-7 in neurons and abnormalities in short-term plasticity. *Neuron*, **37**, 383–401.
 154. Huang, S., Ling, J.J., Yang, S., Li, X.-J. and Li, S. (2011) Neuronal expression of TATA box-binding protein containing expanded polyglutamine in knock-in mice reduces chaperone protein response by impairing the function of nuclear factor-Y transcription factor. *Brain*, **134**, 1943–1958.
 155. Harris, G.M. (2011) Toward understanding the role of protein context in the polyglutamine disease, SCA3.

156. Geiser, M., Cebe, R., Drewello, D. and Schmitz, R. (2001) Integration of PCR fragments at any specific site within cloning vectors without the use of restriction enzymes and DNA ligase. *Biotechniques*, **31**, 88–90.
157. Laccone, F., Maiwald, R. and Bingemann, S. (1999) A fast polymerase chain reaction-mediated strategy for introducing repeat expansions into CAG-repeat containing genes. *Hum. Mutat.*, **13**, 497–502.
158. Hughes, E.D., Qu, Y.Y., Genik, S.J., Lyons, R.H., Pacheco, C.D., Lieberman, A.P., Samuelson, L.C., Nasonkin, I.O., Camper, S. a, Van Keuren, M.L., et al. (2007) Genetic variation in C57BL/6 ES cell lines and genetic instability in the Bruce4 C57BL/6 ES cell line. *Mamm. Genome*, **18**, 549–558.
159. Cemal, C.K., Carroll, C.J., Lawrence, L., Lowrie, M.B., Ruddle, P., Al-Mahdawi, S., King, R.H.M., Pook, M. a, Huxley, C. and Chamberlain, S. (2002) YAC transgenic mice carrying pathological alleles of the MJD1 locus exhibit a mild and slowly progressive cerebellar deficit. *Hum. Mol. Genet.*, **11**, 1075–1094.
160. Paulson, H.L., Das, S.S., Crino, P.B., Perez, M.K., Patel, S.C., Gotsdiner, D., Fischbeck, K.H. and Pittman, R.N. (1997) Machado-Joseph disease gene product is a cytoplasmic protein widely expressed in brain. *Ann. Neurol.*, **41**, 453–462.
161. Perkowski, J.J. and Murphy, G.G. (2011) Deletion of the mouse homolog of KCNAB2, a gene linked to monosomy 1p36, results in associative memory impairments and amygdala hyperexcitability. *J. Neurosci.*, **31**, 46–54.
162. Robinson, J.T., Thorvaldsdottir, H., Winckler, W., Guttman, M., Lander, E., Getz, G. and Mesirov, J.P. (2011) Integrative genomics viewer. *Nat. Biotechnol.*, **29**, 24–26.
163. Thorvaldsdóttir, H., Robinson, J.T. and Mesirov, J.P. (2013) Integrative Genomics Viewer (IGV): high-performance genomics data visualization and exploration. *Brief. Bioinform.*, **14**, 178–192.
164. Chen, J., Bardes, E.E., Aronow, B.J. and Jegga, A.G. (2009) ToppGene Suite for gene list enrichment analysis and candidate gene prioritization. *Nucleic Acids Res.*, **37**, 305–311.
165. Zhang, Y., Chen, K., Sloan, S. a, Bennett, M.L., Scholze, A.R., Keefe, S.O., Phatnani, H.P., Guarnieri, X.P., Caneda, C., Ruderisch, N., et al. (2014) An RNA-Sequencing Transcriptome and Splicing Database of Glia, Neurons, and Vascular Cells of the Cerebral Cortex. *J. Neurosci.*, **34**, 11929–11947.
166. Livak, K.J. and Schmittgen, T.D. (2001) Analysis of relative gene expression data using real-time quantitative PCR and the 2(-Delta Delta C(T)) Method. *Methods*, **25**, 402–408.
167. Orr, H.T. and Zoghbi, H.Y. (2007) Trinucleotide Repeat Disorders. *Annu. Rev. Neurosci.*, **30**, 575–621.
168. Hartl, F.U., Bracher, A. and Hayer-Hartl, M. (2011) Molecular chaperones in protein folding and proteostasis. *Nature*, **475**, 324–332.
169. Maciel, P., Costa, M.C., Ferro, A., Rousseau, M., Santos, C.S., Gaspar, C., Barros, J., Rouleau, G. a, Coutinho, P. and Sequeiros, J. (2001) Improvement in the molecular diagnosis of Machado-Joseph disease. *Arch. Neurol.*, **58**, 1821–1827.
170. Watase, K., Venken, K.J.T., Sun, Y., Orr, H.T. and Zoghbi, H.Y. (2003) Regional differences of somatic CAG repeat instability do not account for selective neuronal

- vulnerability in a knock-in mouse model of SCA1. *Hum. Mol. Genet.*, **12**, 2789–2795.
171. Goti, D., Katzen, S.M., Mez, J., Kurtis, N., Kiluk, J., Ben-Haïem, L., Jenkins, N.A., Copeland, N.G., Kakizuka, A., Sharp, A.H., et al. (2004) A mutant ataxin-3 putative-cleavage fragment in brains of Machado-Joseph disease patients and transgenic mice is cytotoxic above a critical concentration. *J. Neurosci.*, **24**, 10266–10279.
 172. Mori, F., Tanji, K., Odagiri, S., Toyoshima, Y., Yoshida, M., Kakita, A., Takahashi, H. and Wakabayashi, K. (2012) Autophagy-related proteins (p62, NBR1 and LC3) in intranuclear inclusions in neurodegenerative diseases. *Neurosci. Lett.*, **522**, 134–138.
 173. Nascimento-Ferreira, I., Santos-Ferreira, T., Sousa-Ferreira, L., Auregan, G., Onofre, I., Alves, S., Dufour, N., Colomer Gould, V.F., Koeppen, A., Déglon, N., et al. (2011) Overexpression of the autophagic beclin-1 protein clears mutant ataxin-3 and alleviates Machado-Joseph disease. *Brain*, **134**, 1400–1415.
 174. Seidel, K., Meister, M., Dugbartey, G.J., Zijlstra, M.P., Vinet, J., Brunt, E.R.P., van Leeuwen, F.W., Rüb, U., Kampinga, H.H. and den Dunnen, W.F. a (2012) Cellular protein quality control and the evolution of aggregates in spinocerebellar ataxia type 3 (SCA3). *Neuropathol. Appl. Neurobiol.*, **38**, 548–558.
 175. Hu, X., Shi, Q., Zhou, X., He, W., Yi, H., Yin, X., Gearing, M., Levey, A. and Yan, R. (2007) Transgenic mice overexpressing reticulon 3 develop neuritic abnormalities. *EMBO J.*, **26**, 2755–2767.
 176. Shi, Q., Hu, X., Prior, M. and Yan, R. (2009) The occurrence of aging-dependent reticulon 3 immunoreactive dystrophic neurites decreases cognitive function. *J. Neurosci.*, **29**, 5108–5115.
 177. Maren, S. (2001) Neurobiology of Pavlovian fear conditioning. *Annu. Rev. Neurosci.*, **24**, 897–931.
 178. Schmidt, T., Landwehrmeyer, G.B., Schmitt, I., Trottier, Y., Auburger, G., Laccone, F., Klockgether, T., Völpel, M., Epplen, J.T., Schöls, L., et al. (1998) An isoform of ataxin-3 accumulates in the nucleus of neuronal cells in affected brain regions of SCA3 patients. *Brain Pathol.*, **8**, 669–679.
 179. Kurosawa, M., Matsumoto, G., Kino, Y., Okuno, M., Kurosawa-Yamada, M., Washizu, C., Taniguchi, H., Nakaso, K., Yanagawa, T., Warabi, E., et al. (2014) Depletion of p62 reduces nuclear inclusions and paradoxically ameliorates disease phenotypes in Huntington’s model mice. *Hum. Mol. Genet.*, **24**, 1092–1105.
 180. Koch, P., Breuer, P., Peitz, M., Jungverdorben, J., Kesavan, J., Poppe, D., Doerr, J., Ladewig, J., Mertens, J., Tüting, T., et al. (2011) Excitation-induced ataxin-3 aggregation in neurons from patients with Machado-Joseph disease. *Nature*, **480**, 543–546.
 181. Gipson, T.A., Neueder, A., Wexler, N.S., Bates, G.P. and Housman, D.E. (2013) Aberrantly spliced HTT , a new player in Huntington’s disease pathogenesis. *RNA Biol.*, **10**, 1–6.
 182. Elkon, R., Ugalde, A.P. and Agami, R. (2013) Alternative cleavage and polyadenylation: extent, regulation and function. *Nat. Rev. Genet.*, **14**, 496–506.

183. Mata, M. De, Alonso, C.R., Fededa, J.P., Pelisch, F., Cramer, P., Bentley, D. and Kornblihtt, A.R. (2003) A Slow RNA Polymerase II Affects Alternative Splicing In Vivo. *Mol. Cell*, **12**, 525–532.
184. Pinto, P. a B., Henriques, T., Freitas, M.O., Martins, T., Domingues, R.G., Wyrzykowska, P.S., Coelho, P. a, Carmo, A.M., Sunkel, C.E., Proudfoot, N.J., et al. (2011) RNA polymerase II kinetics in polo polyadenylation signal selection. *EMBO J.*, **30**, 2431–2444.
185. Gestwicki, J.E. and Garza, D. (2012) Protein quality control in neurodegenerative disease. *Prog. Mol. Biol. Transl. Sci.*, **107**, 327–353.
186. Sakahira, H., Breuer, P., Hayer-Hartl, M.K. and Hartl, F.U. (2002) Molecular chaperones as modulators of polyglutamine protein aggregation and toxicity. *Proc. Natl. Acad. Sci. U. S. A.*, **99 Suppl 4**, 16412–16418.
187. Muchowski, P.J. and Wacker, J.L. (2005) Modulation of neurodegeneration by molecular chaperones. *Nat. Rev. Neurosci.*, **6**, 11–22.
188. Kumar, A., Vaish, M. and Ratan, R.R. (2014) Transcriptional dysregulation in Huntington’s disease: a failure of adaptive transcriptional homeostasis. *Drug Discov. Today*, **19**, 956–962.
189. Mohan, A., Goodwin, M. and Swanson, M.S. (2014) RNA-protein interactions in unstable microsatellite diseases. *Brain Res.*, **1584**, 1–12.
190. Adanyeguh, I., Pierre-Gilles, H., Nguyen, T., Rinaldi, D., Jauffret, C., Valabregue, R., Emir, U., Deelchand, D., Brice, A., Eberly, L., et al. (2015) In vivo neurometabolic profiling in Patients with Spinocerebellar Ataxia Types 1, 2, 3, and 7. *Mov. Disord.*, **30**, 662–670.
191. Menzies, F.M., Huebener, J., Renna, M., Bonin, M., Riess, O. and Rubinsztein, D.C. (2010) Autophagy induction reduces mutant ataxin-3 levels and toxicity in a mouse model of spinocerebellar ataxia type 3. *Brain*, **133**, 93–104.
192. Stack, E.C., Del Signore, S.J., Luthi-Carter, R., Soh, B.Y., Goldstein, D.R., Matson, S., Goodrich, S., Markey, A.L., Cormier, K., Hagerty, S.W., et al. (2007) Modulation of nucleosome dynamics in Huntington’s disease. *Hum. Mol. Genet.*, **16**, 1164–1175.
193. Thomas, E.A., Coppola, G., Tang, B., Kuhn, A., Kim, S., Geschwind, D.H., Brown, T.B., Luthi-Carter, R. and Ehrlich, M.E. (2011) In vivo cell-autonomous transcriptional abnormalities revealed in mice expressing mutant huntingtin in striatal but not cortical neurons. *Hum. Mol. Genet.*, **20**, 1049–1060.
194. Sambataro, F. and Pennuto, M. (2012) Cell-autonomous and non-cell-autonomous toxicity in polyglutamine diseases. *Prog. Neurobiol.*, **97**, 152–172.
195. Custer, S.K., Garden, G. a, Gill, N., Rueb, U., Libby, R.T., Schultz, C., Guyenet, S.J., Deller, T., Westrum, L.E., Sopher, B.L., et al. (2006) Bergmann glia expression of polyglutamine-expanded ataxin-7 produces neurodegeneration by impairing glutamate transport. *Nat. Neurosci.*, **9**, 1302–1311.
196. Furrer, S.A., Mohanachandran, M.S., Waldherr, S.M., Chang, C., Damian, V.A., Sopher, B.L., Garden, G.A. and La Spada, A.R. (2011) Spinocerebellar ataxia type 7 cerebellar disease requires the coordinated action of mutant ataxin-7 in neurons and glia, and displays non-cell-autonomous bergmann glia degeneration. *J. Neurosci.*, **31**, 16269–16278.

197. Huang, B., Wei, W., Wang, G., Gaertig, M.A., Feng, Y., Wang, W., Li, X.-J. and Li, S. (2015) Mutant Huntingtin Downregulates Myelin Regulatory Factor-Mediated Myelin Gene Expression and Affects Mature Oligodendrocytes. *Neuron*, **85**, 1212–1226.
198. Nonneman, A., Robberecht, W. and Den Bosch, L. Van (2014) The role of oligodendroglial dysfunction in amyotrophic lateral sclerosis. *Neurodegener. Dis. Manag.*, **4**, 223–239.
199. Philips, T., Bento-Abreu, A., Nonneman, A., Haeck, W., Staats, K., Geelen, V., Hersmus, N., Küsters, B., Van Den Bosch, L., Van Damme, P., et al. (2013) Oligodendrocyte dysfunction in the pathogenesis of amyotrophic lateral sclerosis. *Brain*, **136**, 471–482.
200. Kang, J.S., Klein, J.C., Baudrexel, S., Deichmann, R., Nolte, D. and Hilker, R. (2014) White matter damage is related to ataxia severity in SCA3. *J. Neurol.*, **261**, 291–299.
201. Lukas, C., Schöls, L., Bellenberg, B., Rüb, U., Przuntek, H., Schmid, G., Köster, O. and Suchan, B. (2006) Dissociation of grey and white matter reduction in spinocerebellar ataxia type 3 and 6: A voxel-based morphometry study. *Neurosci. Lett.*, **408**, 230–235.
202. Suga, N., Katsuno, M., Koike, H., Banno, H., Suzuki, K., Hashizume, A., Mano, T., Iijima, M., Kawagashira, Y., Hirayama, M., et al. (2014) Schwann cell involvement in the peripheral neuropathy of spinocerebellar ataxia type 3. *Neuropathol. Appl. Neurobiol.*, **40**, 628–639.
203. Katsuno, M., Tanaka, F., Adachi, H., Banno, H., Suzuki, K., Watanabe, H. and Sobue, G. (2012) Pathogenesis and therapy of spinal and bulbar muscular atrophy (SBMA). *Prog. Neurobiol.*, **99**, 246–256.
204. Sander, J.D. and Joung, J.K. (2014) CRISPR-Cas systems for editing, regulating and targeting genomes. *Nat. Biotechnol.*, **32**, 347–355.
205. Fiszer, A. and Krzyzosiak, W.J. (2014) Oligonucleotide-based strategies to combat polyglutamine diseases. *Nucleic Acids Res.*, **42**, 6787–6810.
206. Du, X., Wang, J., Zhu, H., Rinaldo, L., Lamar, K.M., Palmenberg, A.C., Hansel, C. and Gomez, C.M. (2013) Second cistron in CACNA1A gene encodes a transcription factor mediating cerebellar development and SCA6. *Cell*, **154**, 118–133.
207. Banfi, S., Servadio, A., Chung, M.Y., Kwiatkowski, T.J., McCall, A., Duvick, L.A., Shen, Y., Roth, E.J., Orr, H.T. and Zoghbi, H.Y. (1994) Identification and characterization of the gene causing type 1 spinocerebellar ataxia. *Nat. Genet.*, **7**, 513–520.
208. Affaitati, A., de Cristofaro, T., Feliciello, A. and Varrone, S. (2001) Identification of alternative splicing of spinocerebellar ataxia type 2 gene. *Gene*, **267**, 89–93.
209. Tsunemi, T., Ishikawa, K., Jin, H. and Mizusawa, H. (2008) Cell-type-specific alternative splicing in spinocerebellar ataxia type 6. *Neurosci. Lett.*, **447**, 78–81.
210. Einum, D.D., Clark, A.M., Townsend, J.J., Ptacek, L.J. and Fu, Y.-H. (2003) A novel central nervous system-enriched spinocerebellar ataxia type 7 gene product. *Arch. Neurol.*, **60**, 97–103.
211. Reid, S.J., Whittaker, D.J., Greenwood, D. and Snell, R.G. (2009) A splice variant of the TATA-box binding protein encoding the polyglutamine-containing N-

- terminal domain that accumulates in Alzheimer's disease. *Brain Res.*, **1268**, 190–199.
212. Hirata, S., Shoda, T., Kato, J. and Hoshi, K. (2003) Isoform/variant mRNAs for sex steroid hormone receptors in humans. *Trends Endocrinol. Metab.*, **14**, 124–129.
213. Tadokoro, K., Yamazaki-Inoue, M., Tachibana, M., Fujishiro, M., Nagao, K., Toyoda, M., Ozaki, M., Ono, M., Miki, N., Miyashita, T., et al. (2005) Frequent occurrence of protein isoforms with or without a single amino acid residue by subtle alternative splicing: The case of Gln in DRPLA affects subcellular localization of the products. *J. Hum. Genet.*, **50**, 382–394.
214. Costa, M.D.C., Luna-Cancelon, K., Fischer, S., Ashraf, N.S., Ouyang, M., Dharia, R.M., Martin-Fishman, L., Yang, Y., Shakkottai, V.G., Davidson, B.L., et al. (2013) Toward RNAi therapy for the polyglutamine disease Machado-Joseph disease. *Mol. Ther.*, **21**, 1898–1908.
215. Rodríguez-Lebrón, E., Costa, M. do C., Luna-Cancelon, K., Peron, T.M., Fischer, S., Boudreau, R.L., Davidson, B.L. and Paulson, H.L. (2013) Silencing mutant ATXN3 expression resolves molecular phenotypes in SCA3 transgenic mice. *Mol. Ther.*, **21**, 1909–1918.
216. Musunuru, K. (2013) Genome editing of human pluripotent stem cells to generate human cellular disease models. *Dis. Model. Mech.*, **6**, 896–904.
217. Shakkottai, V.G., do Carmo Costa, M., Dell'Orco, J.M., Sankaranarayanan, A., Wulff, H. and Paulson, H.L. (2011) Early changes in cerebellar physiology accompany motor dysfunction in the polyglutamine disease spinocerebellar ataxia type 3. *J. Neurosci.*, **31**, 13002–13014.
218. Pennuto, M., Palazzolo, I. and Poletti, A. (2009) Post-translational modifications of expanded polyglutamine proteins: Impact on neurotoxicity. *Hum. Mol. Genet.*, **18**, 40–47.
219. Gillis, J., Schipper-Krom, S., Juenemann, K., Gruber, A., Coolen, S., van den Nieuwendijk, R., van Veen, H., Overkleeft, H., Goedhart, J., Kampinga, H.H., et al. (2013) The DNAJB6 and DNAJB8 protein chaperones prevent intracellular aggregation of polyglutamine peptides. *J. Biol. Chem.*, **288**, 17225–17237.
220. Jimenez-Sanchez, M., Thomson, F., Zavodszky, E. and Rubinsztein, D.C. (2012) Autophagy and polyglutamine diseases. *Prog. Neurobiol.*, **97**, 67–82.
221. Simões, A.T., Gonçalves, N., Nobre, R.J., Duarte, C.B. and Pereira de Almeida, L. (2014) Calpain inhibition reduces ataxin-3 cleavage alleviating neuropathology and motor impairments in mouse models of Machado-Joseph disease. *Hum. Mol. Genet.*, **23**, 4932–4944.
222. Pratt, W.B., Gestwicki, J.E., Osawa, Y. and Lieberman, A.P. (2015) Targeting Hsp90/Hsp70-Based Protein Quality Control for Treatment of Adult Onset Neurodegenerative Diseases. *Annu. Rev. Pharmacol. Toxicol.*, **55**, 353–371.
223. Barabási, A.-L., Gulbahce, N. and Loscalzo, J. (2011) Network medicine: a network-based approach to human disease. *Nat. Rev. Genet.*, **12**, 56–68.
224. Bettencourt, C., Ryten, M., Forabosco, P., Schorge, S., Hersheson, J., Hardy, J. and Houlden, H. (2014) Insights From Cerebellar Transcriptomic Analysis Into the Pathogenesis of Ataxia. *JAMA Neurol.*, **71**, 831–839.

225. Miller, J. a, Oldham, M.C. and Geschwind, D.H. (2008) A systems level analysis of transcriptional changes in Alzheimer's disease and normal aging. *J. Neurosci.*, **28**, 1410–1420.
226. Zhu, F., Shi, L., Li, H., Eksi, R., Engel, J.D. and Guan, Y. (2014) Modeling Dynamic Functional Relationship Networks and Application to Ex Vivo Human Erythroid Differentiation. *Bioinformatics*, **30**, 3325–3333.
227. Nalavade, R., Griesche, N., Ryan, D.P., Hildebrand, S. and Krauss, S. (2013) Mechanisms of RNA-induced toxicity in CAG repeat disorders. *Cell Death Dis.*, **4**, e752.
228. Cech, T.R. and Steitz, J. a. (2014) The noncoding RNA revolution - Trashing old rules to forge new ones. *Cell*, **157**, 77–94.
229. Bilen, J., Liu, N., Burnett, B.G., Pittman, R.N. and Bonini, N.M. (2006) MicroRNA pathways modulate polyglutamine-induced neurodegeneration. *Mol. Cell*, **24**, 157–63.
230. Hébert, S.S. and De Strooper, B. (2009) Alterations of the microRNA network cause neurodegenerative disease. *Trends Neurosci.*, **32**, 199–206.
231. Johnson, R. (2012) Long non-coding RNAs in Huntington's disease neurodegeneration. *Neurobiol. Dis.*, **46**, 245–254.
232. Johnson, R., Richter, N., Jauch, R., Gaughwin, P.M., Zuccato, C., Cattaneo, E. and Stanton, L.W. (2010) Human accelerated region 1 noncoding RNA is repressed by REST in Huntington's disease. *Physiol. Genomics*, **41**, 269–274.
233. Francelle, L., Galvan, L., Gaillard, M.-C., Petit, F., Bernay, B., Guillermier, M., Bonvento, G., Dufour, N., Elalouf, J.-M., Hantraye, P., et al. (2015) The striatal long noncoding RNA *Abhd11os* is neuroprotective against an N-terminal fragment of mutant huntingtin in vivo. *Neurobiol. Aging*, **36**, 1601.e7–1601.e16.
234. Tan, J.Y., Vance, K.W., Varela, M. a, Sirey, T., Watson, L.M., Curtis, H.J., Marinello, M., Alves, S., Steinkraus, B.R., Cooper, S., et al. (2014) Cross-talking noncoding RNAs contribute to cell-specific neurodegeneration in SCA7. *Nat. Struct. Mol. Biol.*, **21**, 955–961.
235. Verkhatsky, A., Parpura, V., Pekna, M., Pekny, M. and Sofroniew, M. (2014) Glia in the pathogenesis of neurodegenerative diseases. *Biochem Soc Trans.*, **42**, 1291–1301.